Cobalt, Silicon and Silica GLAD films for SMALDI-MS, UTLC and Tissue Imaging

by

Reshma Singh

A thesis submitted in partial fulfillment of the requirements for the degree of

Doctor of Philosophy

Department of Chemistry
University of Alberta

Abstract

The detection and identification of biomarkers and metabolites in the low mass range has become prominent in clinical diagnoses, disease monitoring and for tracking drug interactions. Laser desorption/ionization techniques have been applied as a powerful tool in this field because of their speed and simplicity. Further, the development of matrix-free substrates has emerged as an improvement for LDI in the low mass range eliminating the high background. The need for reproducibility in the fabrication of substrates has now become the focus for future development.

This thesis investigates the application of cobalt, silicon and silica nano-thin films fabricated by glancing angle deposition (GLAD) for solid matrix assisted laser desorption/ionization mass spectrometry (SMALDI-MS), ultra-thin layer chromatography and tissue imaging in the low mass range. The GLAD technique produces films whose morphology in terms of pore size, density and shape can be dictated and is highly reproducible. It is also applicable to a wide range of material types, such as metals, semiconductors and oxides, this offers an exciting avenue for exploring different materials for LDI-MS applications.

In the first segment of this research project, the application of cobalt GLAD films as a SMALDI-MS material was explored. Physical parameters of the films such as deposition angle and film thickness were found to have a direct impact on the SMALDI-MS performance. The selection of the optimum conditions was found to have an improvement on the signal to noise ratios of

mass spectra and hence, the limit of detection. Matrix-free detection of carbohydrates, peptides and metabolites was achieved at the femtomole level. The films were also found to be highly reproducible in terms of SMALDI performance from, spot-to-spot and batch-to-batch. Next, the application of silicon GLAD films for the detection of glycolipids was investigated. Several classes of glycolipids were detected both in standard solutions and in a biofluid sample at femtomole levels. Sample cleanup on the same film was also achieved by employing the UTLC capability of GLAD. Hyphenated UTLC-SMALDI-MS was further examined in the next phase of investigation. Silica GLAD films were determined to be the optimum substrate for this combined application with a mixture of carbohydrates and peptides. Finally, silicon GLAD films were applied for the matrix free tissue imaging by LDI-MS. Animal tissue was used as the test material and lipid compounds were targeted for detection.

GLAD films as a matrix-free substrate was carefully explored and has been proven as a viable material for the application. The potential of the films has also been extended to the areas of hyphenated separation and detection and to molecular imaging.

Preface

Some of the research conducted for this thesis forms part of a research collaboration with Professor Michael Brett of the Department of Department of Electrical and Computer Engineering, University of Alberta. Professor Jed Harrison was the lead collaborator in the Department of Chemistry, University of Alberta. The Glancing Angle Deposition (GLAD) films referred to throughout this thesis were fabricated by Zhen Wang and Jason Sorge with the assistance of Professor Michael Brett.

The mass spectrometry tests, characterization tests and data analyses in Chapters 2, 3, 4 and 5 are my original work, as well as the literature review in Chapter 1. A portion of Chapter 2 of this thesis will be submitted for publication. The work was done in collaboration with Zhen Wang, L. W. Bezuidenhout and Abebaw B. Jemere. My role includes evaluation of cobalt GLAD films for laser desorption/ionization mass spectrometry, contact angle determinations and some of the performance comparisons for slanted and vertical post silicon GLAD films. I am responsible for the manuscript composition and some of the data collection as mentioned above. Zhen Wang was responsible for the film fabrication and L. W. Bezuidenhout and Abebaw B. Jemere contributed some of the data for the silicon films. Jed Harrison will be the supervisory author and was involved with concept formation and manuscript composition.

Contents

List of Tables

List of Figures

List of Abbreviations

3-AQ: 3-aminoquinoline

9-AA: 9-aminoacridine

a.u.: Arbitrary units

CNS: Central nervous system

CVD: Chemical vapour deposition

DCTB: *trans*-2-[3-(4-*tert*-Butylphenyl)-2-methyl-2-propenylidene] malononitrile

DHB: 2,5-dihydroxybenzoic acid

DIOS-MS: Desorption/ionisation on porous silicon mass spectrometry

FTICR: Fourier transform ion cyclotron resonance

ESI MS: Electrospray ionisation mass spectrometry

GLAD: Glancing angle deposition

HPTLC: High performance thin layer chromatography

IUPAC-IUB: International Union of Pure and Applied Chemistry-International Union of Biochemistry and Molecular Biology

LC: Liquid Chromatography

LDI MS: Laser desorption/ionization mass spectrometry

MALDI MS: Matrix assisted laser desorption/ionization mass spectrometry

NANA: N-acetylneuraminic acid

NALDI: Nanowire assisted laser desorption ionization

NMR: Nuclear magnetic resonance

PECVD: Plasma-enhanced chemical vapour deposition

RIE: Reactive ion etching

R_F: Retardation factor

S/N: Signal-to-noise ratio

SALDI: Surface assisted laser desorption/ionization

SMALDI: Solid matrix assisted laser desorption/ionization

TFA: Trifluoracetic acid

TOF: Time of flight

UTLC: Ultra-thin layer chromatography

Chapter 1

Introduction

Sir J.J Thomson and Francis W. Aston are credited with designing the first mass spectrometers in the early twentieth century. They were both awarded Nobel Prizes for their work, Thomson in 1906 and Aston in 1922. It was Aston's instrument that actually dispersed ions by mass and focused them by velocity. This allowed for the detection of isotopes and was the basis for Aston receiving the Nobel Prize. Mass spectrometers became more popular after World War II, when they were being manufactured by several companies. By the 1940s and 1950s variations of the early magnetic deflection instruments introduced by Thomson and Aston were being used in the petroleum industry for detecting and monitoring hydrocarbon abundancies. The usefulness and applicability of the technique could not be denied and was actively promoted by scientists such as Carl Djerassi and Fred McLafferty, who explored mass spectrometry for gathering structural information of natural product molecules beginning in the 1960s.

Matrix assisted laser desorption ionization (MALDI) is a relatively new development in the field of mass spectrometry, emerging in the late 1980s along with another soft ionization technique, electrospray ionization (ESI). These techniques were remarkable in that they could be applied to large biomolecules and macromolecules that other mass spectrometry approaches struggled to detect. With the electron impact and chemical ionization methods employed by these other approaches[6] larger biomolecules could not be detected intact.

MALDI and ESI were also more budget friendly and accessible to more researchers. Other mass spectrometry instrumentation available at the time were based on the more expensive magnetic sector machines, while ESI and MALDI could be used with the more affordable quadrupole, ion trap, and TOF mass analyzers.[7] MALDI's advantage over ESI has mainly been due to its higher tolerance to contaminants, its simpler mass spectra, with mostly singly charged peaks versus multiply charged peaks in ESI, and its ability to detect non-volatile compounds.[6]

Franz Hillenkamp and Michael Karas, then of the University of Fankfurt and Koichi Tanaka of Shimadzu Corp., Japan are independently credited with pioneering MALDI. However, in the strictest sense, while both groups developed techniques that were laser desorption/ionization-based, Tanaka's work is the first matrix-free laser desorption/ionization mass spectrometry (LDI-MS), using a suspension of cobalt nanoparticles. Hillenkamp and Karas on the other hand, were the first to identify and explore the applicability of using an organic matrices for ionization and desorption of biomolecules.

Today, MALDI-MS is an established technique for biomolecular studies and Tanaka's initial matrix-free approach has inspired a generation of researchers to explore the field. It particular, his work has served as the foundation of some of the work in this thesis. As mentioned before, the most common form of LDI-MS is MALDI, first developed by Karas and Hillenkamp in 1988.[8] Their early work concentrated on the analysis of large molecular weight proteins and for the most part, high mass compounds have remained the domain of MALDI in the years since.

In MALDI, the analyte is dissolved with organic matrix molecules in solution. Co-crystallization with the analyte and matrix molecules occurs when a small droplet of the solution is deposited onto a metal plate and allowed to dry. The ratio of matrix molecules to analyte molecules is very high, usually greater than 1000. Matrices are small, low molecular weight compounds that absorb light in the range of the laser used for desorption, typically a nitrogen laser with $\lambda = 337$ nm. Irradiation by the laser causes the matrix molecules to absorb photons or energy, they undergo a phase transition, desorb and move into the gas phase, taking the analyte molecules with them. In many cases, the matrix is also acidic, servering to protonate/ionize the analyte in the gas plume by intermolecular interactions. Some matrix molecules are ionized during the expansion process and collide with the analyte molecules in the gas phase to convert the neutral analyte molecules into ions. The charged ions are now detected by the mass spectrometer.[9]

There are three types of mass analyzers currently being used for MALDI MS, linear time-of-flight (TOF), a TOF reflectron, and a Fourier transform mass analyzer.[10]

With the linear TOF mass analyzer, the ions generated from the sample plate are accelerated in a flight tube towards the detector with the same amount of energy. But because the ions have different masses, they arrive at the detector at correspondingly different times. The lighter, smaller molecules arrive first because of their greater velocity and the heavier, larger molecules arrive later. The arrival time at the detector is dependent upon the mass, charge, and kinetic energy of the ion. Because the length of the flight tube is fixed, the time of arrival can be used to calculate the mass to charge ratio.

Linear TOF is limited in terms of resolution and mass accuracy because an initial kinetic energy distribution exits even for ions of the same mass and this creates different flight times for the same mass to charge ratios. Reflectron TOF mass analyzers are used to compensate for the energy distribution. The reflectron consists of an ion mirror or ion reflector which is located at the end of the flight tube, Figure 1.1. The ion mirror is a series of evenly spaced electrodes onto which an electric field is applied. Ions of higher energy penetrate deeper into the mirror than those of lower energy, resulting in a longer flight time in the reflector than for the slower, less energetic ions.[11] The reflectron increases the amount of time higher energy ions need to reach the detector, thereby reducing their temporal distribution. This results in an overall increase in resolution. Linear mass analyzers can achieve a resolution of about 300, while with a reflectron TOF, this can increase to 5000. MALDI combined with a Fourier transform ion cyclotron resonance (FTICR) mass analyzer can achieve a resolution of up to $>10^5$.[10] In FTICR the charged ion orbits in the presence of a magnetic field. A radio frequency (RF) signal is used to excite the ions producing a current. The current is then Fourier transformed to frequencies corresponding to mass to charge ratios.[10,12]

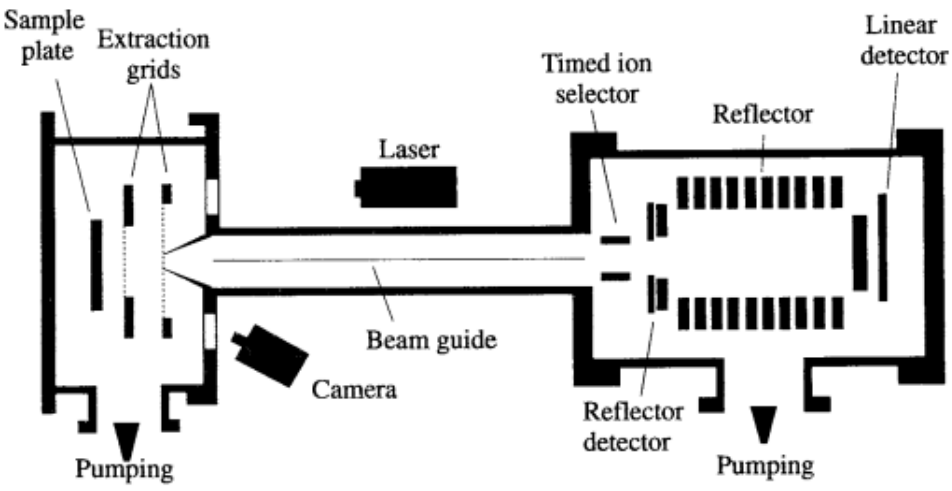

Figure 1.1. Schematic diagram of time-of-flight mass analyzer with linear and reflectron detection. (Reprinted with permission from M.L. Vestal et al.[13] © 1995, John Wiley & Sons, Ltd.)

The MALDI technique has proven very successful with high ionization and desorption efficiencies for the detection of a wide range of compounds including proteins,[14,15] nucleic acids,[16,17] biomolecules[18,19] and polymers.[20] However, choosing the correct matrix for more unusual or less common analytes can be difficult and has a direct effect on the quality of the spectra. For example, mass resolution and sensitivity for certain nucleotide compounds can be difficult and a series of investigations, spanning several years, on a range of potential matrices including 3-hydroxypicolinic acid,[21] picolinic acid,[22] 2-hydroxybenzophenones[23] and 4-nitrophenol[24] had to be performed by different research groups in order to identify the best possible matrix and conditions for detection.[25] The MALDI analysis of glycosaminoglycan-derived oligosaccharides, octasulfated disaccharides and octasulfated pentasaccharides also proved a challenge in recent times. A series of publications dedicated to these compounds by Linhardt and coworkers[18,26,27] suggested that ionic liquid matrices were the best.

Figure 1.2. Picture of MALDI TOF AB Sciex 4800 by Applied Biosystems.

Figure 1.3. Picture of AB Sciex Voyager Elite MALDI by Applied Biosystems.

Even with the correct matrix, uniform co-crystallization in the sample spot is critical. Heterogeneity within the spot can lead to what is known as “hot” and “mute” spots, the former corresponds to regions within the spot where analyte signals are obtained and the latter, to regions where no signal is generated.[28] Because of this non-reproducibility in spot development, it is often necessary to test several sample spots in any given analysis, consuming time and resources. There has been some success with improving sample spots by using a two-layer sample preparation method, [29] a thick-layer method and a sandwich method,[30] among others.

One of the most notable short comings of MADLI has been the difficulty in applying the technique to low mass range analytes, below approximately 1000 Da. Matrix molecules pose a problem in this range, since they are themselves of low molecular weight and dominate the spectra, often masking the actual analyte molecular ions. It is mainly for this reason that much research has been invested in alternative matrix-free methods for LDI-MS. One of the earliest organic matrix-free studies was by Tanaka et al. with 300 Å cobalt powder in glycerol used to detect proteins and polymers of m/z up to 100 000.[31] The high photoabsorption of cobalt, low heat capacity and large surface area were thought to promote the LDI function. Since then, several other studies have tried similar matrix-free approaches with a variety of substrates. Sunner and Chen first coined the term surface-assisted laser desorption ionization (SALDI) in their work with micrometer scale graphite particles for the detection of peptides and proteins.[32] SALDI now generally refers to any LDI technique where the organic matrix is replaced with an active surface. In a 2011 review of these SALDI techniques by Law and Larkin, they classified SALDI surfaces into three categories: carbon, semiconductor and metal-based[33]. However, within these categories, the actual morphology of the surfaces varies widely and can include, nanoparticles[34-37], sol gel[38], nanotubes[39], nanowires (also called NALDI, nanowire assisted laser desorption ionization, trademarked by Burker Daltonics) and porous surfaces.[40] What they all have in common is the background from matrix peaks is eliminated in the low mass range.

Arguably, the most successful of these methods has been desorption/ionization mass spectrometry on porous silicon (DIOS). DIOS was first introduced by Siuzdak et al.

in 1999,[40] and has been applied for the analysis of a wide range of compounds including, metabolites, drugs and peptides with attomole detection limits.[40-43]

The success of DIOS as a matrix free method has mainly been credited to its porous surface, along with the semiconductor properties of silicon itself. Several studies have attested to the necessity of roughness on matrix-free surfaces for LDI-MS,[44-47] regardless of the type of material.[46] However, the efficiency of LDI is much improved if the surface is porous, with significantly higher ion intensities.[48] Specifically, the pore size should be macro porous for reproducible signals.[46] There is strong evidence to suggest the porosity serves several purposes in the desorption/ionization process. First, the pores promote signal reproducibility by acting as reservoirs for analyte and solvent molecules by re-supplying the surface after laser irradiation.[45,48] Second, the porous surface with its increased surface area, provides a large absorption cross section. This, in combination with the high optical absorptivity and high thermal conductivity of silicon ensures efficient energy transfer to analytes and solvent for desorption.[44] In addition, while the pores increase the overall surface area, they also increase the amount of surface defects, thereby increasing the population of surface silanol groups which act as a proton source during ionization.[48]

Further, Xiao et al. suggest in their work that the degree of porosity, i.e., high versus low, and the size and depth of the pores, play a critical role in the desorption mechanism[47]. For low porosity, shallow pores, very little solvent coadsorbs with the analyte, and desorption of the analyte molecules is primarily by heat transfer from the laser irradiated surface. For the high porosity substrates, there is sufficient solvent coadsorbed with the analyte, so that the explosive evaporation of the solvent lifts both solvent and analyte molecules off the surface. Consequently, the energy for desorption, and hence the laser fluence, is less than that for the low porosity surface and this can have an impact on the degree of fragmentation observed.

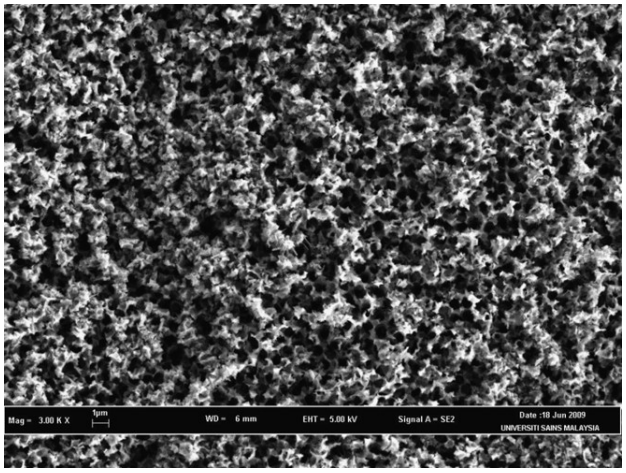

Figure 1.4. SEM of porous silicon prepared by electrochemical etching (Reprinted with permission from A. Ramizy et al.[1] © 2010, Emerald Group Publishing Limited).

The chemical wet-etching fabrication of DIOS can result in irreproducible pore morphologies, Figure 1.4. The most common method of DIOS fabrication involves galvanostatic etching with hydrofluoric acid and ethanol as the electrolyte, to create a micrometers-thick porous layer on piranha cleaned silicon wafers.[40,42,49,50] Wet chemical fabrication suffers in terms of reproducibility, since changes in the fabrication conditions such as etching solution, etching time, etching current, light intensity, exposure, type of bulk silicon, etc., can alter the morphology and more specifically, the nature of the porosity of the film.[9,33,51,52] This is problematic for a technique in which porosity is critical to its efficacy.

Another limitation of DIOS has been the high reactivity of the freshly-made porous surface. This leads to the adsorption of hydrocarbons from the atmosphere and of contaminants within the chamber of the mass spectrometer.[33] As a result, the spectra suffer from high background peaks, especially in the low mass region, and the films suffer from a limited shelf life. One way of countering this has been to store DIOS films in ethanol directly after production.[9] But this solution was somewhat impractical in terms of commercialization.

Some researchers have attempted to address these issues by exploring alternative steps after the initial electrochemical etching. In one study, further etching the porous surface with laser pulses after wet etching produced better results than electrochemical etching alone.[42] Many of the other processes have been fairly complicated, with nanoparticle surface derivatization steps,[53,54] combined electrochemical etching, derivatization and chemical washing,[55] polymer spin coating, lithography, reactive ion etching, and solvent washing[47] and photolithography, reactive ion etching, acid washing and drying.[46] Aside from being lengthy and complicated,[42,46,55] these alternative fabrication techniques are usually only achieved under specific laboratory conditions and are not simple and straight forward enough to be widely applicable and user friendly. Several of these methods also failed to come up with a simple way of addressing the highly reactive porous silicon surface without washing with highly corrosive chemicals.

Despite the complexity of these previous investigations, what is clear is that the most successful fabrications for porous materials involved physical methods, since they are mostly computer controlled, and are better at maintaining the fabrication parameters for a reproducible porous surface with every batch of substrate.[33]

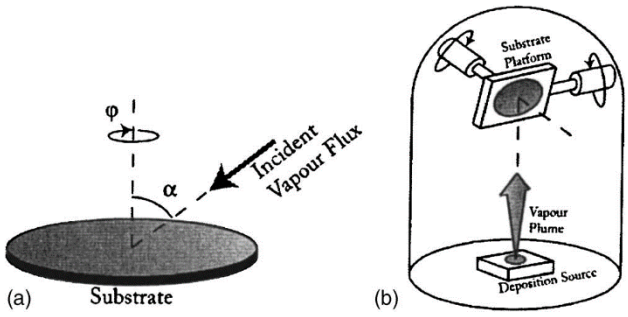

Figure 1.5. (a) Definition of the deposition angle α and the substrate rotation angle φ. The deposition plane is defined by plane containing the incident flux direction and the substrate normal, (b) The GLAD apparatus as it is typically implemented in a standard physical vapour deposition system. Substrate movement is accomplished by two independent motors. The motors are computer controlled, receiving feedback from thickness monitors. (Reprinted with permission from M. Hawkeye et al.[5] © 2007, American Vacuum Society).

A fabrication technique that addresses these issues, by being physical in nature, computer-controlled and relatively straightforward is Glancing Angle Deposition (GLAD). GLAD was pioneered by Dr. Michael Brett's research group of the Department of Electrical and Computer Engineering at the University of Alberta.[2,56-61] It is a physical vapor deposition technique used to fabricate nano-scaled columnar thin films with controlled morphologies, porosities and thicknesses. The computer-controlled GLAD fabrication apparatus regulates the oblique angle at which the vapor flux hits the substrate surface and also determines the rate at which the substrate platform itself rotates, Figure 1.5. The deposition is performed in a custom made high vacuum system from Kurt J. Lesker Co., Clairton, PA, USA (Figure 1.6), with computer-controlled stepper motors for rotating and tilting the substrate holder.

(a)

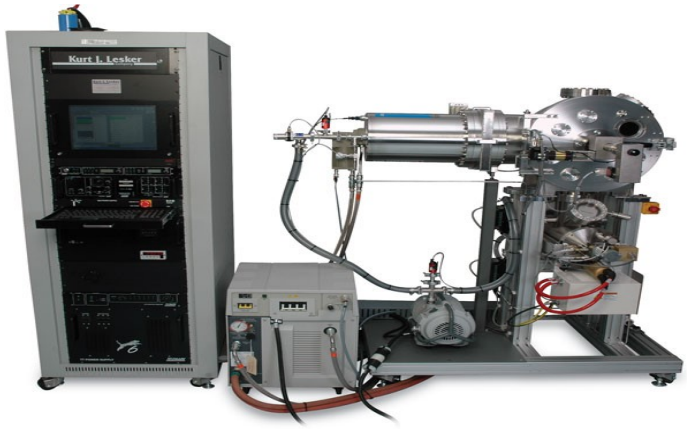

(b)

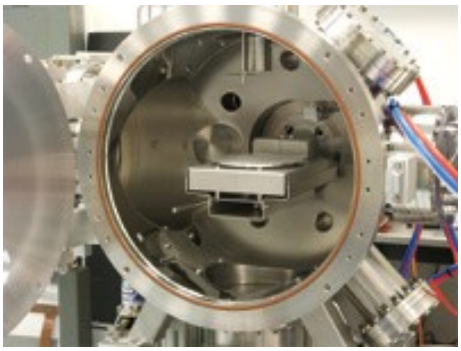

Figure 1.6. (a) The AXXIS-Co-Sputtering, Thermal Evaporation, and Electron Beam Physical Vapour Deposition System from Kurt J. Lesker Co., (b) a closer view of the vacuum deposition chamber of (a).

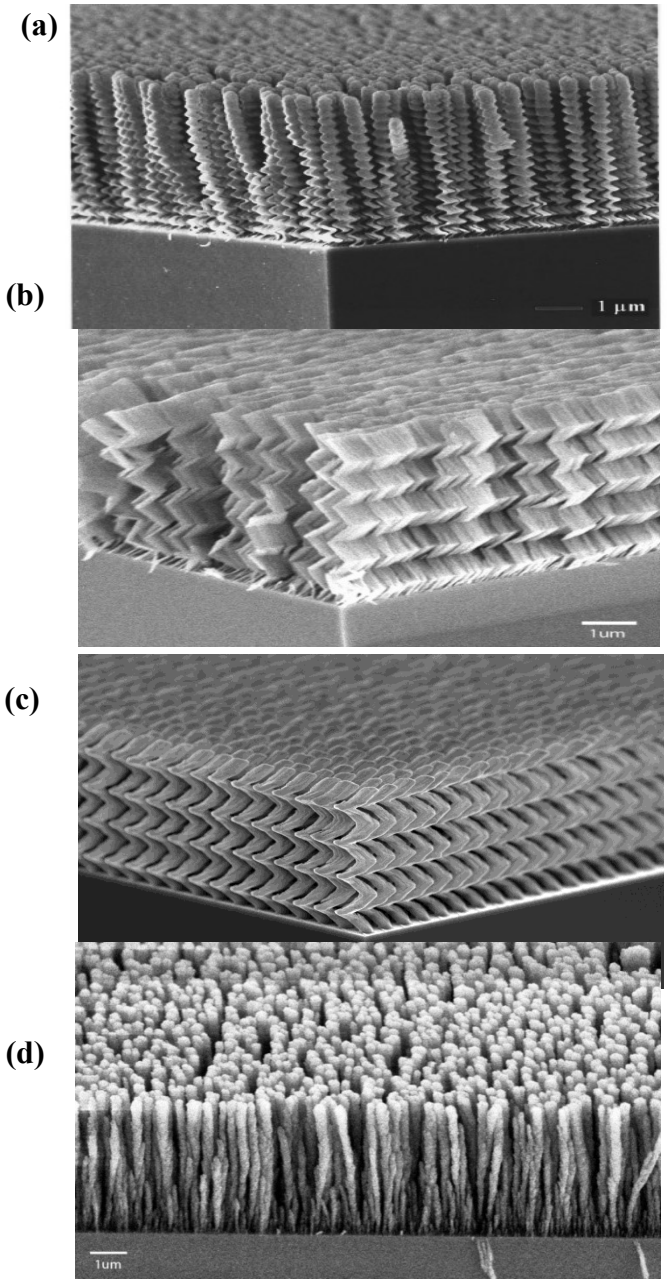

Figure 1.7. Types of SiO_2 GLAD film structures, (a) helix, (b) chevron, (c) square spiral and (d) vertical posts. (Reprinted with permission from K. Robbie et al.[2] Copyright 1997, ©American Vacuum Society).

With GLAD, films of finely tuned morphologies can be fabricated, Figure 1.7, by simply changing the deposition angle of the incident vapor and the speed, direction and angle of the substrate rotation. What is also exciting about GLAD is that it can be used with different types of materials, for example, metals (cobalt, copper, manganese, titanium), semiconductors (silicon), oxides (silicon dioxide, titanium dioxide), etc. Some of the successful applications of the GLAD technique include adsorbate-induced electrochromic phenomenon of indium–tin oxide[62], humidity sensors[60,63], photonic crystal switching,[58] solar cells,[64] microchannel fabrication in microfluidics for DNA separation[65] and ultra-thin layer chromatography (ultra-thin layer chromatography).[66-71]

In a 2010 collaboration between the Harrison and Brett research groups,[72] 500 nm silicon GLAD films were successfully used as a substrate for matrix-free laser desorption/ionization mass spectrometry. The films were shown to be highly reproducible in terms of morphology and signal generation, with detection limits in the attomole and femtomole ranges. Several of the issues with MALDI and DIOS were also addressed. Sample spots were found to be free of "mute" and "hot" spots and background in the low mass range was eliminated. The fabrication and morphology of the GLAD films themselves was also highly reproducible from batch to batch. This study also addressed the limited shelf life of porous silicon surfaces without the need for chemical washing. The films were exposed to UV light and oxygen for 15 minutes in a standard ozone cleaner; contaminants from the surface were removed and did not show up in the mass spectra.

We have since coined the term SMALDI, solid matrix-assisted laser desorption/ionization, in reference to the organic matrix-free use of GLAD films for LDI-MS. This thesis further explores the potential of cobalt, silicon and silica GLAD films for SMALDI-MS and UTLC applications with small molecules, metabolites and biomarkers.

Chapter 2 examines the application of cobalt as a SMALDI-MS material. Specifically, the effects of physical parameters, such as deposition angle, the post orientation and film thickness on the LDI-MS performance is examined. The feasibility of generating mass spectra for carbohydrate compounds by a matrix-free method is also explored in detail.

In Chapter 3, the use of silicon GLAD films for the SMALDI-MS detection of several classes of glycolipid biomarkers is discussed. The limits of detection of these compounds in both standard solution, and in a spiked biofluid sample is also addressed. Additionally, the use of GLAD films for sample preparation on the same film used for SMALDI-MS is explored.

The proven UTLC ability of GLAD films is further discussed in Chapter 4 for a hyphenated UTLC-SMALDI-MS device and finally, the application of silicon GLAD films for tissue imaging is briefly described in Chapter 5.

Chapter 2

Cobalt SMALDI-MS for Carbohydrates, Peptides and Metabolites

2.1 Introduction

Laser desorption/ionisation (LDI) based on nanoporous surfaces has in recent years proven to be a successful matrix-free mass spectrometry approach for small molecule detection. The active surface of the target material along with the solvent molecules of the analyte solution are thought to replace the function of organic matrices in traditional matrix assisted laser desorption/ionisation (MALDI).[1],[73] Desorption/ionisation on porous silicon mass spectrometry (DIOS-MS) has been one of the most successful of these techniques with results matching and in some cases surpassing MALDI.[40] However, it soon became apparent that the early wet chemical etching fabrication techniques for DIOS suffered from irreproducibility. Computer-controlled fabrication techniques such as plasma-enhanced chemical vapour deposition (PECVD), reactive ion etching (RIE) and chemical vapour deposition (CVD) eliminated the problem of poor reproducibility. However, these procedures tend to be complicated and in many cases pre- and post- fabrication chemical treatments were still required to deal with oxidation and hydrocarbon adsorption onto the silicon surface.[33]

Previously our group reported the successful use of Glancing Angle Deposition (GLAD) technique to fabricate porous, vertical post silicon thin films for LDI-MS.[74] GLAD is a computer-controlled physical vapour deposition used to fabricate nano-scaled columnar films with controlled morphologies, porosities and thicknesses on a 10 nm scale. GLAD combines oblique angle deposition with controlled substrate motion to produce reproducible porous targets from materials

[1] A version of this chapter will be submitted for publication. The work was done in collaboration with co-authors, Zhen Wang, L. W. Bezuidenhout and Abebaw B. Jemere. My role includes evaluation of Co GLAD films for LDI-MS, contact angle determinations and some LDI-MS performance comparisons for slanted and vertical post silicon GLAD films.

ranging from metals, semiconductors and oxides to organics.[5,75-77] Based on the success of the Si GLAD films and exploiting the broad application of the GLAD technique led to the current reported work on the performance of cobalt GLAD films for LDI-MS.

Tanaka et al. in 1988 used cobalt powder in glycerol and proved that cobalt can function as an LDI material.[78] The high photoabsorption due to light scattering between the nanoparticles, low heat capacity and large surface area were thought to promote the LDI. In 2002, Yalcin and Li studied a range of metal particle powders as substrates for LDI.[79] Cobalt powder was superior; however, the MS performance was impacted by the size of the particles used. This was thought to be as a result of the effect the different particle sizes had on the packing on the target surface, and in turn the effect this had on heat absorption and dissipation. This approach also suffered from instrumental limitation, where loose fine cobalt particles could possibly damage the mass spectrometer.

The researchers followed this work with experiments using vapour deposited cobalt coated silicon substrates.[80] The mass spectra in this study suffered from alkali metal adducts with relative intensities higher than the protonated molecular ion. Ultrasonically cleaning the substrate with water prior to spotting removed these peaks; however, overall, the intensity of the molecular ion peaks were not much improved given the micromolar analyte concentrations used.

These previous works all emphasize the potential of cobalt as an LDI material. However, both particle and vapour deposited coated surfaces offer poor control over uniformity and porosity. These studies also highlight the fact that a somewhat solid substrate with a uniform surface, controlled thickness and morphology is required to fully explore cobalt's LDI capability. In this chapter, the highly controlled GLAD technique is used to fabricate uniform and reproducible cobalt films for matrix-free LDI-MS.

2.2 Experimental

2.2.1 Materials and Reagents

Verapamil, bradykinin fragment 1-5, ribose, beta-cyclodextrin, triacetyl beta cyclodextrin, 2,5-dihydroxybenzoic acid (DHB) matrix, NaCl, trifluoroacetic acid (TFA) and methanol were from Sigma-Aldrich Chemical Co. (Milwaukee, WI, USA). Carbohydrates 440MW, 498MW and 832MW were obtained from the Lowry research group, Department of Chemistry, University of Alberta (Edmonton, AB, Canada); gangliosides GM1 and MJ7 from the Cairo research group, also of the Department of Chemistry, University of Alberta. Verapamil stock solution was prepared by reconstituting the lyophilized powder in water and was diluted in methanol or methanol/0.1% trifluoroacetic acid (TFA) ($30/70^{V/}_{V}$) as required. Carbohydrate and ganglioside stock solutions were prepared by dissolving in methanol at 1 $mgml^{-1}$. Dilutions were prepared by mixing stock solution/1 mg ml^{-1} sodium chloride (NaCl) ($50/50\ ^{V/}_{V}$) or with methanol. Ultrapure water used for sample preparation was from a deionizing system (Millipore Canada, Mississauga, ON, Canada).

2.2.2 GLAD Film Fabrication

Porous thin film deposition was performed in a high vacuum system (Kurt J. Lesker Co., Clairton, PA, USA).[5] Silicon wafer substrates were cleaned prior to deposition by submersion in piranha (3:1 sulfuric acid: hydrogen peroxide) for 20 minutes followed by a deionized water rinse and drying with nitrogen gas. For vertical post films, silicon (99.9% pure, Cerac Inc., Milwaukee, WI, USA) and cobalt (99.9% pure, Kurt J. Lesker Co. Toronto, ON, Canada) were deposited onto the silicon substrate at the specified deposition angles relative to the substrate normal. Substrate rotation rate was 1.2 rpm and deposition rate was 0.6 nm/s.[74] Slanted posts were deposited at the specified angles, with no substrate rotation at a deposition rate of 0.3-0.7 nm/s. The films were deposited by electron beam evaporation under vacuum (base pressure $<10^{-6}$ Torr) onto three inch diameter single crystal silicon wafer substrates (University Wafer, Boston, MA, USA).

2.2.3 Mass Spectrometry

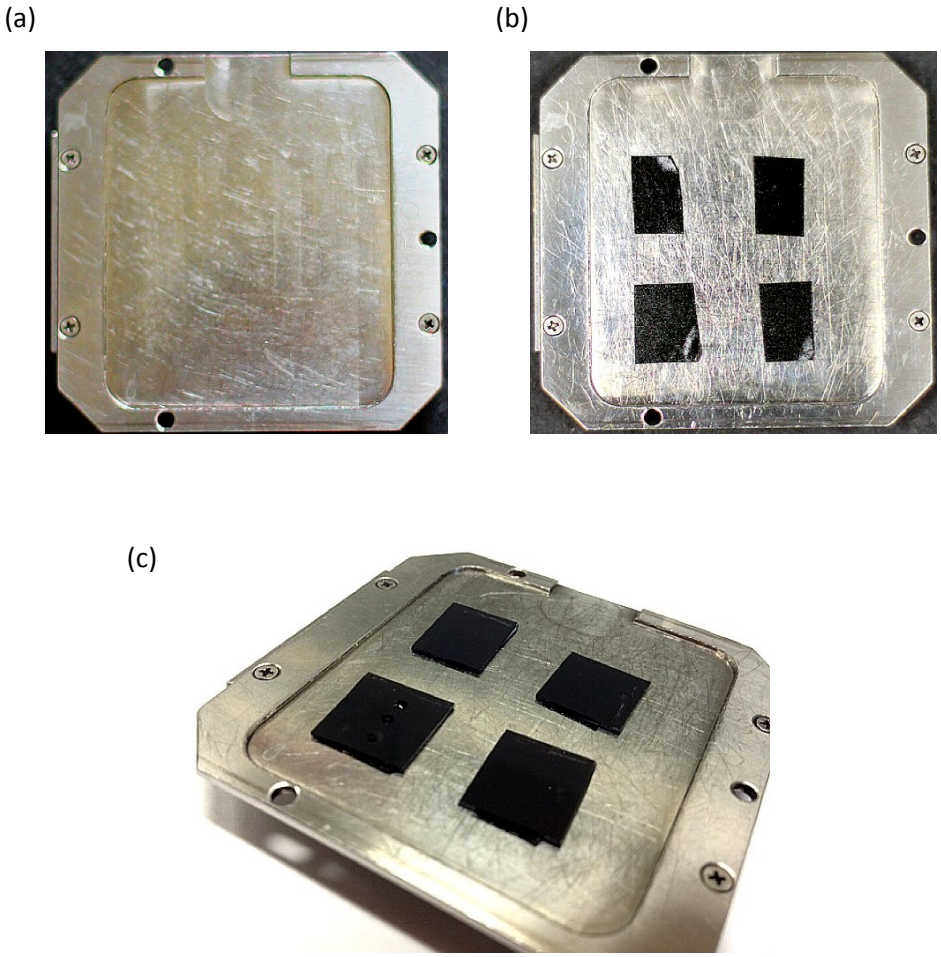

Figure 2.1. Picture of a) adapted MALDI plate, b) attached double ended sticky tape and c) Co film attached to film with deposited analyte spots. Plate dimensions are the same as the standard plate for the AB Sciex Voyager Elite MALDI TOF mass spectrometer.

Mass spectra were obtained using an AB Sciex Voyager Elite MALDI TOF instrument with a pulsed N_2 laser (332 nm) at a repetition rate of 3.0 Hz. Spectra were acquired in positive ion mode using delayed ion extraction. Grid voltage was set at 74% and extraction delay time was 250 ns. Each spectrum consists of 100 shots. GLAD films were secured to a modified MALDI plate using double sided adhesive tape. Figure 2.1 shows cobalt films after they have been attached to the MALDI target plate. Aliquots of 0.5µL of samples were

spotted onto films and allowed to air dry prior to mass spectrometry analysis. MALDI samples were prepared using the dried droplet method,[81] deposited onto a MALDI steel plate and allowed to air dry prior to mass spectrometry analysis as described above for GLAD films. Signal-to-noise ratios were calculated using Voyager Data Explorer version 4.0 software (Applied Biosystems, Framingham, MA, USA).

2.2.4 Film Characterisation

Optical absorption of cobalt films was measured using a Variable Angle Spectroscopic Ellipsometer (J.A. Woollam Co., Lincoln, NE, USA) in the reflectance mode. Scanning Electron Micrographs (SEMs) were obtained with a JEOL 6301F Scanning Electron Microscope (JEOL Canada, Inc., QC, Canada), following carbon coating with a Leica EM SCD005 evaporative carbon coater (Leica Microsystems Inc., Concord, Ontario, Canada). Contact angles were measured with the FTA200 Contact Angle Measurement system, First 10 Angtroms (Portsmouth, VA, USA).

2.3 Results and Discussion

2.3.1 Deposition Angle

Four deposition angles, 1°, 70°, 85° and 88º were studied with verapamil for the optimal LDI-MS performance of the films. (Verapamil, is a drug used to treat a variety of cardiovascular conditions.[82]) These angles were chosen to provide a range of deposition angles for evaluation. Previous investigations of the LDI-MS performance of silicon films had better performance when the deposition angle increased beyond 80º.[72] The film with a 1° deposition angle appears almost flat, Figure 2.2 (a), with densely packed nucleation sites, but no developed columns.

The columns are tightly packed at 70° creating a very dense film. At 85° and 88º, the films achieve pore sizes exceeding 10 nm.[83] Increasing the deposition angle for GLAD films increases the self-shadowing effect and the porosity.[2,84]

Essentially, as the deposition angle increases, some columns are sacrificed for the growth of others and the overall porosity increases as the film becomes less dense.

Since the column vapor is deposited at an angle, some columns will screen neighboring columns from incoming vapor flux, suppressing their growth. Eventually, smaller columns become completely shadowed and stop growing. This process is referred to as column extinction and results in larger spaces between fully grown columns as the deposition angle increases[85].

Self-shadowing has significant effects on the morphology of GLAD films. In a detailed study of the morphology of GLAD films[86], it was reported that as the deposition angle increased from 75° to 87°, the dominant column spacing increased from 37 nm to 85 nm. Porosity is linked to the column packing density with GLAD films; a high packing density results in low porosity and vice versa. The number of fully formed columns was observed to drop from 4300 to 175 μm^{-2} from 75° to 87° deposition angles. So increasing the deposition angle results in both an increase in the size of the pores between columns and an increase in the porosity, by reducing the packing density.

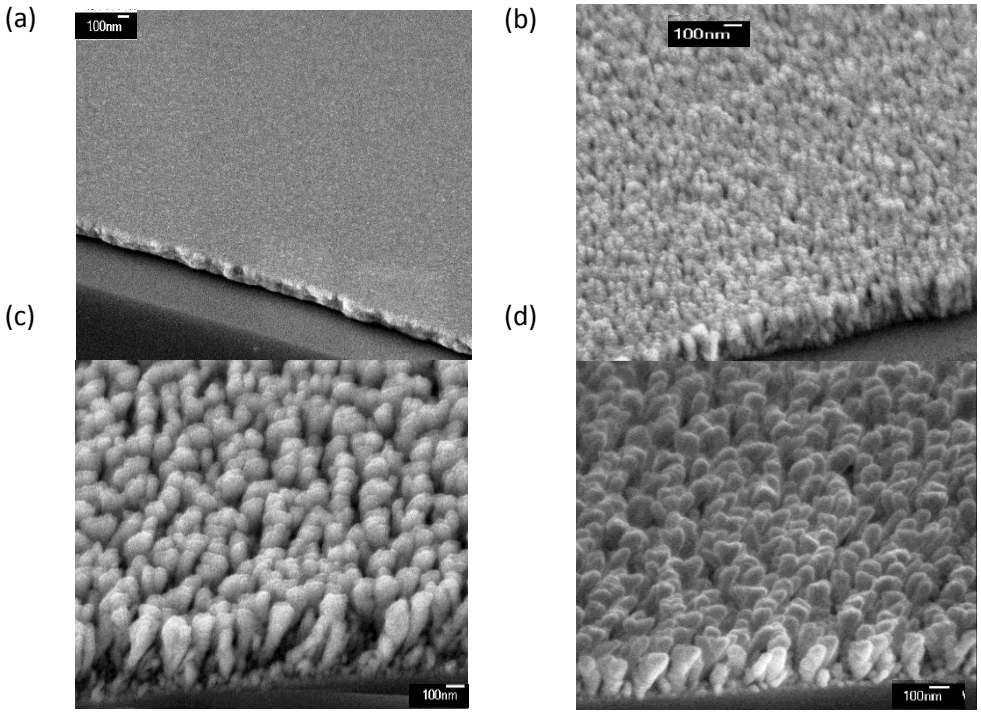

Figure 2.2. Scanning Electron Micrographs of cobalt films deposited at (a) 1°, (b) 70°, (c) 85° and (d) 88°.

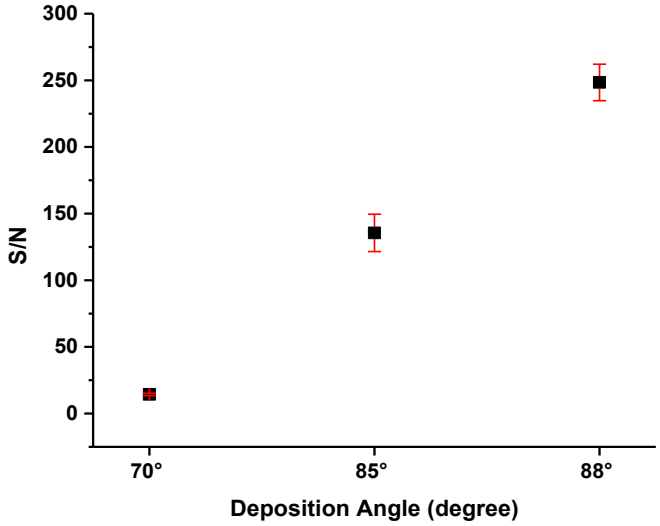

Figure 2.3. Effect of deposition angle on SMALDI-MS performance. S/N was measured for 1 pmol verapamil on Co GLAD films deposited at 70, 85 and 88°.

The signal to noise ratios calculated for 1 pmol verapamil, were 14, 136 and 248 for 70°, 85° and 88º, respectively, Figure 2.3. Signal-to-noise ratios were calculated using Voyager Data Explorer, Version 4.0, (Applied Biosystems, Framingham, MA, USA). No signal was observed from films deposited at 1°. Previous studies with silicon GLAD films showed a similar trend of improved LDI performance as the porosity increased.[72] From these observations we conclude that a sufficiently porous GLAD film is essential for LDI-MS. This is comparable to the findings of other surface-based LDI studies. Alimpiev et al. reported that as the porosity increases, higher LDI yields are achieved and more specifically, that nanoscale roughness was most efficient.[48] They surmised that this improvement arises because pores are more able to effectively contain and resupply analyte and solution during LDI.[45]

2.3.2 Post Orientation

Our collaborators previously demonstrated that slanted Si GLAD posts require a lower arbitrary laser fluence than vertical posts for the generation of LDI-MS peaks and this has been reported as its advantage over vertical posts.[87] It was concluded that this better performance was due to the coupling of the laser light with the slanted posts, and the resulting alignment of the posts with the electric field of the laser.

In a study with posts with diameters ranging from 50-600 nm it was found that polarized light couples into the posts[88]. The coupling is promoted when the electric field of the incoming light is parallel or in-line with the posts.

This observation was tested by our collaborators in their slanted post study.[89] The laser beam of the mass spectrometer incidents on the MALDI target at 45^{o}. When the slanted posts were aligned with the laser so that the incoming beam was perpendicular to the posts, as suggested on Figure 2.4, the SMALDI-MS results were superior to other alignments and to vertical posts with similar parameters (thickness and deposition angle). The alignment was achieved by marking the direction of the slanted posts on the wafer during fabrication, then attaching the film to the MALDI target so that the desired alignment is obtained with the laser. The electric field of the laser is perpendicular to the direction of the beam itself, and therefore the slanted posts as shown in Figure 2.4, provides the largest cross section for coupling with the incoming electric field. According to Walker et al.[88], this coupling causes the near-field enhancement of the laser near the surface of the posts and can be up to 200 times greater than the incident laser intensity. This increased intensity promotes more desorption/ionization of the molecules on the surface.

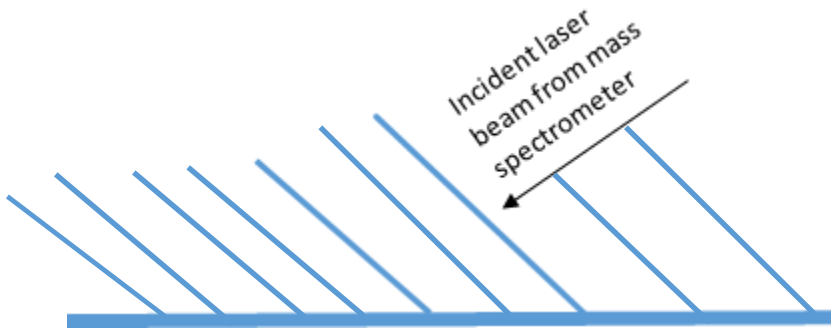

Figure 2.4. Side view of the orientation of slanted post GLAD films in the mass spectrometer that produced the best SMALDI-MS results. Mass spectrometer laser beam is incident on posts perpendicularly.

It was this improvement of the SMALDI-MS performance with slanted post over vertical posts that prompted us to further investigate using them for our studies. We further examined three different, visually identifiable regions of Si slanted post films on the substrate wafer (after column deposition, but prior to dicing into 2 cm by 2 cm portions for LDI-MS), and compared the results to Si vertical post films. We categorized the slanted post regions as "light", "intermediate" and "dark" based on the distinct regions observed by a top-view visual inspection of the uncut, circular film wafer, see Figure 2.5 (a). By comparison, vertical post films are uniform in colour and matches the light region of the slanted post film, Figure 2.5 (b).

Ganglioside GM1 was used at three concentrations, 6.6, 1.1 and 0.09 pmol, to determine if the SMALDI-MS performance changes with the different regions of the substrate, see Table 2.1. There is a significant drop in S/N of the SMALDI-MS spectra in moving from the light region, through the intermediate region to the dark region. For the dark region, a peak was only observed for the highest concentration tested. For the intermediate region, no peak was observed at 0.09 pmol and the variability in S/N was very high at 1.1 pmol.

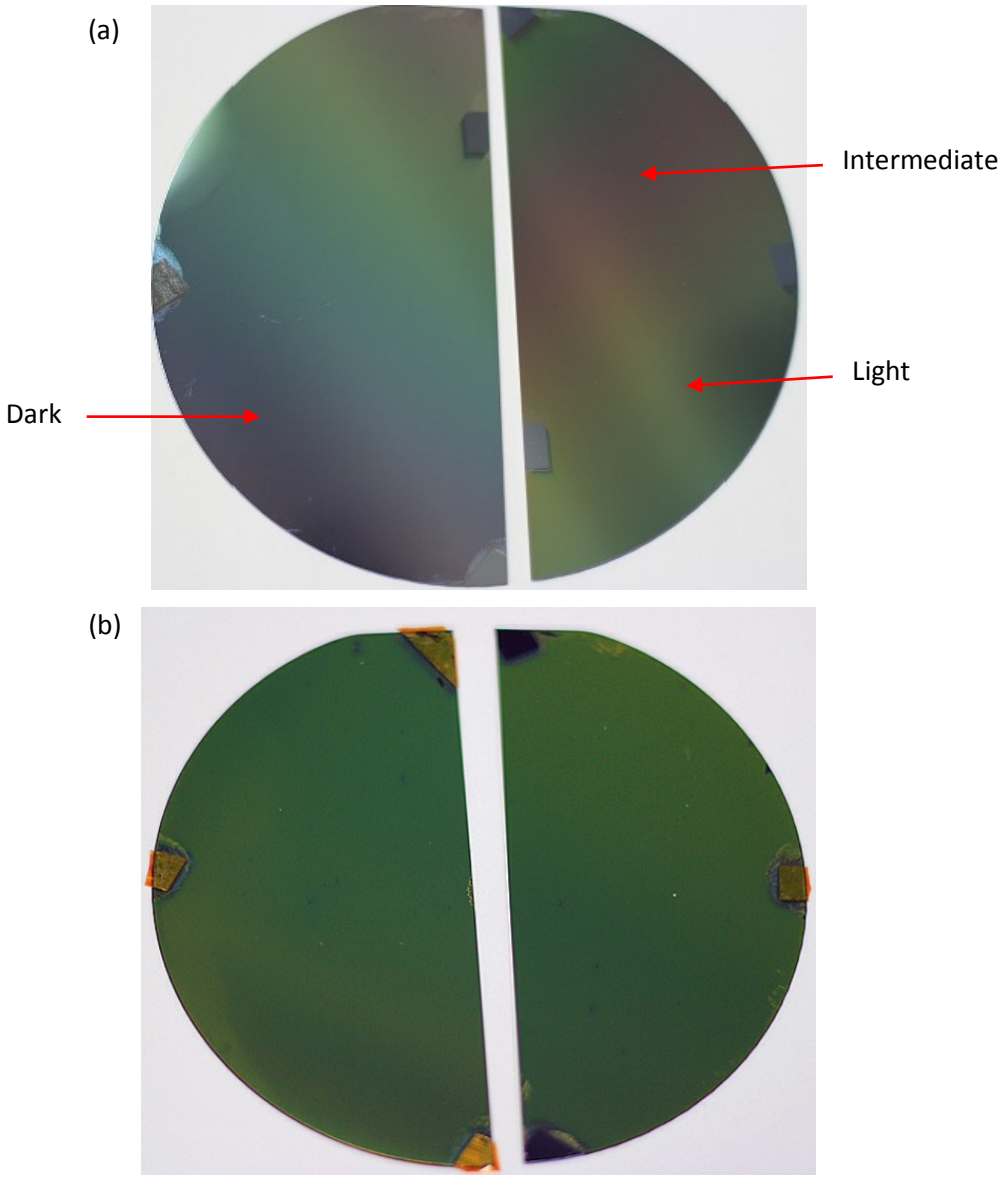

Figure 2.5. Picture of a) slanted angle deposited 500 nm Si film and b) vertical posts 500 nm Si film. Both sets of film deposited at a deposition angle of 88°.

Table 2. 1. Comparison of S/N obtained at different regions of Si slanted post and on Si vertical post films. All films were deposited at 88° deposition angle.

Concentration (pmol)	6.6	1.1	0.09
Slanted Posts Light	157.34 ±23.59	40.44 ±8.91	15.48 ±0.93
Slanted Post Intermediate	128.78 ±15.98	53.56 ±38.62	No Peak
Slanted Post Dark	98.44 ±13.99	No Peak	No Peak
Vertical Posts	52.24 ±2.68	20.36 ±2.56	14.92 ±2.25
			[2]*27.5 ±2.34

Consequently, for investigations involving concentrations below 1 pmol, at least one third of the wafer would be unusable and potentially, two thirds may be unusable (depending on what is the cut off concentration of detection for the intermediate region).

The performance of the vertical post films lags behind that of the light and intermediate regions of slanted post films. However, it is still possible to obtain signals at low concentrations from any portion of the Si film wafer. Also of note, the S/N of 0.09 pmol of both the light slanted post region and vertical posts are the same statistically. At this concentration, the performance of the light section of slanted post wafer and any section of vertical post wafers, is the same and no benefit comes from using slanted posts. Increasing the laser fluence by 200 a.u. increases the S/N for vertical posts by approximately 45% without inducing analyte fragmentation. This ability of vertical post to match the performance of the best portion of a slanted post wafer at low concentration, combined with the uniformity of the film response across the wafer, means that vertical posts can be used preferentially for low concentration work and to avoid wastage.

Our findings were corroborated by a subsequent study by our collaborators[61] on the non-uniformity of slanted post films. The deposition technique for slanted posts creates specific sections of non-uniformity on the

[2] *S/N obtained at 200 a.u. higher laser fluence.

substrate material. For an eight cm diameter substrate, the non-uniformity in the deposited mass per unit area is greater on the half of the substrate closest to the deposition source, with an overall percent non-uniformity across the wafer of up to fifty four percent measured along the x axis; for vertical post films, the non-uniformity is ±2% for the same region.[61] This non-uniformity in the deposited mass per unit area of slanted posts results in appreciable differences in film thickness and density across the wafer and explains why the LDI performance measured is varied. The light coloured regions correspond to the more uniform areas of the wafer. To maintain reproducible LDI-MS results, certain sections of the deposited film wafer cannot be used for generating mass spectra, leading to wastage. Given that the LDI-MS results can be significantly improved by higher deposition angles for vertical posts, Figure 2.1, we chose to use vertical posts for our characterization of cobalt GLAD films as a LDI-MS material.

2.3.3 Film Thickness

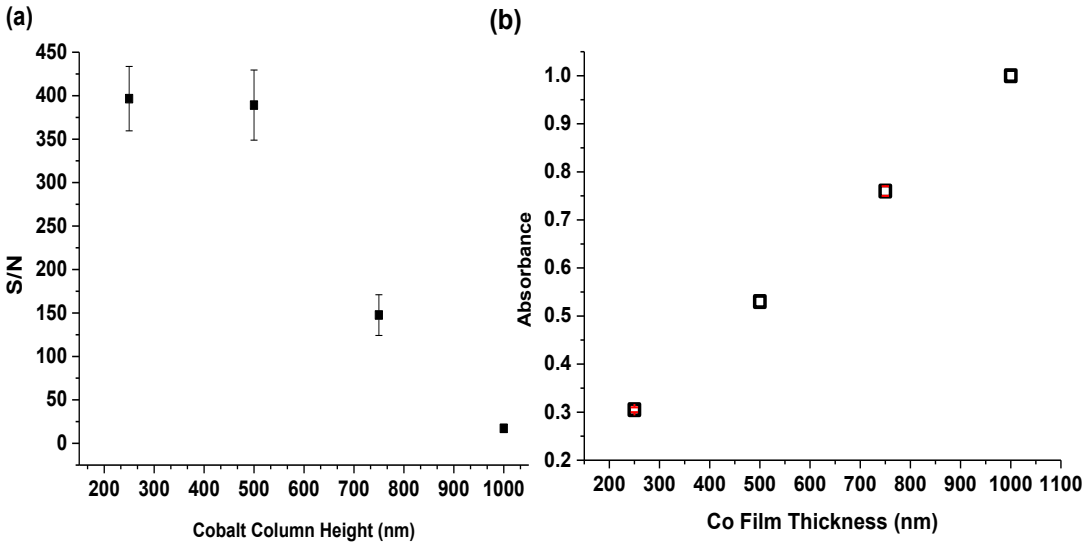

Figure 2.6. Effect of film thickness on SMALDI-MS performance. (a) S/N of 1 pmol verapamil obtained from Co GLAD films of different thicknesses. The same laser intensity was used for each film. (b) The UV absorption at 337 nm wavelength for Co GLAD films at different thicknesses. Optical absorption of cobalt films was measured using a Variable Angle Spectroscopic Ellipsometer in the reflectance mode. Column height is monitored during deposition by measuring the deposition

The optimum thickness of the Co GLAD films was determined based on the S/N of the verapamil peak taken at varying film thicknesses with the same arbitrary laser fluence. S/N was measured for five spectra taken at each film thickness and averaged. There was no significant difference in the SMALDI-MS performance in terms of S/N between the 250 nm and 500 nm films as seen in Figure 2.6 (a). The optimum cobalt film thickness was therefore taken as 250 nm since these films require less material for fabrication than 500 nm. While the performance of the 250 nm and 500 nm films are high (and statistically the same), performance markedly decreases with 750 nm and 1000 nm films. This may be due to the combined effect of the longer longer distance over which heat must now be conducted for the thicker films and the lower conductivity of porous cobalt vs. bulk cobalt. The thermal conductivity of parallel cobalt nanowires 2 μm

long is nearly 30 times less than bulk cobalt.[90] Additionally, as film thickness increases, the average size of the macropores of titanium dioxide and silicon GLAD films also increases,[61,66] and analyte solution can reach the base of the posts more easily. The absorbed heat must now travel a longer distance to reach the analyte and solution molecules in 750 nm and 1000 nm films during the time allotted for desorption. But this heat may possibly remain trapped in the posts. It has been shown for porous silicon that the desorption of the ionized analyte is controlled by surface heating and subsequent thermal activation. A minimum surface heating of about 800 K is required for desorption to occur,[48] which is induced by the laser. If this threshold is not met by the thicker films due to the poorer conductivity, desorption is negatively impacted.

On the other hand, the poor performance of the 170 nm may be due to films of this thickness not having enough material for sufficiently high laser absorption which is necessary for desorption and ionisation of analyte molecules. Alternatively, as columns become longer, the self-shadowing effect becomes more dominant at oblique angle deposition.[91] As previously mentioned, a minimum pore space between columns of tens of nanometers is required for LDI-MS performance. However, our results indicate that for cobalt, performance drops off when porosities become much larger.

2.3.4 Contact Angle

The contact angle is related to the wettability of a film surface. Angles less than 90^{o} indicate that wettability is high.[92] In Figure 2.6, the contact angles for the 168 nm films was the highest, but still slightly below 90^{o}. There was a drastic drop in the contact angle at 250 nm to $32^{o} \pm 3$, from $72^{o} \pm 7$ nm at 168 nm. This is the start of the plateau region of the curve. The overall trend matches that of a similar contact angle study with hydrophilic GLAD films by Fan and coworkers where the increase in column thickness was seen to increase the hydrophilicity until it plateaus after a thickness of 154 ±5 nm.[3] Based on this correlation, we can conclude that our Co GLAD films are also hydrophilic, but with the 168 nm films bordering on hydrophobic.

According to Wenzel's law for hydrophilic films, the 168 nm films, above the plateau region, Figure 2.6 (f), are classified as *rough*.[3] The thicker films in the plateau region can be considered as *porous*. This porous characteristic of the thicker Co GLAD films is responsible for its better LDI-MS performance. In the case of DIOS, surface defects and increased surface area play a significant role in the ionization process by increasing the population of surface silanol groups which act as a proton source during ionization.[45] These contact angle related predictions on the roughness and porosity of our Co films also match our previous discussions on the increasing porosity as film thickness increases (Section 2.3.3).

Wetting for films in the porous region of the graph, Figure 2.6, has been described as "hemi-wicking".[3,93] Hemi-wicking is a combination of spreading and imbibition (absorption of solvent into a solid or colloid). A portion of the deposited drop on the surface of the GLAD posts is sucked (absorbed) into the space between the posts. The drop now sits both as liquid between the posts and as a small remainder on the top of the solid posts, Figure 2.7. It progresses downward, leaving a fraction of the posts dry as the liquid recedes.

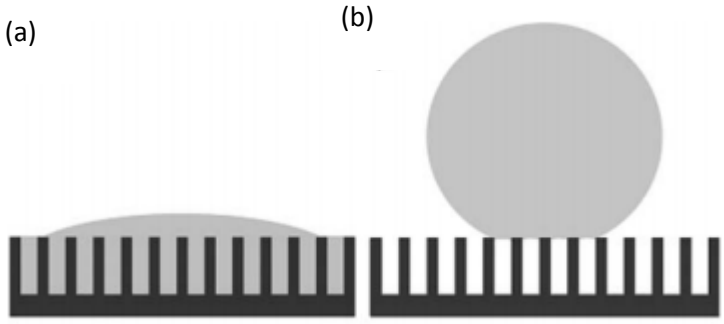

Figure 2.7. A schematic model for the two cases when a water droplet contacts a surface. (a) Hemi-wicking: water first absorbs into the channels, then spreads across, (b) hydrophobic surface: water only wets the surface of the nano columns. (Reproduced from Fan et al.[3] with permission of ©The Royal Society of Chemistry (RSC) on behalf of the Centre National de la Recherche Scientifique (CNRS) and the RSC.)

Hemi-wicking has implications for the LDI-MS function of the Co GLAD films. Other LDI materials such as porous silicon, are known to hold solvents well within their porous structures.[47] This ability is credited for easing the desorption/ionization process. Xiao et al. put forward two models for desorption/ ionization which they believe co-exist[47]. The first model, and the one that applies to our hemi-wicking findings, is termed "pseudo-MALDI". The solvent and analyte molecules are co-adsorbed within the porous structure and the explosive evaporation of the solvent propels both the analyte and solvent molecules off the surface.[47] In the second model, known as the "LDI" or "dry" model, the analyte molecules lift from the surface of the material when the critical energy required for desorption is met by heating. This process is reliant on a sufficiently high laser intensity.[47,94]

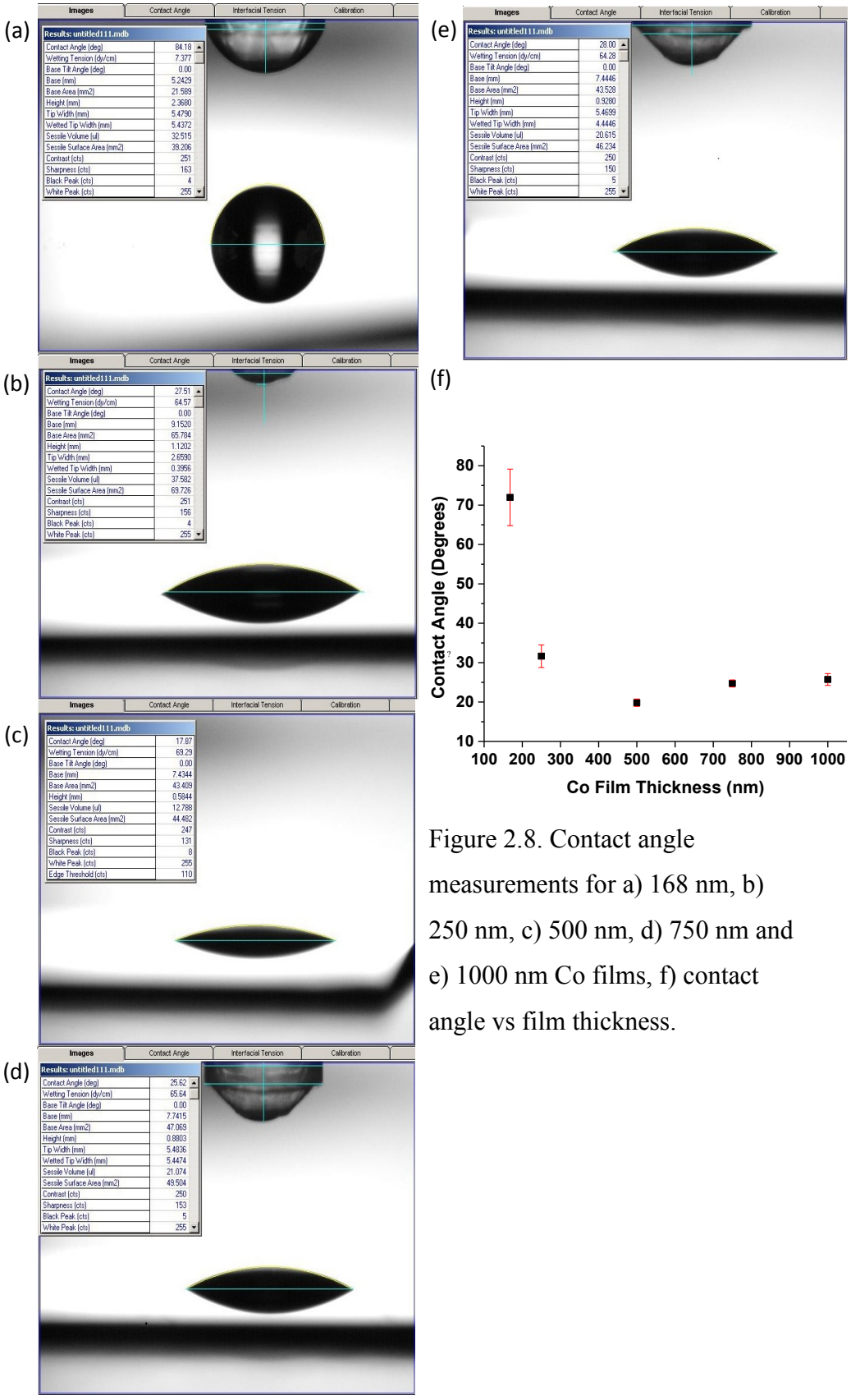

Figure 2.8. Contact angle measurements for a) 168 nm, b) 250 nm, c) 500 nm, d) 750 nm and e) 1000 nm Co films, f) contact angle vs film thickness.

2.3.5 Laser Fluence

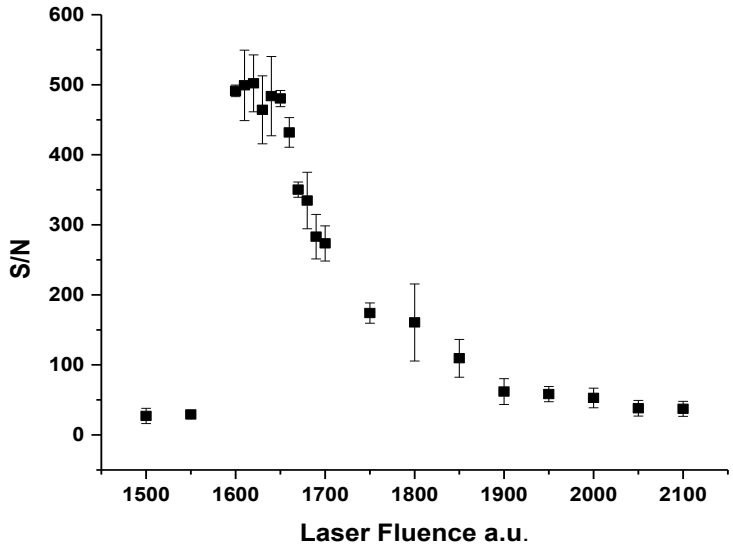

Figure 2.9. Determination of the optimum arbitrary unit (a.u.) laser fluence for SMALDI-MS on 250 nm Co films. S/N for 10 pmol verapamil was measured for five spectra at each a.u. laser fluence.

The optimum arbitrary laser fluence for the 250 nm Co films was taken to be 1650 units, Figure 2.7. There is a minimum temperature threshold that SALDI surface must overcome to provide sufficient heat for desorption of molecules on its surface, this has been estimated to be around 500K (~ 576 ºC).[45,48] We conclude that this threshold was met at 1650 a.u. for our MADLI instrument. This was the fluence corresponding to the highest S/N in an incremental study of 10 pmol verapamil, see Figure 2.9. The S/N steadily declined after this point, due to the rise in the background noise and the fragmentation of the analyte ion.

2.3.6 Film Reproducibility

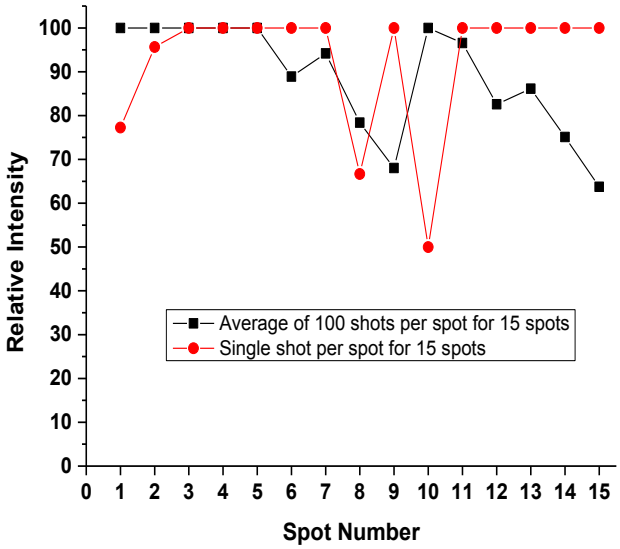

Figure 2.10. Relative peak intensity (maximum intensity = 100%) from 15 different sample spots on 250 nm Co GLAD vertical post films.

The shot-to-shot reproducibility of the GLAD films was examined by measuring the signal intensity (100 shots/spectrum) for verapamil on 15 different cobalt targets fabricated under the same deposition conditions, Figure 2.10. The average signal intensity of 1 pmol verapamil was 90% with a relative standard deviation of ± 14% (100% = maximum signal observed). In contrast, a similar reproducibility study performed with MALDI yielded much poorer results, even when the spectra were collected from sample areas identified as potential sweet spots.[28] A two-layer spot development method has been found to reduce these problems,[29] but this too adds complexity to the preparation. This high degree of reproducibility with GLAD suggests that the films are uniform and that achieving an even sample distribution on the surface does not require much effort, skill or time.

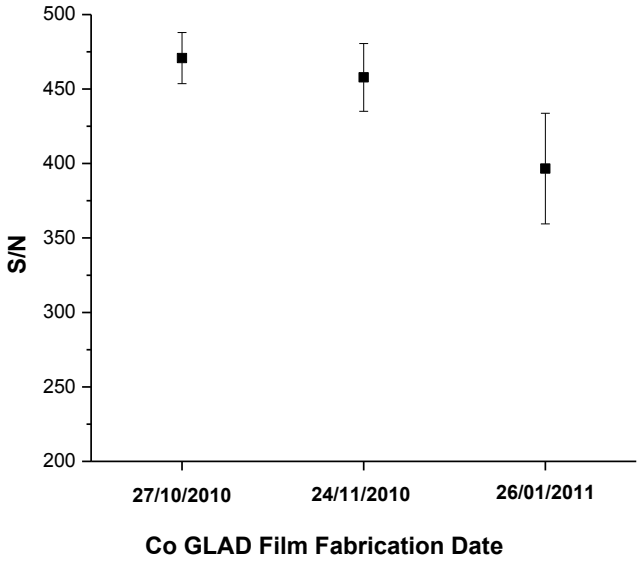

Figure 2.11. Comparison of SMALDI-MS performance of Co films fabricated on different dates. S/N of 50 pmol verapamil was measured for five spectra from films produced on each dated. Spectra collected at 1800 a.u. laser fluence

The reproducibility of the GLAD fabrication technique was also evaluated by testing three separate batches of films deposited on different dates under the same conditions, Figure 2.11. 50 pmol verapamil was used as the model analyte. Overall, the different batches of films did not deviate by more than 100 S/N units in their performance.

2.3.7 Limit of Detection

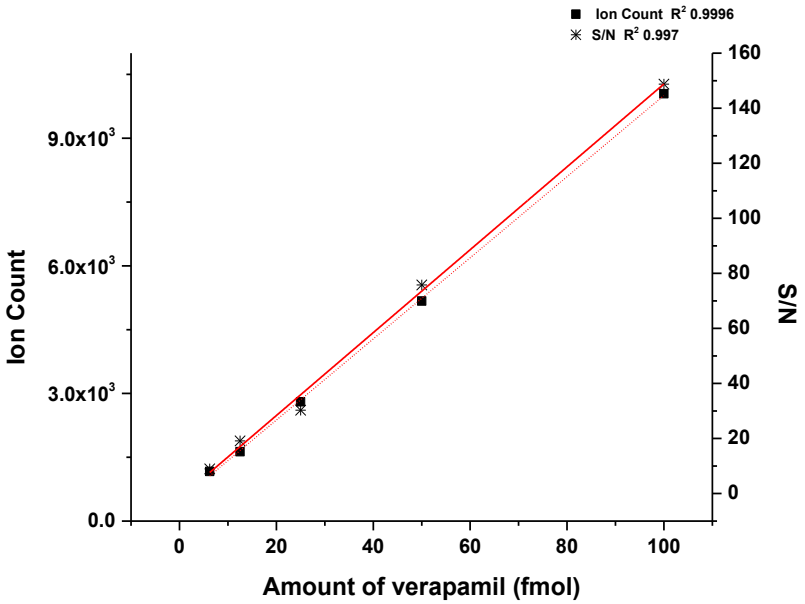

Figure 2.12. Plot of S/N and ion count vs. amount of verapamil on 250 nm Co GLAD films for limit of detection. Spectra collected at 1800 a.u, laser fluence.

The limit-of-quantification of verapamil was 6.25 fmol at a S/N of 10. The signal responses were also found to linearly decrease with decreasing analyte quantity as is seen in Figure 2.12.

2.3.8 Effect of TFA on LDI – MS

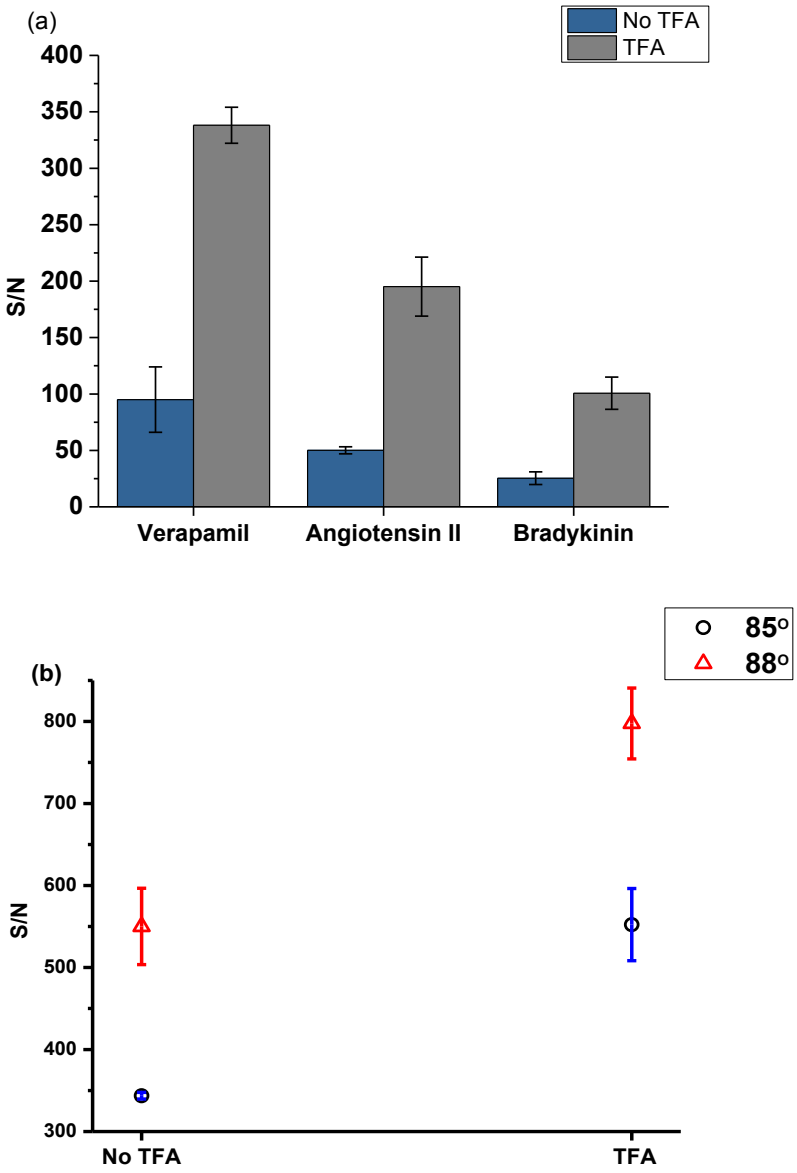

Figure 2.13. The effect of TFA on SMALDI-MS performance. S/N of (a) 10 pmol verapamil, 48 pmol angiotensin II and 55 pmol bradykinin, on 250 nm thick Co films deposited at 88°, and (b) 11 pmol verapamil on 85° and 88° Co films. S/N was measured for five spectra and averaged.

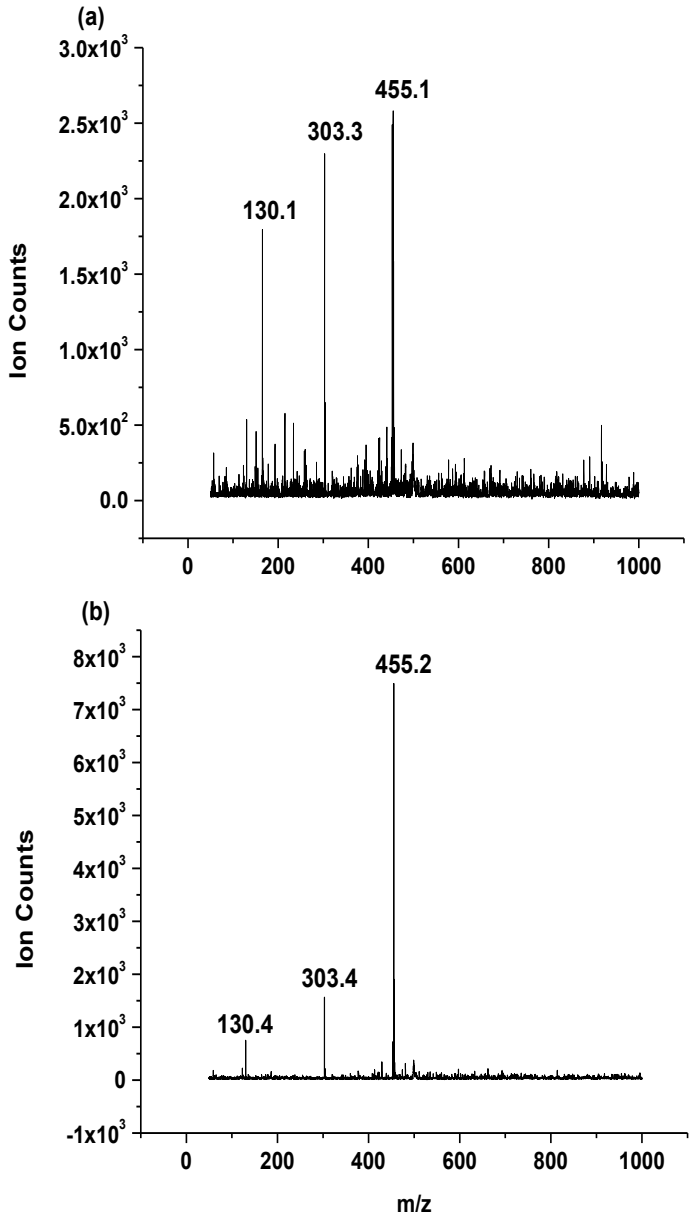

Figure 2.14. Effect of TFA on the background signals of SMALDI-MS mass spectra. Spectrum for 10 pmol verapamil (a) without TFA and (b) with TFA, on Co films.

The presence of 0.1% trifluoracetic acid (TFA) had a marked improvement on the LDI performance of several compounds, verapamil (drug), angiotensin II and bradykinin (peptides), as seen in Figure 2.13. This improvement can be tied to the protonation by TFA observed in both MALDI and ESI-MS.[95,96] While it is possible to obtain analyte signals without TFA, the quality of the spectrum is significantly improved when it was used, Figure 2.14 (a) and (b). The peaks at 303 and 130 are a fragment ion[97] and a common contaminant found in matrix free laser desorption/ ionization spectra.[53,98]

2.3.9 Small Molecule LDI-MS

Figure 2.15 shows mass spectra of six different carbohydrate compounds with masses below 1000 Da. Typical MALDI mass spectra within this mass region tend to suffer from high background due to the presence of peaks from the organic matrix, however, this was not an issue with GLAD films. In Figures 2.16 and 2.17, the mass spectra obtained for β-cyclodextrin and triacetyl β-cyclodextrin from GLAD films do not have background in this range.

One of the earlier works to explore MALDI-MS for oligosaccharide detection used 2,5-dihydroxybenzoic acid (DHB) to study enzymatic kinetics.[99] Notable in this study was the fact that the signals observed below 500 Da were only from the matrix. DHB is the most commonly used MALDI matrix for carbohydrate analysis.[100] However, it is known to suffer from the common MALDI handicap of non-uniform crystallization[33].

A matrix has been proven to overcome the crystallization issue, is 3-aminoquinoline (3-AQ), but it tends to promote the formation of Schiff base imines with reducing sugars. Some researchers have capitalized on this tendency to form imines by ensuring that the derivatisation process is quantitative.[101] However, derivatisation is not always useful, for example, for the evaluation of unknown compound mixtures where we do not know the chemical nature of all the molecules present.

Furthermore, while high efficiency derivatisation and uniform crystal formation was achievable with 3-AQ, its use is also limited by several reaction conditions, including pH (and type of acid used for adjustment), the organic content of the solution/type of organic solvent added and the spot preparation technique. All of which can be problematic for the unskilled and requires extra time during sample preparation.

It is well established that generating the protonated (MH^+) ion for carbohydrates is difficult, but that ionization is promoted by introduction of alkali metal salts.[102] Even so, for traditional carbohydrate MALDI, obtaining a suitably sensitive mass spectrum requires careful selection of a matrix and meticulous spot development.[100,103] We were able to overcome this difficulty by simply mixing aqueous solutions of alkali metal salts (Na^+) with the carbohydrate compounds for ionization, spotting the sample onto GLAD films and obtaining mass spectra by LDI.

Figures 2.15 through 2.17 show the detection of carbohydrates by SMALDI, in many cases enhanced by the addition of alkali salts. A comparison to the spectra with the best MALDI matrix is also shown in Figures 2.16 and 17. The performance between SMALDI and MALDI is similar, except for the larger background at low mass in MALDI. However the data was obtained with no effort to identify a functional matrix material.

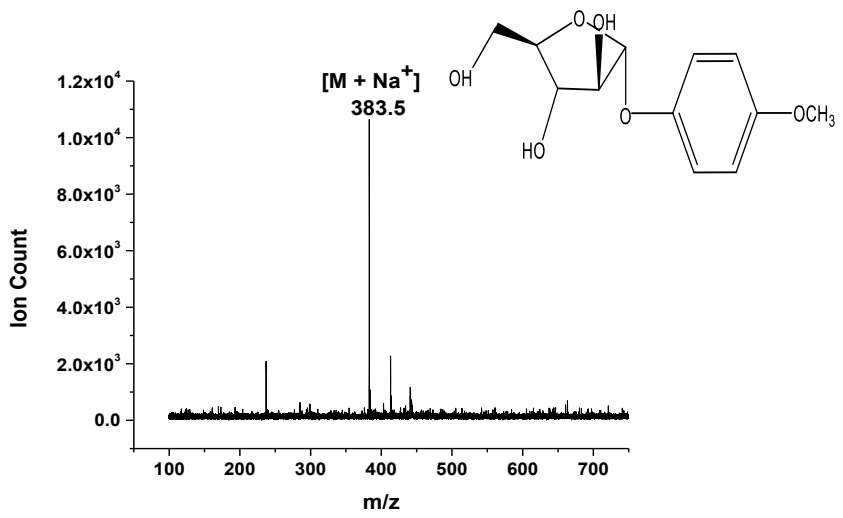
[M + Na+]
383.5
Ion Count
m/z
OH
HO
O
OCH3

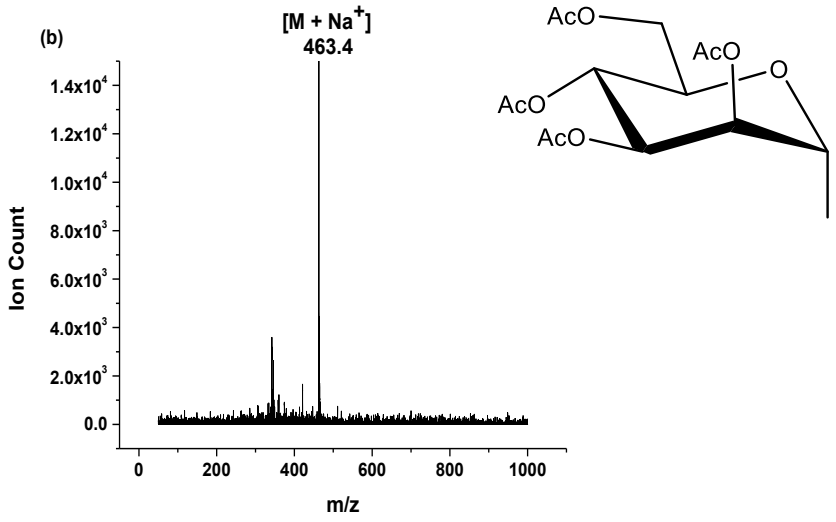
(b)
[M + Na+]
463.4
Ion Count
m/z
AcO
AcO
AcO
O

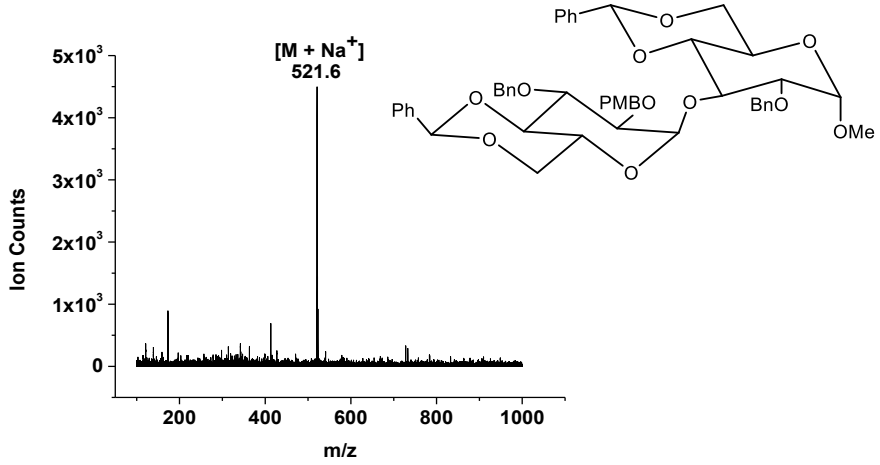
[M + Na+]
521.6
Ion Counts
m/z
Ph
BnO
PMBO
BnO
OMe
O

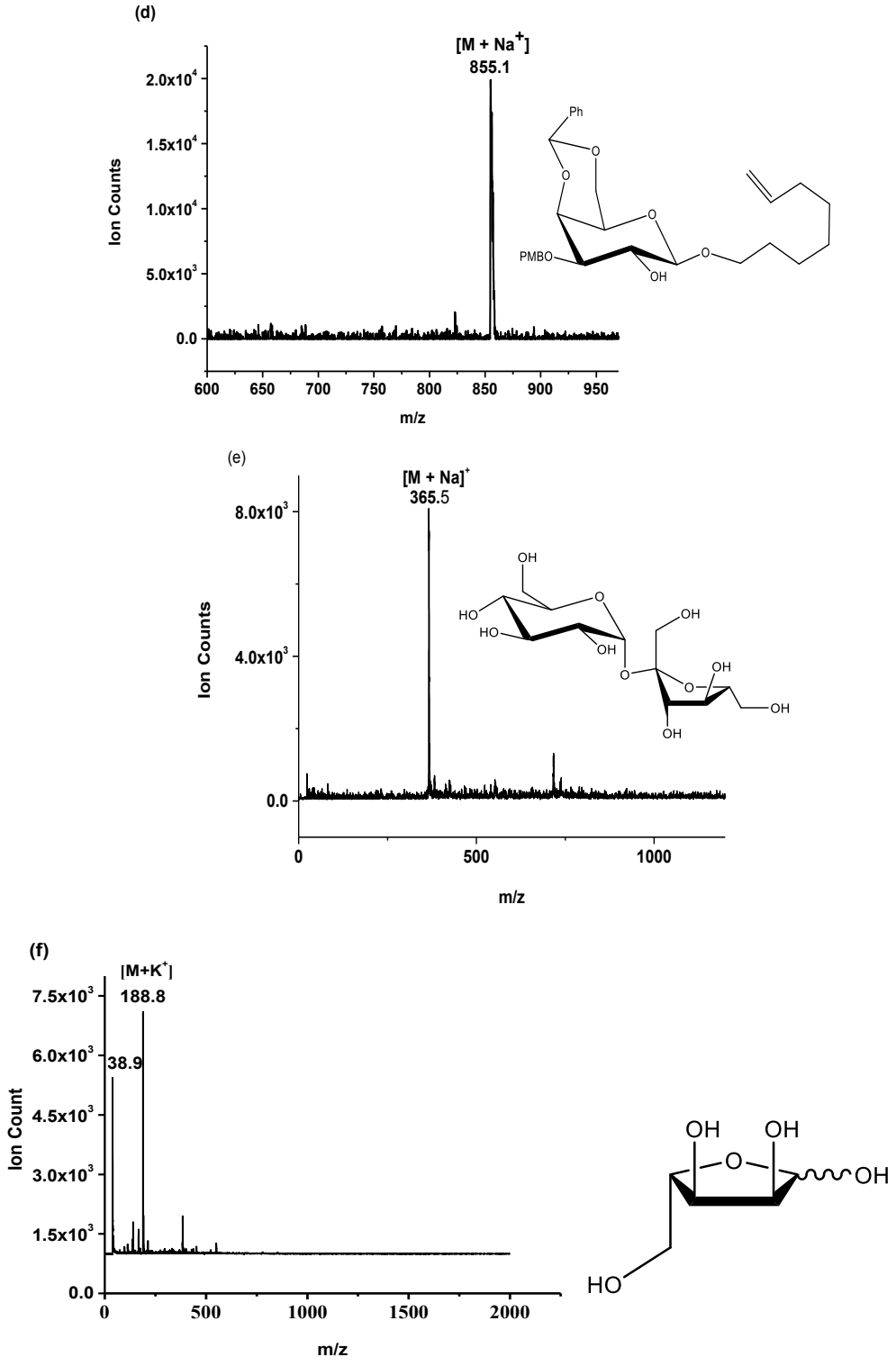

Figure 2.15. Mass spectrum of (a) 35 pmol MJ7, (b) 20 pmol 440MW carbohydrate (c) 5 pmol 498MW carbohydrate (d) 0.3 nmol 832MW carbohydrate (e) sucrose and (f) ribose on 250 nm Co GLAD film.

Lower detection limits (femtomole range) for small molecules were achieved with Co GLAD films, Figure 2.12, compared to other researchers' work using alternative cobalt substrates; [78,79] as well as greater control over whether the molecular ion peak or adduct ion peak was generated. In a study by Yalcin and Li with glutamic acid as the test compound, the presence of alkali metal ions were not added to the test solutions but were a source of contamination and the detection was in the micromole range The metal ion adduct peaks and the molecular ion peaks were both present in spectra. However the metal ion adduct peaks were much stronger than the molecular ion peaks.[80] With our GLAD film, there were no traces of metal ion adduct formation, unless it was intentionally promoted for carbohydrate ionisation. Our highly controlled, vacuum fabrication process ensures that the presence of contaminants on the films is kept to a minimum.

These spectra in Figure 2.15 also demonstrate the ability of Co GLAD films to detect compounds with different structures. The compounds are all carbohydrates but with varying degrees of structural complexity, from the simple monosaccharide ribose to carbohydrates that are intermediates and precursors in biosynthetic pathways. The 498MW compound is a precursor for acceptors in glycosylation in preparation of ABH histo-blood group antigens.[104,105] The 832 MW carbohydrate is prepared in the course of synthesizing a trisaccharide for studies of glycosidase specificities. The ability to detect such intermediates with minimal sample preparation will serve to monitor these synthetic pathways.

The GLAD films also offer the advantage of being able to provide mass spectra of compounds that require specific matrices. In Figures 2.16 and 2.17, we were able to obtain spectra for β-cyclodextrin and its substituted form, triacetyl β-cyclodextrin. To perform MALDI on these same samples, different matrix molecules were tested, with 2,5-dihydroxybenzoic acid (DHB) as the best for β-cyclodextrin and *trans*-2-[3-(4-*tert*-Butylphenyl)-2-methyl-2-propenylidene] malononitrile (DCTB) for triacetyl β-cyclodextrin.

While the ion counts are about the same for each compound in both the MALDI and GLAD spectra, the GLAD spectra have much less background and higher signal to noise ratios.

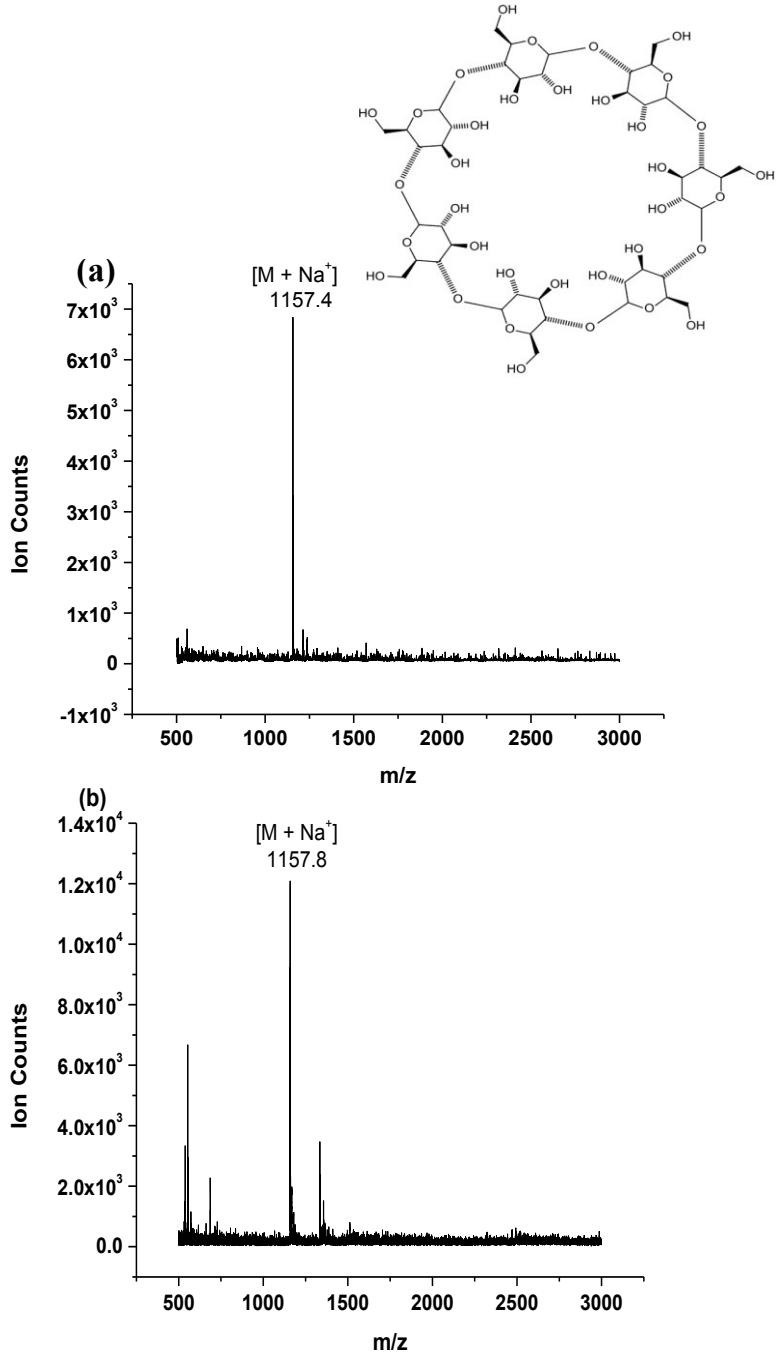

Figure 2.16. Comparison of SMALDI-MS and MALDI-MS mass spectra. Mass spectrum of β cyclodextrin using (a) 250 nm Co GLAD film and (b) DHB matrix.

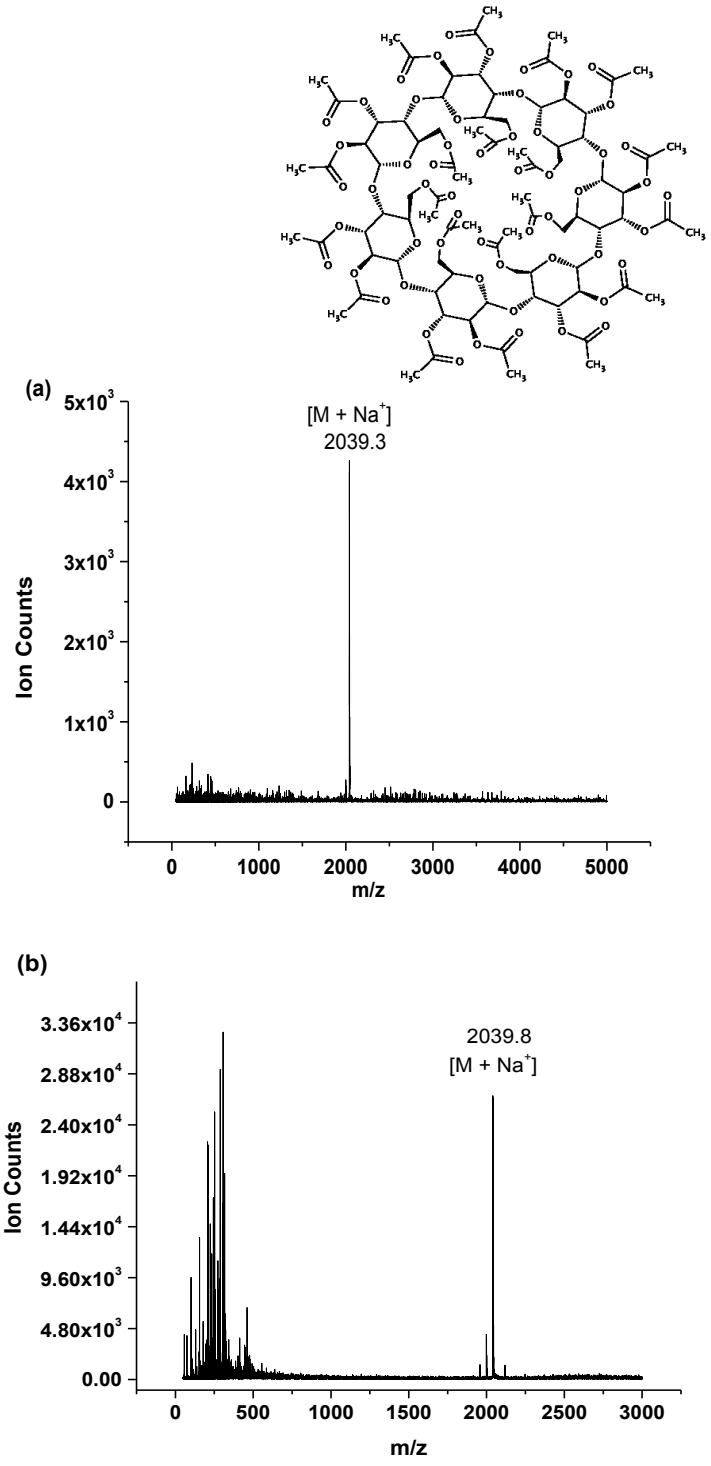

Figure 2.17. Comparison of SMALDI-MS and MALDI-MS mass spectra. Mass spectrum of triacetyl beta cyclodextrin (a) 250 nm Co GLAD film and (b) DCTB matrix.

2.3.10 The Nature of Cobalt Surfaces with Respect to LDI-MS

As-deposited Co GLAD films are known to suffer from oxidation upon exposure to the atmosphere.[106] Very early research demonstrated that the exposure of a clean, bulk cobalt surface to the atmosphere at room temperature leads to the formation of an 8-10 Å film of $Co(OH)_2$ in seconds.[107] Recently, detailed studies of the oxidation of cobalt nanocrystals in a colloidal suspension[108] and of carbon-supported cobalt nanoparticles in oxygen-helium[109], both done at room temperature, reiterated these earlier findings. The oxidation process occurs in two stages, a fast, initial stage, complete in less than 1 minute, and a much slower second stage, occurring gradually over a period of hours. Two notable observations in this first fast stage are that: 1) initial oxidation rate may be proportional to the coverage of metal surface by oxygen;[109] and 2) this coverage is limited by the presence of contaminants, surfactants, solvents, etc.[108] Greater oxidation is observed for surfaces free of impediments. For the nanocrystal and nanoparticle work, the initial oxidation layer extended over only a few atomic layers. However, this layer may extend up to 20 nm.[110]

While the overall mechanism and kinetics of the oxide layer on metals is still not fully understood, it is thought to involve several defined steps proposed by Mott et al.[111,112] The first, fast stage of low temperature oxidation occurs when oxygen molecules chemisorb onto the surface of the metal. This causes the formation of two-dimensional oxide nuclei which subsequently coalescence into the three-dimensional oxide crystallites layer. Place exchange (anions and cations interchanging positions, in this case, electrons tunneling across the oxide layer from oxygen ions formed on the surface) determines the extent of the oxide layer formed by the creation of an electric potential across the oxide layer. The strength of this electric field induces the mobility of metal ions so that oxidation occurs quickly across several layers even at room temperature.[108,109,112] This initial layer to some extent serves as passivation against further oxide formation. Hence the second stage is much slower, and follows a different series of steps. For us the first stage is of the greater interest, since this is the period of greatest oxide

formation and our films are stored in the laboratory under atmosphere after fabrication.

Sources differ on the nature of the reported oxide layer formed at room temperature, cobalt hydroxide[107] or cobalt oxide (CoO).[109] However, it is possible that a combination of both is present in the passivated layer. As numerous studies on the proposed mechanism of DIOS have shown,[43,45,47,48,94] the surface groups of the material plays an integral role in the LDI-MS process. For porous silicon, the silanol groups dominate the surface and hence dictate the mechanism.[45,48] We can conclude that a similar mechanism applies for LDI on cobalt GLAD surfaces, with the -OH groups of the cobalt hydroxide, due to oxidation by air, functioning as they do with silicon surfaces.

2.4 Conclusion and Future Work

This chapter demonstrates the effectiveness of cobalt GLAD films for matrix-free detection and identification of small carbohydrates and drugs and for proteomics application. The GLAD films were able to achieve high sensitivity with a low femtomole limit of detection and low background noise below m/z 1000. The relationship between film thickness and LDI performance was a balance between the degree of film material and porosity and the vertical post height itself. Films ranging from 250 nm to 500 nm possessed the ideal combination. The controlled fabrication of GLAD films ensures that sample distribution on the surface is consistently uniform resulting in reproducible mass spectrometry results (demonstrated over 15 different spots), without lengthy and complicated sample spot preparation as is required for MALDI. Our films also offer the advantage of not requiring cleaning treatments pre and post fabrication as other surface assisted LDI surfaces. Cobalt GLAD films therefore offer advantages over electrochemically etched porous silicon, MALDI and other approaches in terms of cost, contamination control, target uniformity and ease of use.

For future investigations, we recommend investigating the full repertoire of compounds cobalt films can detect, such a glycolipids and low molecular

weight protein biomarkers. Since a significant difference in performance was also found with different column morphology, it might also be useful to further examine other GLAD column types for SMALDI-MS applications.

The determination of the nature of the surface oxide formed on the surface and more in-depth studies into the porous nature of the films would lead to a better understanding of the SMALDI-MS mechanism of cobalt GLAD films.

Chapter 3

Silicon SMALDI-MS for Glycolipid Biomarkers

3.1 Introduction

Several recent studies have demonstrated the potential of glycolipids as biomarkers and metabolites for a wide range of diseases, such as ovarian cancer, dementia, Alzheimer's disease, Huntington disease, cardiovascular disease, hepatic failure and salidosis.[4,103,113-129] The International Union of Pure and Applied Chemistry-International Union of Biochemistry and Molecular Biology (IUPAC-IUB) Joint Commission on Biochemical Nomenclature designates a glycolipid as any compound containing one or more monosaccharide residues bound by a glycosidic linkage to a hydrophobic moiety.[130] A wide range of biomolecule linked saccharides are of biological relevance[131-134] and a number were studied in this work. The nomenclature of these molecules is presented below.

A glycosphingolipid contains at least one monosaccharide residue and either a sphingoid or a ceramide. Sphingoids consist of long-chain aliphatic amino alcohols and are considered a ceramide when they are *N*-acylated.

Sulfatides are formed when hydrogen sulfate forms esters with ceramide-containing glycosphingolipids,[135] Figure 3.1. Sulfatides represent a class of sulfated galactocerebrosides that differ only in the composition of the fatty acid residue that acylates the amino group of the sphingosine.[4]

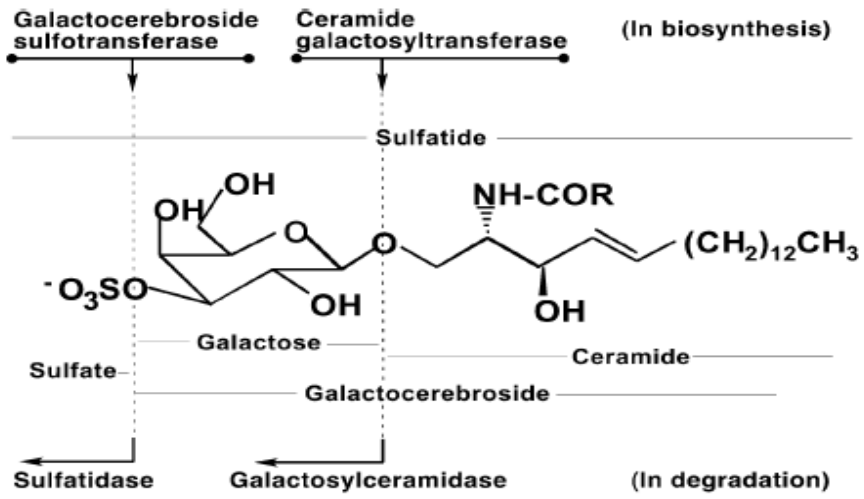

Figure 3.1. General structure of a sulfatide[4] (Reprinted with permission from John Wiley and Sons).

Gangliosides are acidic glycosphingolipids additionally containing one or more sialic acid residues. They are composed of an oligosaccharide, sialic acid(s) and a ceramide (sphingosine and fatty acid). Gangliosides are constituents of plasma membranes, especially in the central nervous system (CNS) and function as cell recognition sites for other cells and hormones, as antigens for toxins, etc. Gangliosides are also linked to cell growth and migration in CNS tumors and are biomarkers for neuronal disorders.[127,136] Many gangliosides are either deplete or accumulate in parts of the CNS at the onset of age dependent dementia. Levels of certain gangliosides/sulfatides vary with the different stages of dementia.[4,118,137]

The sialic acid component of gangliosides is the cause of *salidosis*: failure of the sialidase (neuraminidase) enzymes to remove the terminal sialic acid residue from glycoproteins and glycolipids, which disrupts cell function and

causes accumulation of complex carbohydrates.[138] One of the most common sialic acids is N-acetylneuraminic acid (Neu5Ac or NANA).[139]

The Cairo Research Group of the Department of Chemistry, University of Alberta examines inhibition, substrate specificity, and biological function of the human neuraminidase family, as well as synthetic lipid probes.[140,141] In these investigations, gangliosides, sialic acids and carbohydrate triazoles (five-membered rings of two carbon atoms and three nitrogen atoms) compounds are all studied.[138] Research of this nature requires fast and easy detection of these glycolipid compounds during the course of reactions, and at different stages of the experiment. Currently, NMR (nuclear magnetic resonance) methods can identify these types of compounds. However, this can be time consuming and requires NMR expertise. The researchers of the Cairo group had made attempts to use MADLI-MS for rapid detection of these compounds, but were unable to detect many of them. Currently, there is some difficulty in detecting glycolipids by conventional MALDI-MS. Glycolipids are usually detected by using a matrix.[133,142-144] However, selecting the correct one can be a lengthy and complicated process for this class of compounds. Some glycolipids are also almost impossible to detect even with a wide range of matrices commonly used in conventional MADLI.[145] In addition to the matrix selection issues for different classes of lipids, a minimum threshold proton affinity of the analyte molecule is required to promote ionization in LDI-MS.[45,146] A higher background was also observed as the proton affinities of compounds decreased, which was correlated to matrix suppression and to analyte-analyte suppression effects in MALDI.[146] The higher proton affinities of neutral analytes promote the formation of analyte ion peaks and suppress the matrix ion.[147] Many fatty acid methyl esters, a part of the structure of the compounds we investigate, have proton affinities below this threshold.[147,148] Another important lipid analyte characteristic was its acidity, which had an inverse relationship with ease of protonation.

These limitations experienced with MALDI have also translated into other matrix free methods. One of the limitations of the DIOS and SIMS-MS

techniques has been the poor results for lipid compounds.[146] This is linked to the minimum threshold of proton affinity required for ionization on porous silicon surfaces.

Metal oxide SALDI-MS techniques with ZnO,[34] NiO and MgO[148] have successfully overcome this ionization limitation with lipids. However, they suffered from metal ion adducts above certain laser fluences. These adducts can make identifying peaks in the mass spectra of lipid compounds difficult.[145] Lipid spectra from biological samples tend to be complicated due to the presence of various lipids with varying fatty acid chains, etc., so the added complication of adducts is undesirable. Also, while metal oxide surfaces work for lipid compounds, pretreatment with esters, ketones, carboxylic acids, diesters, and triesters was necessary to provide protons for ionization of other classes of compounds such as carbohydrates and peptides,[149] this limits the overall applicability of these oxides as matrix free surfaces.

There have been offline studies that have combined separation and mass spectrometry of glycolipids extracted from tissue samples.[150] High performance thin layer chromatography (HPTLC) plates were used for the separation of the glycolipids from tissue extract. Standard glycolipids and visualization agents were then required to identify the separated bands. The separated compounds were extracted and reconstituted from each band prior to further analysis by MALDI with 9-aminoacridine matrix, a relatively new MALDI matrix, or by electrospray ionization mass spectrometry (ESI-MS).[151,152] This process can be lengthy and analyte molecules can be lost during the removal from the plate and the subsequent extraction and reconstitution prior to MS analysis.[153,154]

Online HPTLC with MALDI-MS attempts to address issues with offline separation-MS methods.[155] However, one difficulty with this hyphenated approach with standard MALDI TOF instrumentation has been the negative effect on sensitivity. This is due to the irregularity of the silica gel surface of the HPTLC plates.[156] Researchers have overcome this by using IR lasers instead of UV lasers. IR lasers desorb a few micrometers of plate material off the surface of the plates

with each laser shot, providing more analyte molecules for detection in the plume and thus increasing the sensitivity.[157] UV lasers do not remove a layer of material from the surfaces, unless the fluence is extremely high. This can cause fragmentation of the analytes of interest, as well as introduce contaminant peaks in to the mass spectrometer. However, some of the issues with the offline method still plague this online procedure, namely, long separation times (20 minutes), and the need for glycolipid standards and visualization agents.

For biofluid samples such as serum and plasma, LC ESI-MS is used for sample clean up prior to mass detection. While detection with ESI-MS is effective, the method does require some sample preparation and clean up by solvent extraction and liquid chromatography prior to the mass analysis. Overall, the most popular method to detect glycolipids from extracted lipid samples is ESI-MS.[158] ESI-MS can be applied to the direct analysis of solutions, does not require derivatization reactions and has high sensitivity.[159-161] Low picomole detection limits are routinely achieved[159,162] and this is better than the detection in the MALDI-MS studies. [160,162] For work that requires a rapid and simple detection of glycolipids, SMALDI-MS can serve as an alternative method.

Based on the previous success in detecting metabolites with 500 nm silicon SMALDI-MS[72], we chose to further explore the potential of silicon SMALDI-MS to detect the classes of glycolipids described above. The work is relevant because of the role of glycolipids as biomarkers in a wide range of diseases, and the existing need for a simple and rapid detection method. The UTLC capability of GLAD films[66,68,163] was also explored as a simple hyphenated UTLC-SMALDI-MS preparatory step for sample clean up, and for minimizing the matrix effect in mass spectra of a real biofluid sample.

3.2 Experimental

3.2.1 Materials and Reagents

NaCl (sodium chloride), KCl (potassium chloride), 2,5-dihydroxybenzoic acid (DHB), t-2-(3-(4-*t*-butyl-phenyl)-2-methyl-2-propenylidene) malononitrile (DCTB), cyano-4-hydroxycinnamic acid (CHCA) and trifluoroacetic acid (TFA) were from Sigma-Aldrich Chemical Co. (Milwaukee, WI, USA).

Pig brain sulfatide, ceramide, gangliosides GM1, GM3 and GD1, and**,** N-acetylneuraminic acid (Neu5Ac) standards was purchased from Avanti Polar Lipids Inc., (Alabaster, USA).

Stock solutions of standard glycolipids were prepared in methanol at 1 mg/ml. Dilutions were prepared by mixing stock solutions with 1mg/ml NaCl, KCl ($^{V}/_{V}$) or with methanol. Ultrapure water used for sample preparation was from a deionising system (Millipore Canada, Mississauga, ON, Canada). Sterilized pig serum was from Life Technologies Inc. (Grand Island, NY, USA).

3.2.2 GLAD Film Fabrication

Porous thin film deposition was performed in a high vacuum system (Kurt J. Lesker Co., Clairton, PA, USA).[5] Silicon wafer substrates were cleaned prior to deposition by submersion in piranha (3:1 sulfuric acid: hydrogen peroxide) for 20 minutes followed by a deionized water rinse and drying with nitrogen gas. For vertical post films, silicon (99.9% pure, Cerac Inc., Milwaukee, WI, USA) was deposited onto the silicon substrate with a substrate rotation rate of 1.2 rpm and the deposition rate was 0.6 nm/s.[74]

3.2.3 Extraction of Sulfatides from Serum

100 uL of serum was added to 1.8 mL of hexane:2-propanol (3:2, $^{V}/_{V}$) and vortexed for 20 minutes. The supernatant was transferred to a vial and left to dry overnight in a fumehood. The resultant dried lipids were reconstituted in 1 mL chloroform: methanol (2:1,$^{V}/_{V}$) and spotted onto the 500 nm silicon GLAD film and allowed to air dry.

3.2.4 Extraction of Phosphocholines from Serum

100 uL of serum was added to 1.8 mL of hexane: 2-propanol (3:2, $^{V}/_{V}$) and vortexed for 20 minutes. 0.5 µl of the supernatant was spotted onto the GLAD film and allowed to air dry prior to SMALDI detection.

3.2.5 SMALDI and MALDI-MS

Mass spectra were obtained using an AB Sciex Voyager Elite MALDI TOF instrument with a pulsed N_2 laser (wavelength 332 nm) at a repetition rate of 3.0 Hz. Spectra were acquired in positive ion mode using delayed ion extraction. Grid voltage was set at 74% and extraction delay time was 250 ns. Each spectrum consists of 100 shots at randomly selected laser focus spots within a single sample spot. 500 nm silicon GLAD films were secured to a modified MALDI plate using double sided adhesive tape, Figure 3.1. Aliquots of 0.5 µL of samples were spotted onto films and allowed to air dry prior to mass spectrometry analysis. MALDI samples were prepared using the dried droplet method.[81] A 1 µL aliquot of a mixture of sample and matrix was deposited onto a MALDI steel plate and allowed to air dry prior to mass spectrometry analysis as described above for GLAD films. Signal to noise (S/N) ratios were calculated using Voyager Data Explorer version 4.0 software (Applied Biosystems, Framingham, MA, USA).

3.3 Results and Discussion

The most widely used method of detection for glycolipid compounds has been ESI-MS with liquid chromatography.[128,164] However, this approach can result in the overlap of sulfatide, glycerophospholipid and other sphingolipid peaks, minimizing the technique's selectivity,[142] or the compounds might require modification such as alkaline methanolysis,[165] which is time consuming.

With common MALDI matrices such as cyano-4-hydroxycinnamic acid (CHCA), it is difficult to detect some classes of glycolipids such as sulfatides, without some form of modification. For example, saponification,[129,166] which introduces another step in the sample preparation. 2,5-Dihydroxybenzoic acid (DHB), on the other hand, has been more successful with detecting some ganglioside species[133] with Fourier transform ion cyclotron resonance mass spectrometry (FTICR-MS). However, when the same matrix is used for detection of phospholipids, Western blotting with polyvinylidene difluoride (PVDF) membrane was required.[167] A matrix that has emerged as successful for the detection of sulfated glycolipids in recent years is 9-aminoacridine (9-AA),[142,150,168,169] but has not yet proven applicable with other classes of glycolipid biomarkers.

What is evident from these previous studies is that no single, simple, straightforward LDI-MS technique is currently available which can readily detect a wide range of glycolipid species. We know from our discussions with the researchers in the Cairo group in our own department that such a method is desirable, as a rapid means of monitoring reactions involving these biomarker compounds.

We have therefore chosen to compare 500 nm silicon SMALDI with MALDI for the detection of several glycolipid standards. The preferred mode of detection with SMALDI, positive ion versus negative ion mode, was also evaluated. The preferred mode was used to further determine the limit of detection for a standard ganglioside and a sulfatide.

3.3.1 Gangliosides

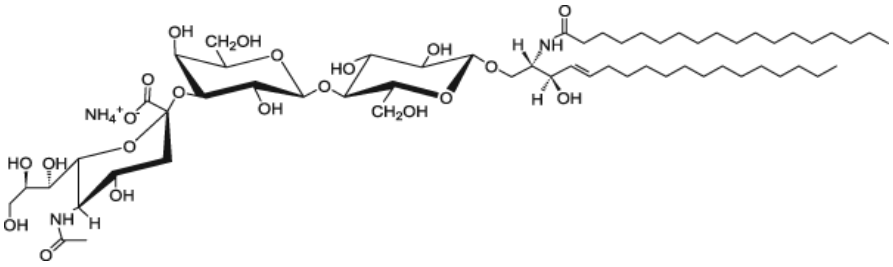

Figure 3.2. Structure of G_{M3} Ganglioside (Milk, Bovine-Ammonium Salt).

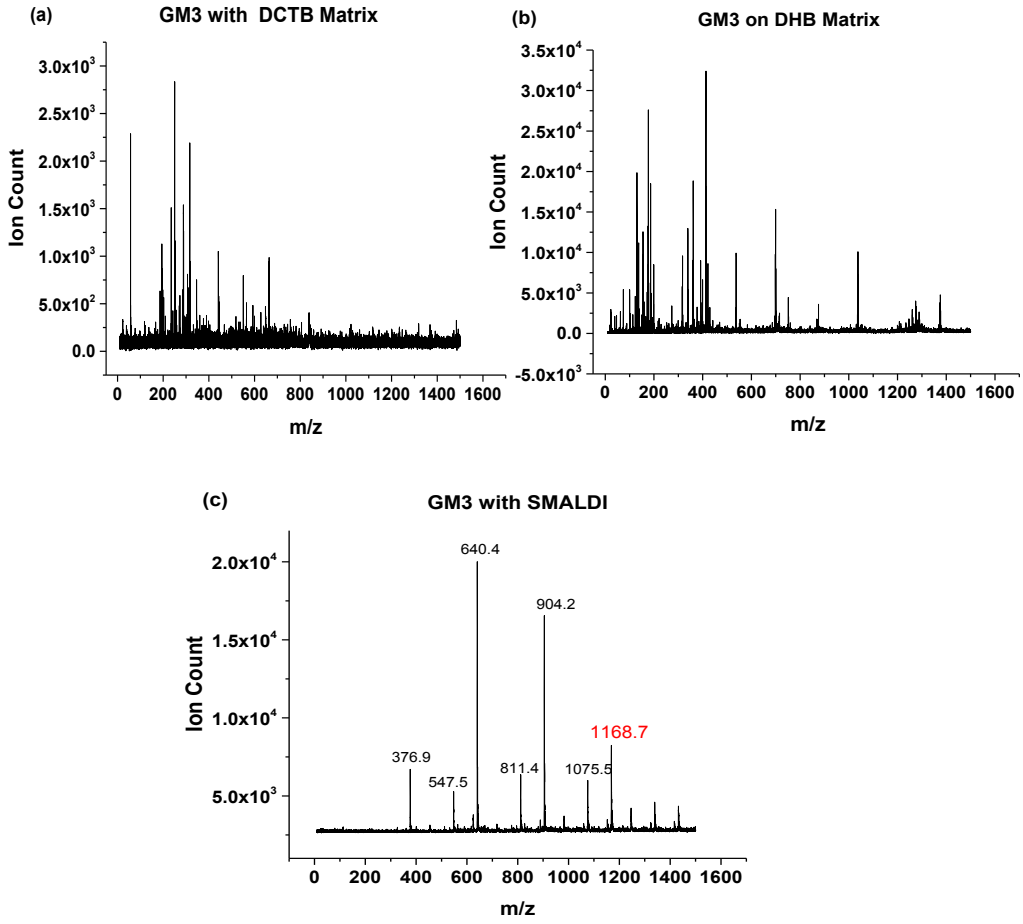

Figure 3.3. Mass Spectra of 20 pmol ganglioside GM3 with (a) DCTB matrix, (b) DHB matrix and (c) on 500 nm silicon GLAD.

Gangliosides

We tested the ganglioside GM3, structure shown in Figure 3.2, with two of the most probable MALDI matrices, 2,5-dihydroxybenzoic acid (DHB) and t-2-(3-(4-*t*-butyl-phenyl)-2-methyl-2-propenylidene) malononitrile (DCTB). DCTB has worked for other glycolipids.[170] However, we were not able to observe any spectra with either matrix. With SMALDI, a major fragment ion of the GM3 was observed at 1169 (see the red peak) in Figure 3.3 (c). Of note in this spectrum of a purchased standard of bovine GM3, are the peaks at 904 and 1076. These peaks are associated with two other types of bovine gangliosides; 904 from ganglioside GD1b and 1076, from GT1b. The other peaks are fragment peaks associated with GM3 gangliosides.[171]

MALDI-MS detection of ovine GM1 was unsuccessful with the range of matrices we tested. In SMALDI positive ion mode, the peak detected was a fragment ion following the loss of Neu5 Ac. From the spectra, we can also conclude that the GM1 standard purchased was not completely pure. The peaks at 1535 and 1563 detected in negative ion mode, in Figure 3.4 (c) are consistent with ceramides present in animal sources[150] and our standard is of ovine origin.

G_{M1} Ganglioside (Brain, Ovine-Ammonium Salt)

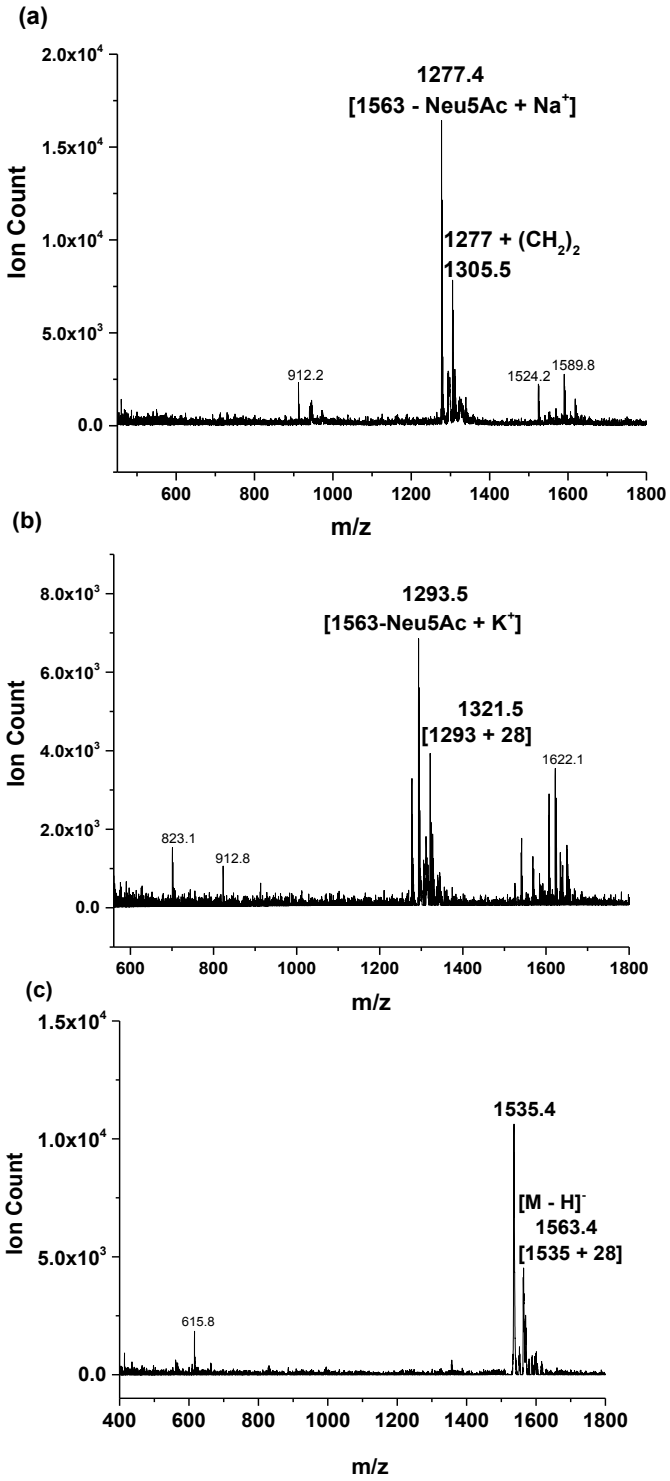

Figure 3. 4. Mass spectrum of 5 nmol GM1 ganglioside with SMALDI (a) positive ion mode with Na^+, (b) positive ion mode with K^+ and (c) negative ion mode. Spectra collected at 1750 a.u. laser fluence.

The molecular mass of the GM1 standard was reported as 1564. However, the 28 unit difference observed in the negative ion mode with peak 1536 can be attributed to the difference in the sphingosine constituent of the ganglioside. A single conjugation within the fatty acid chains results in a 28 unit difference in mass and is quite common in glycolipids extracted from animal sources.[120] As with Neu5 Ac, detection in negative ion mode was achieved without the addition of ionizing agents.

We were able to achieve high attomole detection of standard GM1 ganglioside in solution, as shown in Figure 3.5. This matches current literature that study other ganglioside species as biomarkers with ESI-MS and MALDI-MS respectively.[172,173] For example, in a study probing the immunity of gangliosides, human milk was found to have picomole levels of gangliosides in the extracted sample.[131] Our lower detection in this instance compared to the reported literature may be due to the fact that we studied a pure standard in solution, rather than an extracted sample from a complex, real sample.

However, at this low concentration, fragment ion peaks were more dominant, Figure 3.5. The S/N ratios reported in the graph were taken for the 1536 peak in negative ion mode.

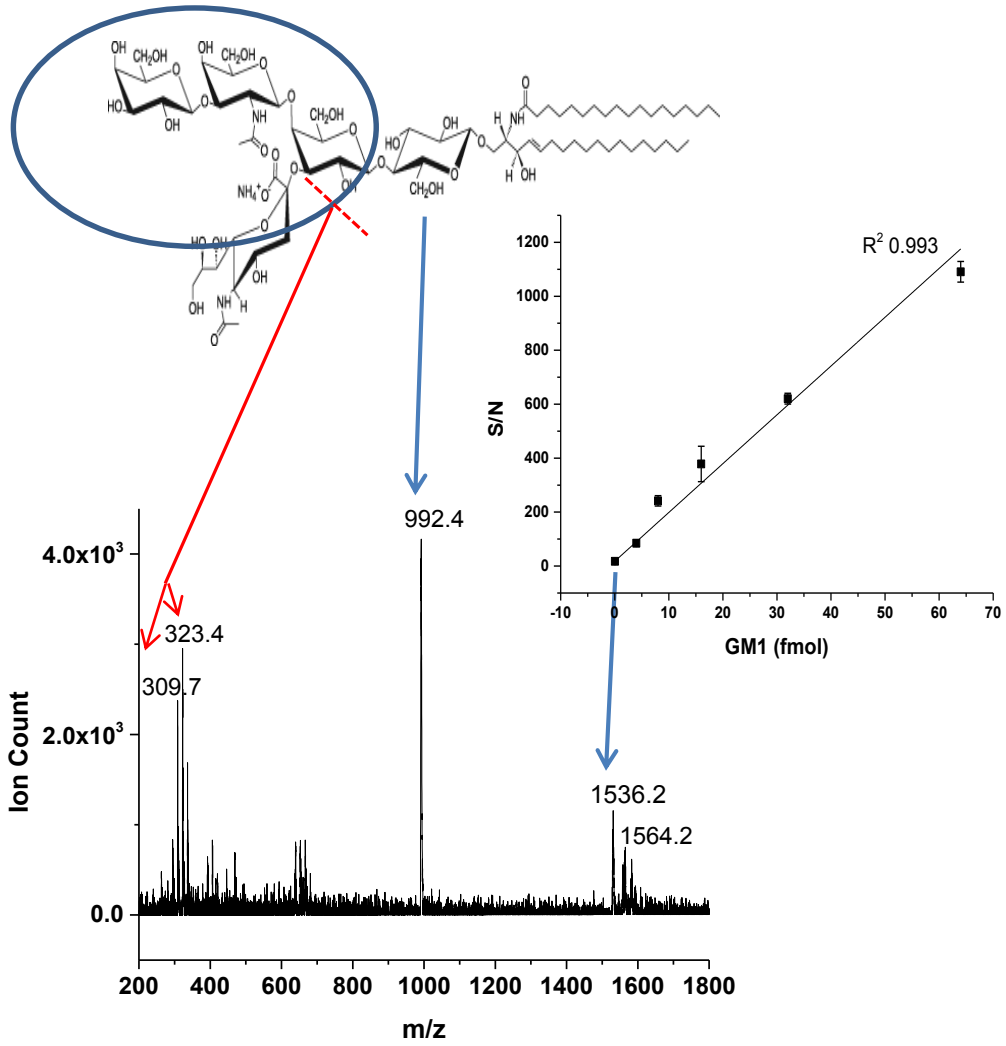

Figure 3.5. Detection of 90 attomole standard GM1 ganglioside with SMALDI-MS on silicon GLAD film. Spectrum collected at 2200 a.u. laser fluence.

GD3 Ganglioside (Milk, Bovine-Ammonium Salt)

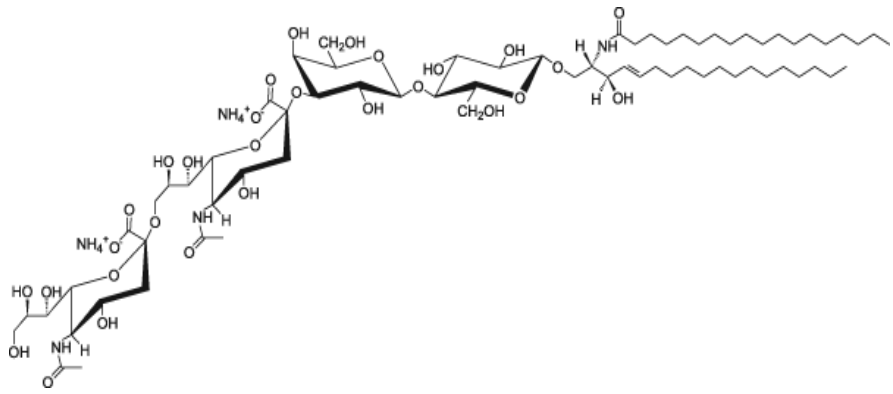

Figure 3.6. Structure of GD3 Ganglioside.

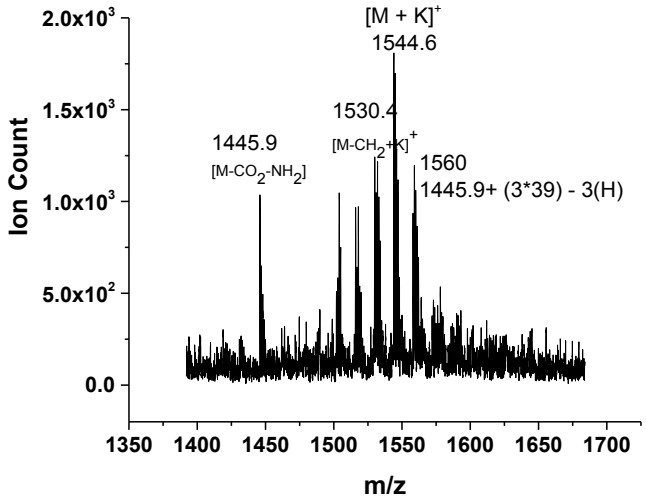

Figure 3.7. Mass spectrum of 8 nmol GD3 Ganglioside with SMALDI.

GD3 ganglioside was also not detected with MALDI – MS, and was only detected in the positive ion mode with SMALDI. While the analyte potassium ion peak was dominant in the spectrum, several fragment ions were also detected[133], Figure 3.7.

3.3.2 Sialic acid, N-acetylneuraminic acid (Neu5Ac)

Sialic acids are a component of gangliosides, structure of N-acetylneuraminic acid shown in Figure 3.8. DHB was able to produce a spectrum for the standard sialic acid Neu5Ac, but DCTB was not. Peaks were observed in both negative and positive ion mode for SMALDI, Figure 3.9 (b) and (c), and the overall quality of the spectra in both modes was better than MALDI. The peak detected with DHB was also a sodium ion adduct peak, however, sodium ions were not added to the sample solution. The peak at 190 is a fragment of the molecular ion. With the SMALDI spectrum in the positive ion mode, we used the same concentration of the analyte as with DHB, but we added KCl to the sample matrix to promote ionization and hence the potassium adduct ion peak was expected in the positive ion mode. With SMALDI, the analyte peak in the negative ion mode was generated without the addition of any ions, Figure 3.9 (c). Overall, the ease of detection and the quality of the spectra was better with SMALDI, especially since there was no need to go through the matrix selection process.

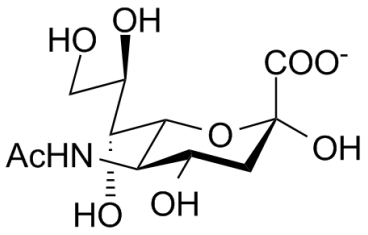

Figure 3.8. Structure of N-acetylneuraminic acid (Neu5Ac), a component of gangliosides.

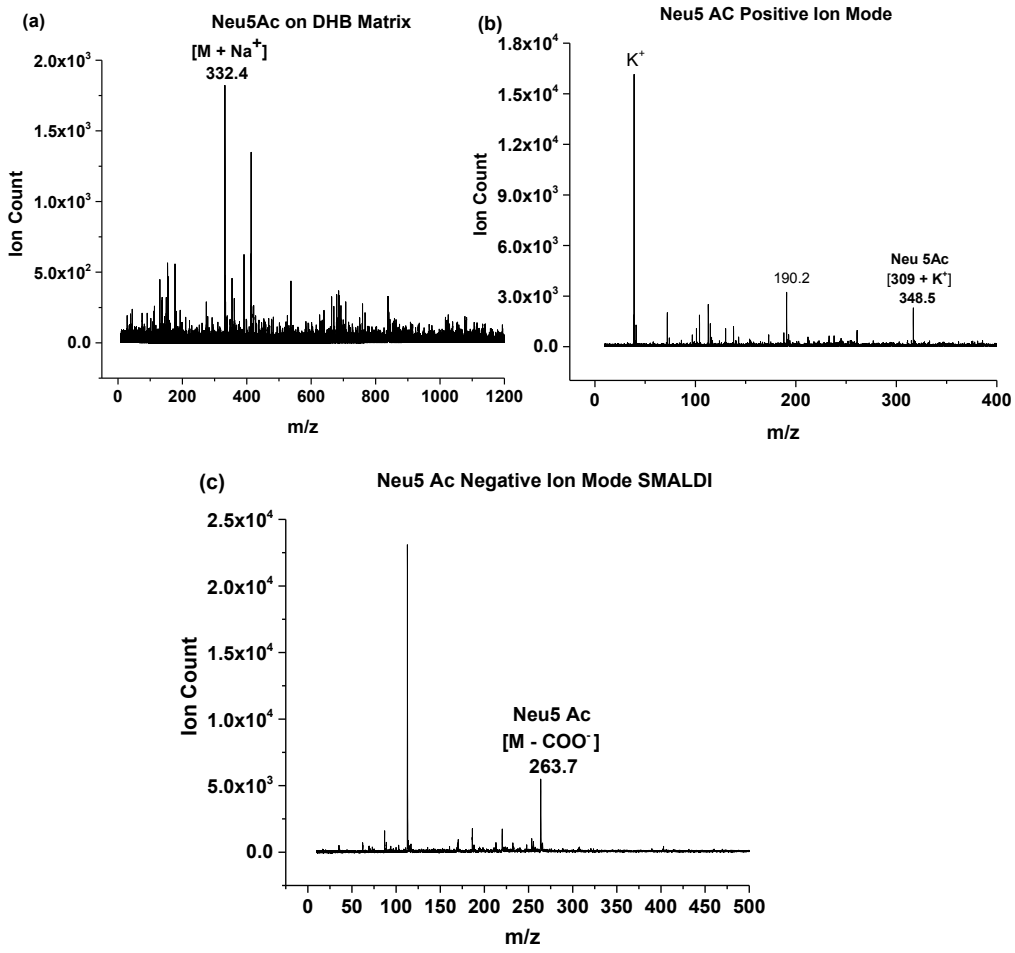

Figure 3.9. Comparison of MADLI and SMALDI-MS detection of sialic acid in positive and negative mode. Mass spectrum of 48 pmol Neu5Ac (a) with DHB matrix, (b) positive ion mode silicon SMALDI and (c) negative ion mode silicon

3.3.3 Triazoles

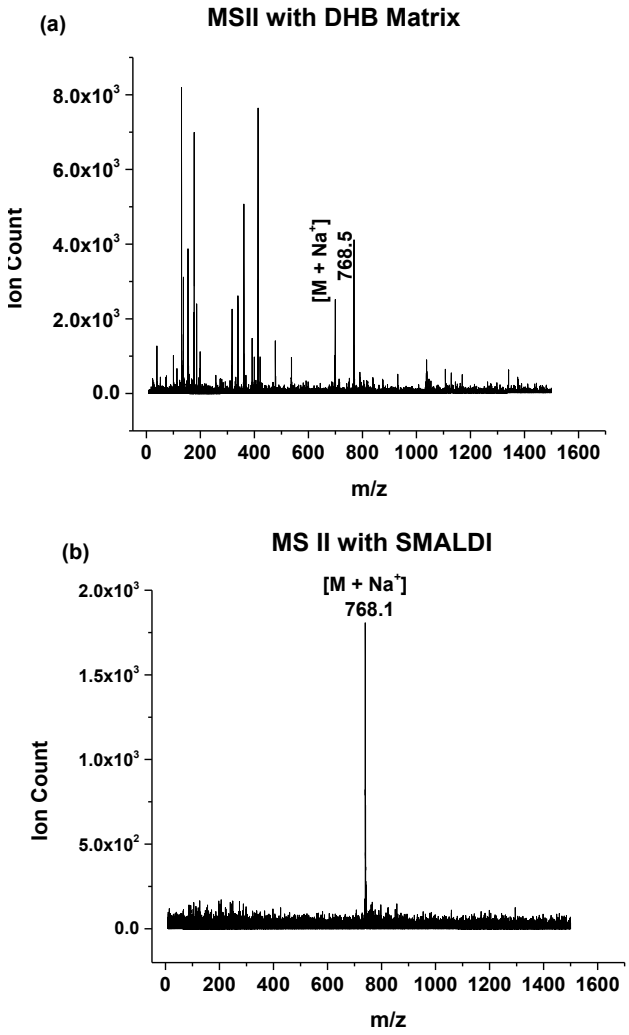

Figure 3.10. Comparison of MALDI and SMALDI-MS detection of triazoles in the positive ion mode. Mass spectrum of 62 pmol triazole carbohydrate MSII (a) with MALDI matrix DHB and (b) on 500 nm Si GLAD.

Triazoles

The triozoles were detected with both MALDI and SMALDI. But as with the other glycolipids detected with MALDI-MS, the major peak was an alkali adduct peak even though alkali adducts were not added to the sample solution. The ion counts for both SMALDI and MALDI were similar, but the background was significantly reduced with SMALDI, Figures 3.11 (a) and (b).

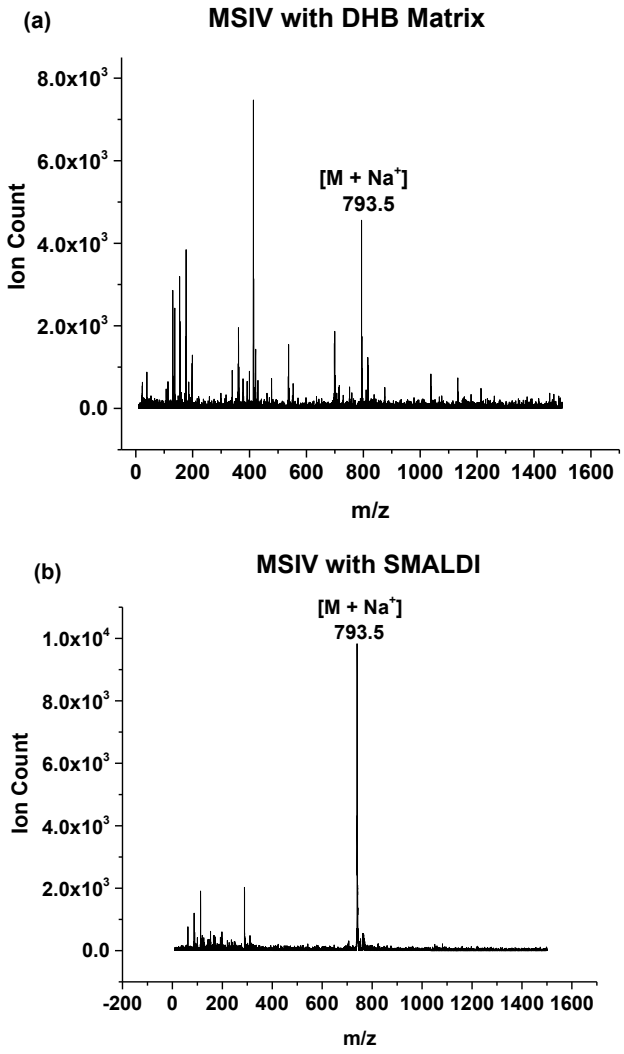

Figure 3.71. Comparison of MALDI and SMALDI-MS detection of triazoles in the positive ion mode. Mass spectrum of 60 pmol triazole carbohydrate MSIV (a) with MALDI matrix DHB and (b) on 500 nm Si GLAD.

3.3.4 Sulfatide and Ceramide

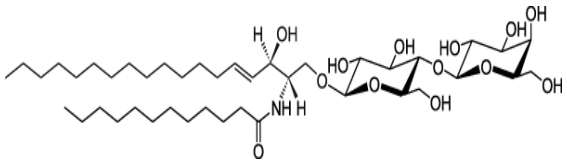

Figure 3.82. Structure of C12 Lactosyl(ß) Ceramide (d18:1/12:0).

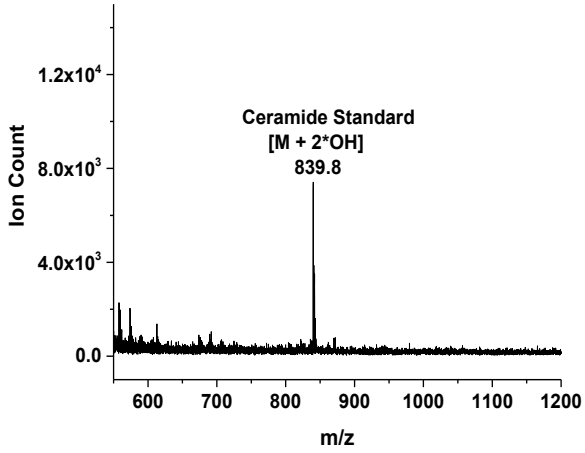

Figure 3.13. Mass spectrum of 15 nmol C12 Lactosyl(ß) Ceramide (d18:1/12:0).

Detection of a standard ceramide was not accomplished with MALDI, but it was detected in negative ion mode with SMALDI, Figure 3.13. Standard pig brain sulfatide on the other hand was detected with a MALDI matrix, but as can be seen from Figure 3.15, the quality and intensity are better with SMALDI. The peaks at 550 and 522 are fragment ions[151] and in both cases, these peaks were more intense than the analyte ion peak. SMALDI in negative ion mode was far superior to the positive ion mode for both MALDI and SMALDI, Figure 3.15 (c). Loss of the sulfate group gives 801 peak and loss of either OH or NH_2 gives the major peak at 882.

For those compounds that were not detected with MALDI matrices, but were detected with SMALDI, it is possible that the minimum threshold proton affinity requirement was responsible.[45,146,147]

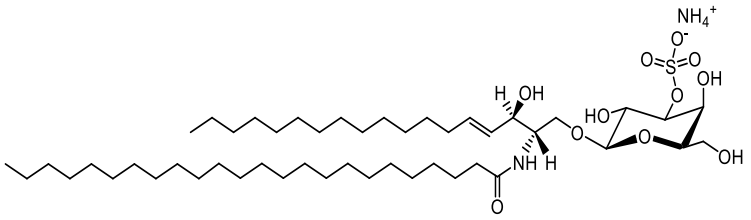

Figure 3. 94. Structure of pig brain sulfatide standard, Mono-Sulfo Galactosyl(ß) Ceramide (d18:1/24:0)

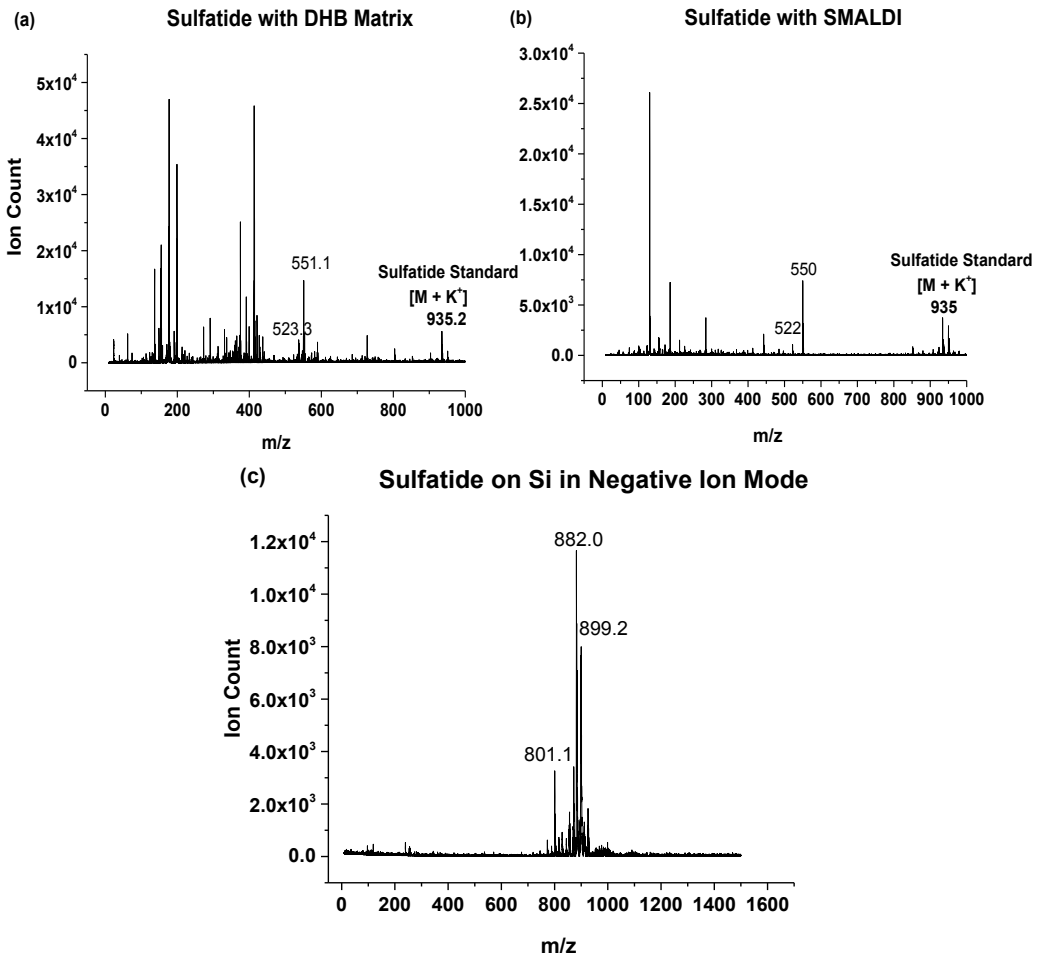

Figure 3.105. Comparison of MALDI and SMALDI-MS detection of standard sulfatide, structure shown in Figure 3.14. Mass spectrum of 65 pmol pig brain sulfatide (a) with DHB matrix, (b) with SMALDI in positive ion mode and (c) with SMALDI in negative ion mode.

3.3.5 Detection of glycolipids in porcine serum

In biologically relevant studies, biomarkers of interest are in real biofluids extracted from test subjects. Most notably, for illnesses associated with changes in sulfatides, cerebrospinal fluid and serum[122,174] are tested. Since SMALDI proved effective in detecting a standard sulfatide, the next step was to test its efficacy for detection of this class of compounds in a biologically relevant sample, and for this we chose pig serum.

We extracted the lipid compounds as a supernatant from pig serum with hexane:2-propanol. This supernatant was dried and reconstituted with a mixture of chloroform and methanol for sulfatide detection with SMALDI, Figure 3.116. Two major pig sulfatides were detected with peaks corresponding to 855 and 881; the 907 peak is most likely the pig epithelial ceramide (S-GalCer, 24:0)[150], Figure 3.16. Interestingly, the 881 peak was also the major peak detected in the standard pig sulfatide, Figure 3.15 (c). We conclude that the presence of this sulfatide is not restricted to just the brain region of pigs. However, the 801 and the 899 peaks were only seen with the brain standard.

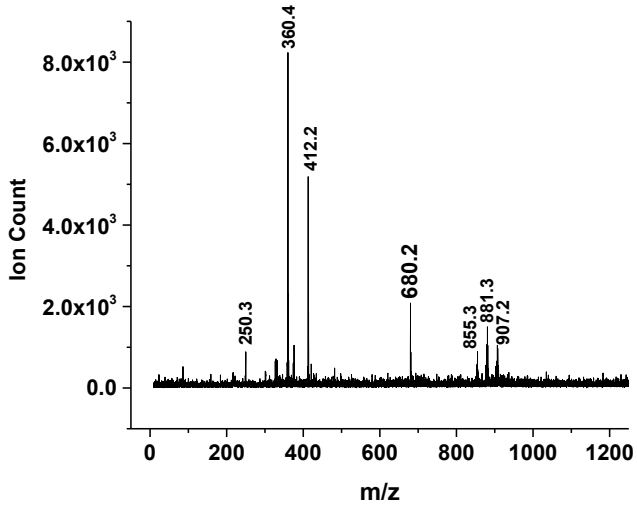

Figure 3.126. SMALDI-MS mass spectrum of sulfatide compounds from serum extracted with hexane:2-propanol and reconstituted with chloroform:methanol.

While working with pig serum, we detected another class of glycolipids, phophatidylcholines, between 700 and 832 m/z, which we did not intentionally set out to detect, see Figure 3.17 for spectrum. During complete lipid extraction, these compounds were detected in the supernatant after vortexing with hexane and 2-propanol. The supernatant was tested with SMALDI and phophatidylcholines were observed. For complete lipid extraction, the supernatant is usually dried and reconstituted prior to detection. When we tested the supernatant, it was found to contain a phophatidylcholine and several of its associated ions. Phosphatidylcholines are known to ionize well in the positive ion mode with MALDI. But often structural information for their identification requires tandem mass spectrometry and specific solvents.[175] This was not a problem with SMALDI, the extent of fragmentation can be controlled by changing the laser fluence, so identification was more easily accomplished.

In Figure 3.17, the phosphatidylcholine species containing the 16:0/18:1 fatty acids has a m/z corresponding to 760. Peak 184 is its head group fragment ion.[175,176] The $[M + Na]^+$ peak is also observed at 782. The 496 and 725 peaks are fragment ions resulting from the loss of a ketene (O=C=CH – R) and of $(CH_3)_3N$) respectively.[176,177] The peaks at 808 and 810 are both $[M + Na]^+$ ions for the phophatidylcholines corresponding to fatty acid components of 18:0/18:2 and 18:1/18:0 respectively. The $[M + H]^+$ peak for 18:1/18:0 is detected at 788. Peak 832 is most likely $[M + Na]^+$ ion of the phophatidylcholine with fatty acid chain 18:0/20:4 and 16:0/22:4. Literature suggests that the 703 peak is the molecular ion peak of the sphingomyelin 16:0.[176]

Several metabolites, Table 3.1, were also identified in the low mass range of the phophatidylcholine spectrum. The mass peaks were compared to literature values.[178] This was expected, since serum is a biofluid and contains an abundance of metabolites.

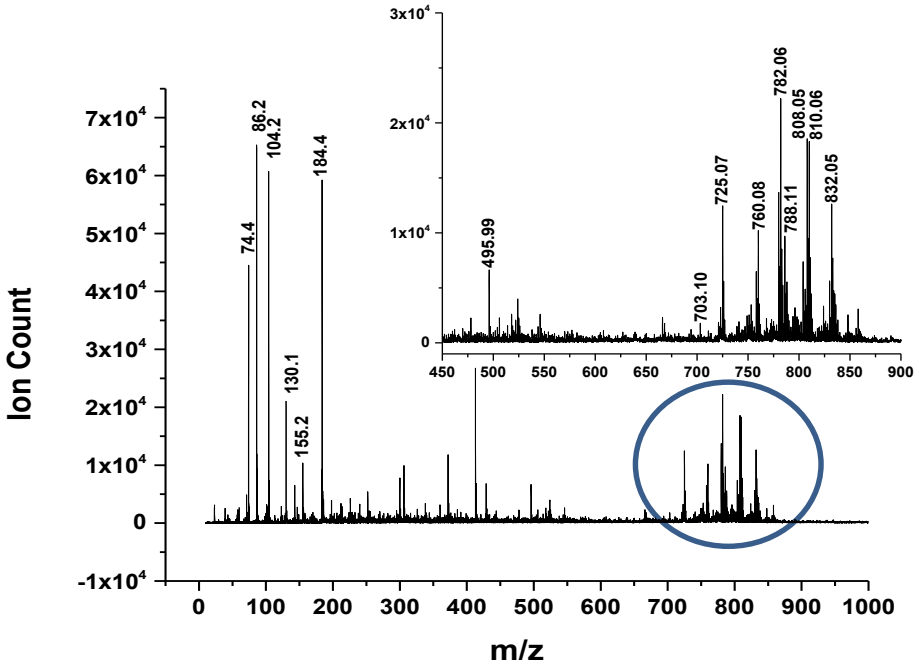

Figure 3.137. SMALDI-MS mass spectrum of metabolites and phosphocholines compounds detected in serum after treatment with hexane and 2-propanol. Inset is expansion of circled region with major phosphatidylcholine peaks.

Table 3. 1 Metabolites detected in pig serum, spectrum shown in Figure 3.17.

m/z	Compound
74	Glycine
86	Pyruvic Acid
104	Serine
130	Oxaloacetate
155	Histadine

3.3.6 Matrix Effect on Sulfatide Detection

We next used serum as a means to study the matrix effect of a biofluid on our detection of sulfatide biomarkers. That is, will the complex nature of the many matrix compounds in a biofluid such as serum mask the detection of a sulfatide biomarker at very low concentration? It was important that we answer this question, since SMALDI-MS would only be viable if it can detect biomarkers in the attomole level, the level at which sulfatides are of interest in diseased individuals.

Pig serum was spiked with standard pig brain sulfatide. Total lipids were extracted using hexane and 2-propanol, dried and reconsituted with chloroform: methanol, 2:1, as previously described. The spectra were then examined for the presence of the peaks associated with only the standard pig brain sulfatide, the 801 and 899 peaks. While the 882 peak, common to both the pig serum and brain, was again dominant, the unique 899 peak of the spiked standard was detected even at low concentrations.

The detection achieved with Si GLAD on our mass spectrometer, AB Sciex Voyager Elite MALDI (acquired in 2000), was in the low femtomole range, Figure 3.18 (a). The spectrum in Figure 3.18 (b) is of 4 femtomole spiked standard pig brain sulfatide. Other serum lipid peaks were also observed (not shown in spectrum). Detection in this range has implications for the applicability of SMALDI in biomarker studies. Glycolipids have been investigated as biomarkers in a wide range of diseases and in a wide range of biofluids and tissue types. In most cases, it is the change in concentration or the presence of certain sulfatide species that is an indication of the onset or progression of an illness. For tissue samples, the quantities of glycolipids are usually extracted and monitored as the mass of lipid per mass of tissue.[4] But for biofluid studies with blood, serum, urine, etc., the concentrations are usually monitored as moles of glycolipid extracted per ml of fluid.

For example, in a study of Type 2 diabetes[179] in pregnant women, phosphocholines were studied in the femtomole per ml range in serum. The serum

was first centrifuged, then filtered before lipid extraction with organic solvent. This extract was centrifuged and diluted prior to detection by ESI-MS. Kidney dysfunction in mice was investigated by monitoring picomole levels of sulfatide in serum and[114] a study of dementia monitored the change of sulfatide levels in cerebrospinal fluid at picomole level per ml.[137] For these last two studies, the sulfatides were separated from the serum samples by mixing with chloroform and methanol. The supernatant was discarded and the residue was dried and reconstituted, then detected by ESI-MS.

A recent MALDI study with the relatively new matrix, 9-aminoacridine,[142] has also been able to detect sulfatides in the high attomole range. The lowest detection of phospholipids from cellular lipid extract with nano-ESI-MS was 2.6 attomole[159] with a triple quadrupole mass spectrometer. The low femtomole detection on our MALDI TOF instrument is probably the best it can achieve given its age and therefore, the SMALDI-MS detection is comparable with some of the best detection currently available.

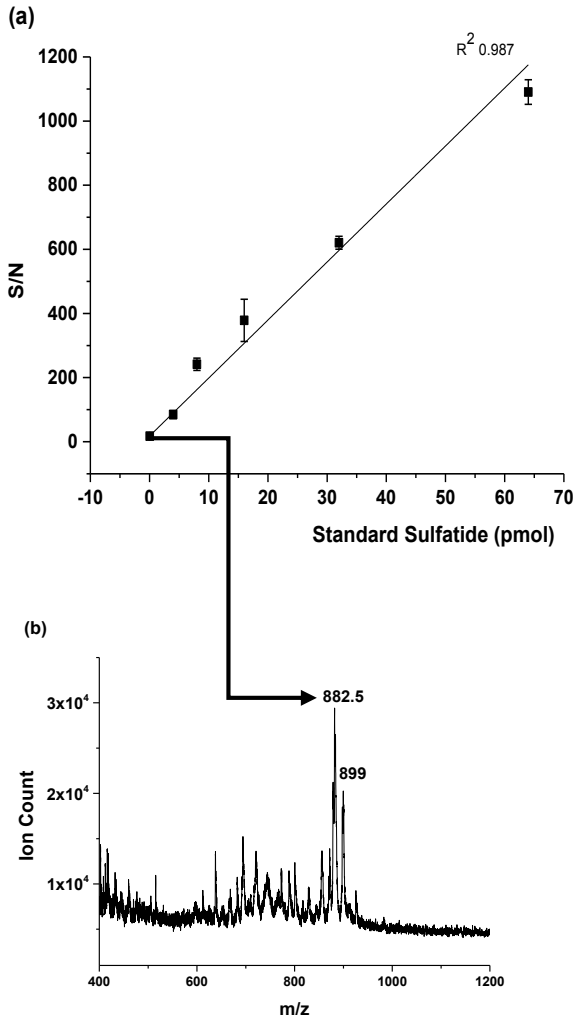

Figure 3.148. Limit of detection of standard sulfatide spiked in pig serum. (a) S/N vs amount of standard sulfatide and (b) SMALDI spectrum taken at 4 fmol sulfatide standard.

It is also important to note, that for the detection limits reported in most of the literature, the compounds of interest were first extracted from the tissue or biofluid with extraction solvents, undergoing some amount of sample clean up and concentration, prior to mass spectrometry detection. Our result is for the detection of the standard analyte in serum without extraction and concentration.

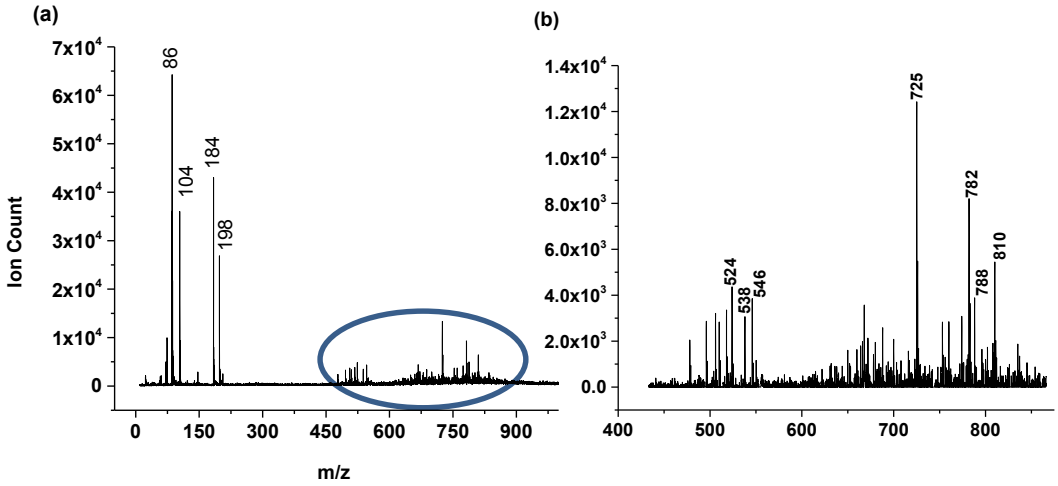

Figure 3.159. (a) Mass spectrum of serum washed by UTLC with chloroform: methanol (2:1, $^{V}/_{V}$) as the mobile phase and (b) expansion of highlighted region in (a).

3.3.7 Simplified Biofluid Sample Preparation with GLAD UTLC

We then wanted to test the proven UTLC ability of GLAD films[66-68,163] to simplify the sample preparation of serum prior to sulfatide detection. Instead of extracting the lipid metabolites from the serum by mixing, vortexing, drying, etc, then doing LDI-MS, the extraction and reconstitution solvents were used as the mobile phase on a spot of untreated serum. The resultant separated spots on the separation film were then simply tested by LDI-MS.

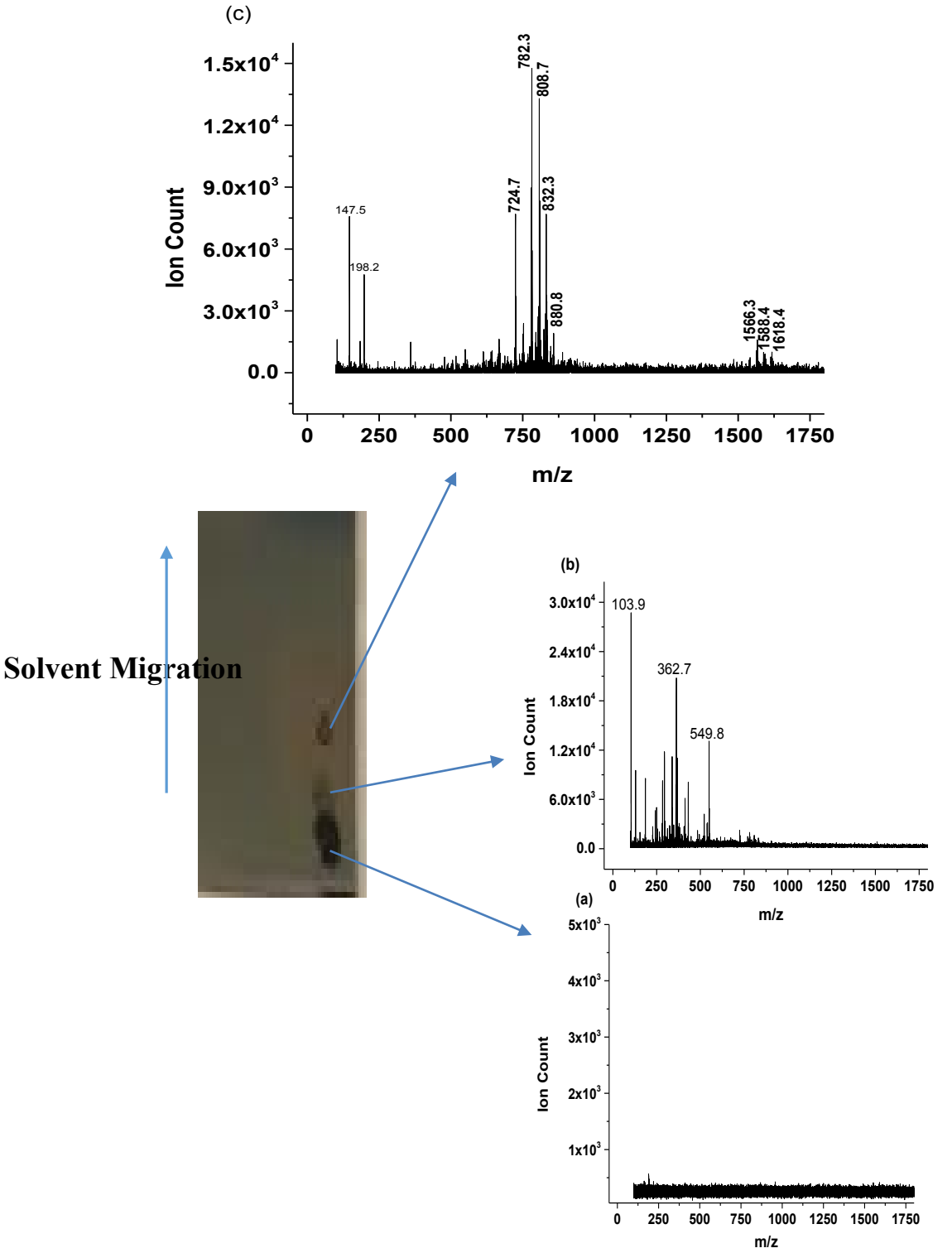

Figure 3.20. Sample clean-up on GLAD film followed by SMALDI-MS. Pig serum separated with Solvent C (a) Original spot, (b) first separated spot and (c) second separated spot with glycolipids.

In the first attempt, we used chloroform:methanol (2:1) as the mobile phase to wash an untreated spot of serum on silicon GLAD, Figure 3.19. This combination of solvents was chosen since it has been used as the separation mobile phase for lipid separation in HPTLC studies.[157] Separated spots were not observed after mobile phase was introduced, but some sulfatides and phophatidylcholines were detected (725 to 810) on the original spot. However, there was a significant amount of background and contaminants (at approximately 524-546). When the solvents, hexane and 2-propanol, used to extract lipids from serum, were used as the mobile phase, this proved to be more successful in separating out the contaminants from the spotted serum.

There was some amount of tailing of the original serum spot, but two distinct separated spots were also observed, Figure 3.20 (a). SMALDI spectrum of the original sample spot shows no peaks. This was due to the fact that since the mobile phase used for sample clean-up was non-polar, many of the water soluble salts and contaminants remained crystallized on the original spot, thus preventing the generation of peaks. The mass spectrum of the first separated spot, Figure 3.20 (b), shows that contaminants were isolated in this spot. In the second spot, the glycolipids-phophatidylcholines, sulfatides and sphingolipids were isolated and detected, Figure 3.20 (c). The peaks at 1558 and 1560 in the separated serum spectra may belong to other sphingolipids, possibly a 24 carbon fatty acid with two to three double bonds.[150]

If we compare the spectrum in Figure 3.20 (a), where GLAD UTLC was used in the sample preparation, with the spectrum in Figure 3.16, which used solvent extraction and reconstitution in the sample preparation, the ion counts for the 881 peak is approximately the same for both approaches. We were also able to detect, in Figure 3.20 (c), some of the major phosphocholine peaks observed in Figure 3.17 in the same spectrum, again with comparable ion counts, without the need for a different sample preparation step. Granted some of the peaks detected in the individual extraction methods did not appear in the UTLC treated spot, but further work on the mobile phase composition may remedy this in the future.

These preliminary results offer an alternative to the current HPTLC-SMALDI-MS separations and detection. This UTLC-SMALDI approach eliminates the need for a visualizing agent,[150,157] organic matrices and, does not restrict the laser choice to an IR laser.[156,157]

This precedent of using the established extraction solvents as the mobile phase on GLAD UTLC for sample clean up demonstrates that there is also great potential for the application of different extraction solvents, and TLC development solvents.[115,132,150,151,171] The separation of different classes of lipid compounds from biofluids on GLAD can be achieved, saving time and effort.

3.4 Conclusions and Future Work

Silicon SMALDI was able to detect some glycolipids that were not detected with MALDI-MS, specifically, the gangliosides GM3, GM1 and GD3. For the compounds that were detected by both MALDI and SMALDI, the quality of the spectra with SMALDI was superior to the MALDI spectra. For SMALDI itself, the SMALDI-MS taken in the negative ion mode produced mass spectra that are superior to the positive ion mode. This was especially evident with the sulfatide compound tested. Overall, the detection with SMALDI-MS was much simpler, since matrix selection was unnecessary, we were able to detect all the test compounds, which included several classes of glycolipids, on GLAD films.

The detection of standard ganglioside and sulfatide (within a real sample matrix, serum) was also achieved at low femtomole levels. This is promising for the application of SMALDI-MS as a high through put technique in biomarker studies, and the data in Figures 3.5 and 3.18 indicate that a quantitative response can be achieved. Diseases such as Alzheimer's disease, dementia, Type II diabetes, Tay Sach's, etc. all involve changes in glycolipid biomarkers in the nano to picomole range. This detection may also be improved with a more advanced mass analyzer to match the current MALDI method of sulfatide detection with 9-aminoacridine at the attomole level.[142]

The UTLC ability of GLAD films was also successful in isolating contaminants and glycolipids in serum prior to SMALDI – MS detection on the same film, eliminating the need for a lengthy extraction process. This sample preparation capability of GLAD films, in addition to its proven high level of SMALDI detection, clearly proves that the material is a high throughput, sensitive alternative for biomarker and metabolite studies.

The application of silicon GLAD films for both SMALDI-MS and sample clean up on the same film offers exciting avenues for future investigations. For example, the detection of other biomarker compounds, metabolites and drugs, at sufficiently low detection limits, in a variety of biofluids such as urine, saliva and blood by changing the migration solvents is promising for high throughput work.

Chapter 4

UTLC-SMALDI-MS

4.1 Introduction

This thesis looks at the applications of GLAD films, in this chapter, one interesting application that has been explored is ultra-thin layer chromatography (UTLC), using 1 μm thick silica or silicon films. Considering the high quality mass spectrometry we have achieved, it makes sense to consider combining these two methods, as the hyphenated UTLC-MS has seen interest over time. A brief review of the field follows.

4.1.1 Ultra-Thin Layer Chromatography

The first commercial UTLC plates were introduced in 2001 by Merck (Darmstadt, Germany). The Merck Ultra-Thin Monolithic plates consist of a 10 μm thick porous silica gel layer with mesopores in the range of 30 to 40 Å and macropores from 1 to 2 μm.[180,181] TLC plate layers are significantly thicker at around 250 μm. The major advantages of UTLC over thin layer chromatography TLC and high performance thin layer chromatography (HPTLC) include faster elution times, lower solvent consumption, higher sensitivity and lower detection limits.[180,181]

However, the same physical characteristics of the plates that offer advantages also lead to several drawbacks, most notably, reduced resolution and separation efficiency due to the shorter elution distances and higher R_F values because of the smaller overall specific adsorption surface area. Additionally, there are difficulties with incorporating UTLC plates with standard equipment designed for the more conventional TLC and HPTLC plates.

4.1.2 Hypenated UTLC-MS

Detection by mass spectrometry is especially useful when the identification of unknown compounds is necessary. It offers the advantage of greater specificity with MS/MS characterization. Until recently, MS detection in

TLC was an offline process, with the separated bands being removed from the TLC plate, the analytes extracted and then detected with a conventional mass spectrometer.[144,182]

One of the disadvantages of direct TLC-vacuum MALDI has been the risk of introducing plate materials such as particulates into the mass spectrometer, as well as peaks from the TLC materials that can show up in the spectra.[6,183] In a study that explored the combined UTLC-Atmospheric Pressure (AP)-MALDI vs UTLC-vacuum MALDI on commercial Merck monolithic plates, the AP MALDI was better than vacuum in terms of sensitivity for both eluted and non-eluted compounds.[184] The limits of detection achieved by spotting the analyte solution onto the surface of the commercial plates were in the picomole range for a S/N (signal to noise ratio) of 3 for AP MALDI. Sample preparation was also not straight forward. A matrix solution was needed and had to be applied with a special commercial sprayer. Additionally, a series of optimization experiments to determine the correct ratio of matrix molecules to analyte ions had be conducted for the UTLC plates. Matrix amounts lower or higher than the optimum, either reduced the sensitivity or increased the background respectively.

In a study by Kauppila et al.,[41] Merck UTLC plates were tested for UTLC (desorption electrospray ionization) DESI-MS coupling. A mixture of metabolites, acetylcholine, dobutamine, midazolam, verapamil, diazepam and testosterone were separated and detected. The limits of detection achieved by spotting the analyte solution onto the surface of the Merck plates were again in the picomole range for a S/N of 3. The authors measured the time required to scan the eluted plate with the DESI scanner from the sample spot to the solvent front relative to each analyte's ion abundance, which is not a common approach relative to reporting R_F values. It was therefore not possible to do a direct comparison of the UTLC results of that study with other work in terms of R_F values. They took this approach because unlike commercial TLC plates, which have a fluorescent indicator that uses a UV lamp as a means of separated spot identification, the Merck UTLC plates do not have a built in visualization function. The DESI method, while effective at picomole sample levels, requires

that several parameters be optimized prior to obtaining favourable results. As a result, DESI is not operator friendly. Considerable expertise is required to optimize the limit of detection, which is dependent on the choice of spray solution and the distance between the sprayer and the surface.

Combined UTLC ESI-MS has also been attempted.[153] The major difficulty with this technique has been coupling the UTLC plates with conventional ESI mass spectrometers. A TLC-MS interface by Camag (Muttenz, Switzerland) works well for extracting samples from HPTLC and TLC plates and transferring them to any LC-MS capable mass spectrometer, but does not couple well with UTLC plates. HPTLC is superior to TLC in terms of automation, separation time, resolution and control of the methodology.[185] UTLC, on the other hand, has thinner plates than both TLC and HPTLC, with even shorter migration distances and development times. This can lead to poorer resolution than the other methods.[180,181] The device extracts the samples from TLC plates by completely pressure sealing each spot with a piston head, using an appropriate solvent to remove the sample, and then transferring this eluent to the mass spectrometer. On UTLC plates, improper sealing between the piston head and the surface causes the solvent to overflow and swamp the plate. The researchers solved this problem by placing a methanol-washed filter paper over the spots to promote the pressure sealing. While this addressed the problem in this study, there might be sensitivity issues with this approach at very low concentrations of analyte. When the TLC-MS interface is used with the HPTLC and TLC plates for which it was designed,[186] the detection limit for small molecules is in the low and sub picomole range.[155,187]

What these hyphenated UTLC ESI-MS investigations highlight is that an additional interface and time consuming sample preparation is required prior to the mass spectrometry analysis, robbing the technique of a quick, simple, direct analysis.

Our collaborators in the M. Brett group have demonstrated that GLAD films made of SiO_2 can be employed for UTLC applications.[68-71,163] Our work

with the Brett group has clearly demonstrated that SMALDI with GLAD films made of Si[72] and Co (Chapter 2) can give femtomole detection limits when used with vacuum MALDI instrumentation. Clearly, a UTLC-SMALDI-MS approach could be attractive, given the good detection limits of SMALDI-MS and the effective UTLC performance of GLAD films. This chapter explores the suitability of Si for UTLC and SiO_2 for SMALDI-MS, in order to establish optimal performance in the combination of these two methods. The results obtained are encouraging, with separation distances and times on par with other UTLC methodologies, and detection limits on par with our previous SMALDI-MS studies.

4.2 Experimental

4.2.1 Mobile Phase Preparation

A mobile phase of isopropanol:hexane:ethyl acetate (6:2:2) was used to separate the mixture of carbohydrates. The peptide separation mobile phase was acetonitrile:ethylacetate:0.1% TFA (4:4:1:1). These reported mobile phases represent the final, optimized versions used for the separations achieved on silica GLAD films reported in the Results (Section 4.3).

4.2.2 UTLC Separation

20 minutes before separation, 0.5 ml of mobile phase was dispensed into both the conditioning trough and the reservoir to saturate the vapour phase in the chamber. A porous glass frit was then placed into its holder in the reservoir and allowed to saturate, refer to Figure 4.1. The mixture of analytes to be separated was spotted 1 mm from one end of the GLAD film (2.5 cm X 2 cm) with a 1/4 in., 32 gauge blunt end stainless steel tip needle, which dispenses approximately 10 nl of solution.

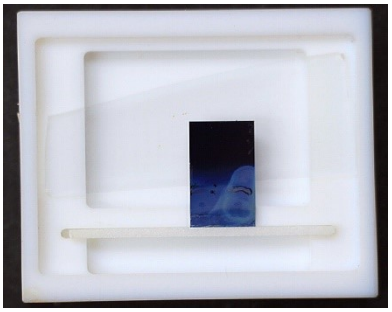

Figure 4.1. Horizontal UTLC development chamber with silica GLAD film.

The spot was allowed to dry for approximately three minutes. The mixture of carbohydrates spotted contained, 35.5 pmol ribose, 45.6 pmol sucrose, 50.4 pmol 498 MW carbohydrate and 48.8 pmol methyl galactopyranoside. The mixture of peptides spotted contained 38.5 pmol angiotensin I, 48.7 pmol angiotensin II, 55.3 pmol bradykinin and 50.3 pmol verapamil.

Prior to separation, an additional 0.5 mL of mobile phase was added to the reservoir. The GLAD film was then placed face up, horizontally between one edge of the porous glass frit and a piece of glass. The glass spacer was used to keep the film from moving. The frit functioned to wick mobile phase to the film in a controlled manner. A glass cover was immediately placed over the entire separation chamber while the UTLC separation progressed. The separation chamber was kept in a fume hood throughout the process.

We used horizontal development for our UTLC. Vertical development can suffer from longer development times and hence evaporation of components of the mobile phase before the separation is complete.[153] To maintain reproducible mobile phase migration, the gas phase in the developing chamber had to be saturated with mobile phase for 20 minutes prior to separation. This limited the uneven adsorption and desorption of the mobile phase from the film bed. For our ultra-thin GLAD films, this pre-saturation step also minimizes the risk of the mobile phase evaporating into the chamber from the film during separation.

4.2.3 Mass Spectrometry

Mass spectra were obtained using an AB Sciex Voyager Elite MALDI TOF instrument with a pulsed N_2 laser (wavelength 332 nm) at a repetition rate of 3.0 Hz. Spectra were acquired in positive ion mode using delayed ion extraction. Grid voltage was set at 74% and extraction delay time was 250 ns. Each spectrum consists of 100 shots. After UTLC separation, GLAD films were secured to a modified MALDI plate using double sided adhesive tape, refer to Figure 2.1 in Chapter 2.

4.2.4 Calculation of R_F Values

R_F values were calculated by dividing the distance from the original spot to the migrated position by the distance from the original spot to the solvent front. This is illustrated in Figure 4.2.

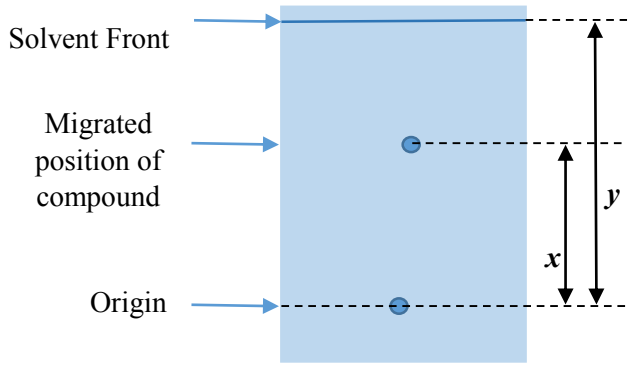

Figure 4.2. Diagram of UTLC plate with measurements taken for the calculation of the R_F value.

4.2.5 Carbohydrate Visualization

The visualization solution was prepared by dissolving 20 mg of naphthoresorcinol in 10 mL of ethanol with 0.2 mL concentrated sulfuric acid.[188] This solution was placed into the separation as described above for mobile phase and used to coat the already separated carbohydrate on UTLC plates. The plates were then left to dry in a fume hood for 10 minutes for colour development.

4.3 Results and Discussion

4.3.1 LDI-MS Measurement

Much of the UTLC[66,68,70,189] and LDI-MS[72] work with GLAD materials has been conducted separately on silica and silicon films, respectively. The previous UTLC experiments were with silica films and lipophilic dyes, while the LDI-MS with metabolites and peptides was performed on silicon. Our first task in attempting to hyphenate the two techniques on GLAD was to determine which material type, silicon versus silica, would produce the optimal results for both separation and mass detection.

Another parameter which had to be fine-tuned was the film thickness. From our own study of the parameters that affect LDI-MS, Section 2.3.3, it was determined that the optimal film thickness of silicon and cobalt films was 250-500 nm, with the sensitivity dropping with increasing thickness. However, UTLC performance was better on thicker films, between 5-7 μm.[87] Thinner films suffer from overload, long development times and poor resolution due to the lack of sufficient stationary phase to provide both pore spaces and functional groups for retention. For the selection of the optimum thickness, it was necessary to keep in mind that the thickness directly determines the largest sample volume that can be applied without overloading the film, and hence determines the LDI sensitivity and the UTLC resolution.

GLAD films tend to clump and form defined spots where sample molecules are deposited.[87] They also display the same tendency with analyte

molecules that have migrated to a spot, as with our UTLC separations. This means that the migrated spots do not require a visualization reagent for identification and isolation of the separated spots. This offers a great advantage with the elimination of a step that is required for all of the current, conventional methods. TLC methods use UV densitometry for the fluorescently embedded plates, while more complicated scanning methods are used for the Merck UTLC plates,[41] which are not fluorescently labelled, but provide no means of definite spot location. However, excessive clumping can lead to poor SMALDI performance,[89] so there is a balance as to the usefulness of this effect.

4.3.2 Film thickness for UTLC Separation

We measured the LDI responses of both silica and silicon films at different thicknesses to determine the maximum thickness we could use for UTLC that would still yield mass spectrometry results. We chose to deposit the silicon films onto conductive Indium Tin Oxide (ITO) glass substrates instead of silicon. The silicon deposited onto silicon substrates in our previous work[72] and in Chapter 3, produced dark brown, opaque films, which made the identification of separated spots difficult. With the ITO backing on the other hand, the films are a light yellow colour and semitransparent, making spot identification simple. Silica films deposited onto silicon substrates are off white in appearance, which did not make spot identification a problem after clumping.

The 1 μm Si-ITO films gave the best S/N out of the three thicknesses tested, Figure 4.3. The performance dropped off significantly as the thickness of the films were increased. On the other hand, silica GLAD films tested with these same compounds, at the same concentrations, did not produce a signal beyond 500 nm thickness, Figures 4.4, 4.5 and 4.6. Increasing the laser fluence did not have the desired effect of improving the performance, since the surface of the film became etched and the spectra were dominated by contaminant peaks.

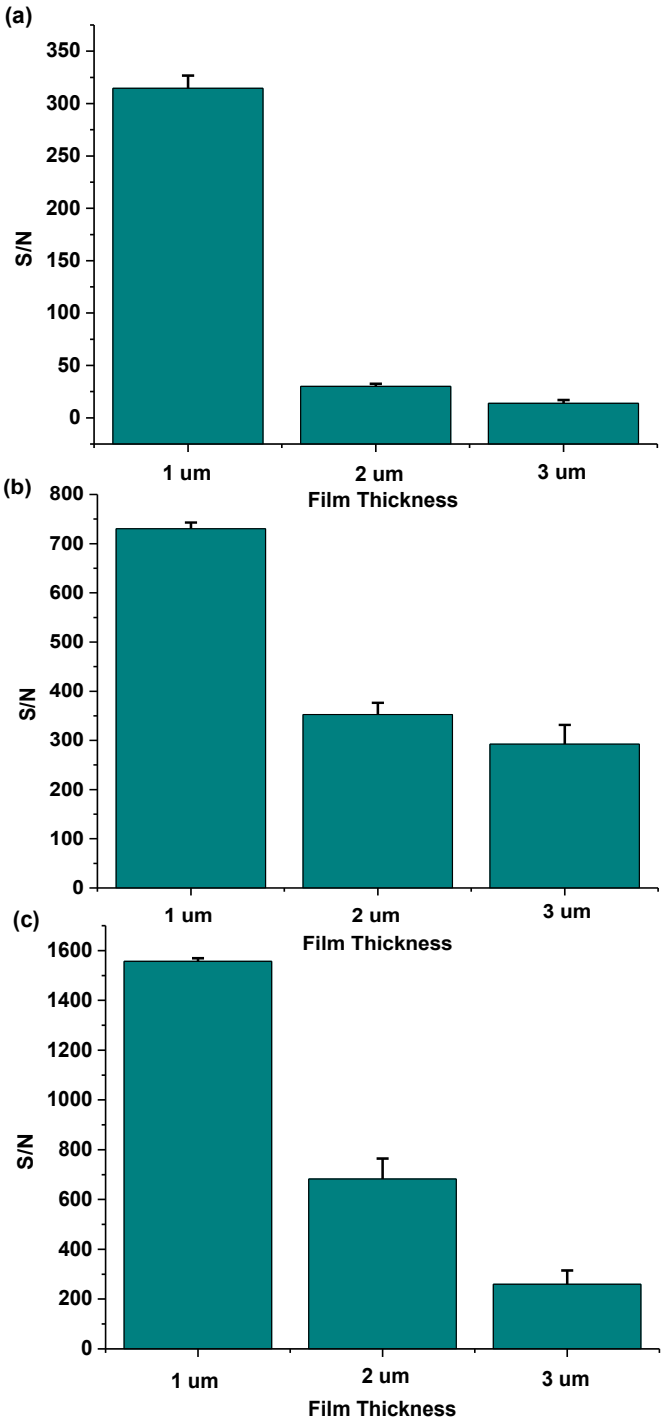

Figure 4.3. Determination of the optimum film thickness for SMALDI-MS of Si GLAD films on ITO glass substrate. S/N of (a) 38.5 pmol angiotensin I, (b) 47.8 pmol angiotensin II and (c) 55.3 pmol bradykinin on Si-ITO GLAD films taken at laser fluence 2000 a.u.

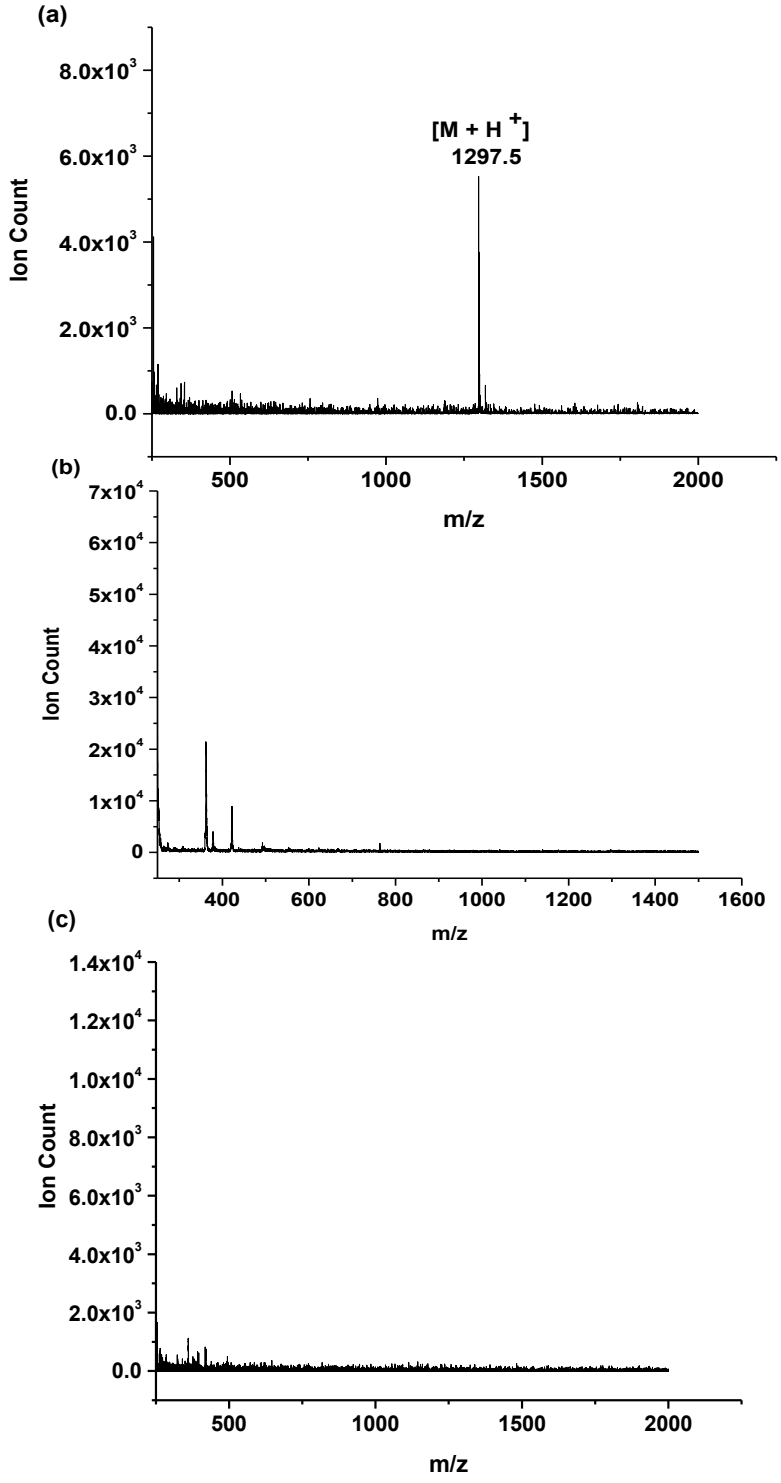

Figure 4.4. Determination of the optimum film thickness for SMALDI-MS of silica GLAD films on ITO substrate. Mass spectrum of 38.5 pmol angiotensin I on (a) 500 nm, (b) 1 μm and (c) 5 μm silica taken at laser fluence 2700 a.u.

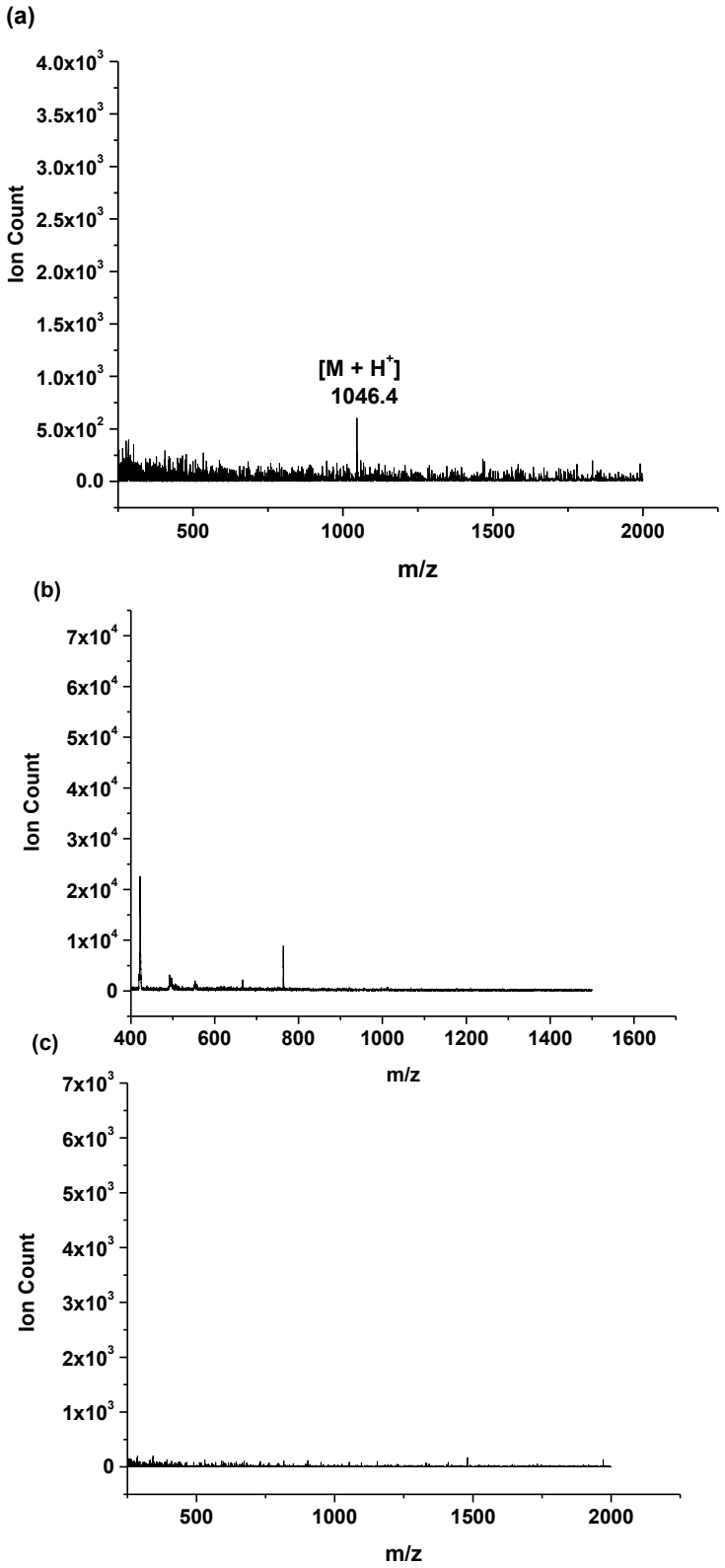

Figure 4.5 . Determination of the optimum film thickness for SMALDI-MS of SiO_2 GLAD films on ITO substrate. Mass spectrum of 47.8 pmol angiotensin II on (a) 500 nm, (b) 1 μm and 5 μm SiO_2 taken at laser fluence 2700 a.u.

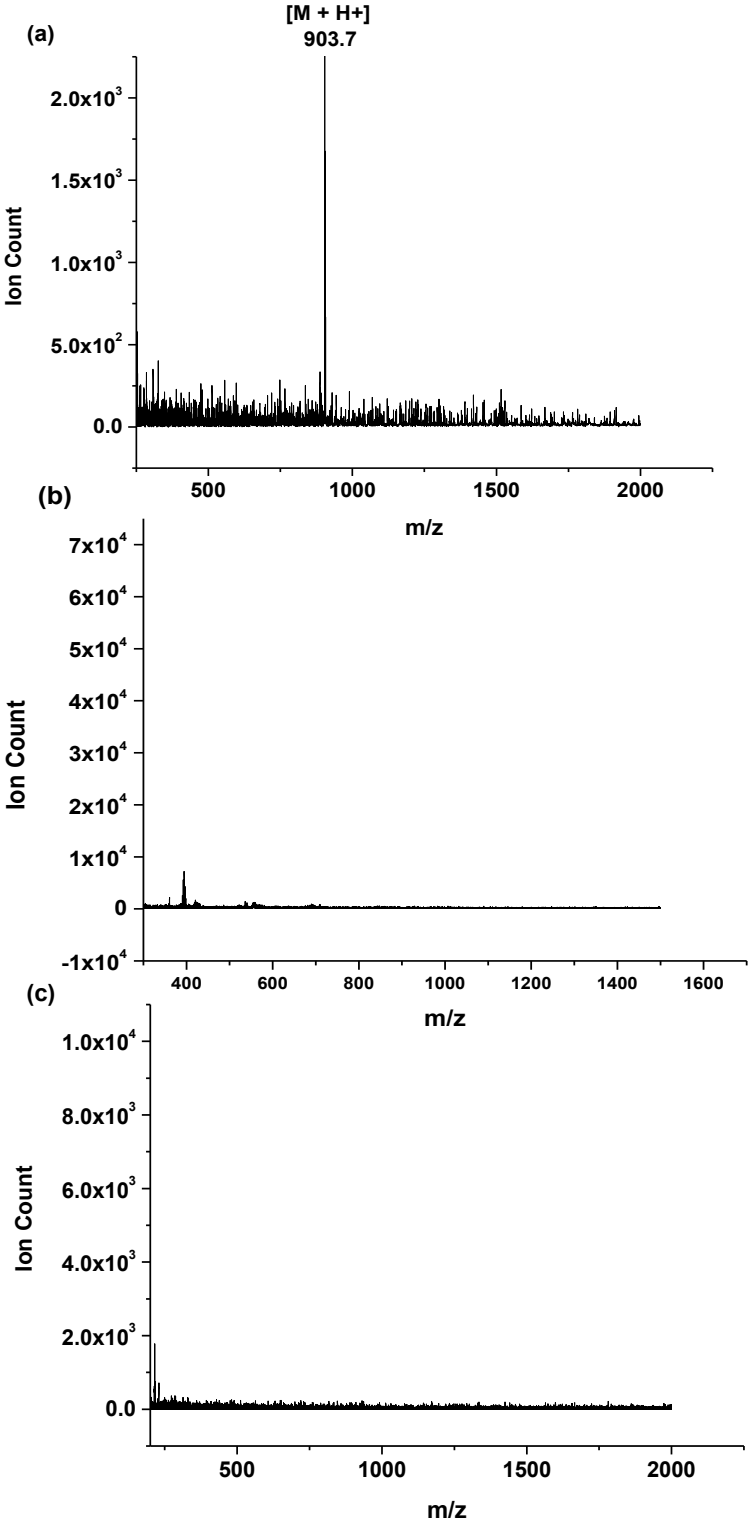

Figure 4.6. Determination of the optimum film thickness for SMALDI-MS of silica GLAD films on ITO substrate. Mass spectrum of 55.3 pmol bradykinin on (a) 500 nm, (b) 1 μm and (c) 5 μm SiO_2 taken at laser fluence 2700 a.u.

We found that the choice of solvent can have an effect on the quality of the spectra. Two common separation solvents, toluene and acetonitrile, were chosen for testing. When the samples were diluted in a mixture of water and toluene or water and acetonitrile, instead of 50%:50% water and methanol, the results were much different. Peaks were observed on the 1 μm silica films, Figure 4.7 (a). Even on the 3 μm films, we were able to detect a peak with acetonitrile, but not with toluene, Figure 4.7 (c) and (d). Overall, acetonitrile produced the greater enhancement in signal.

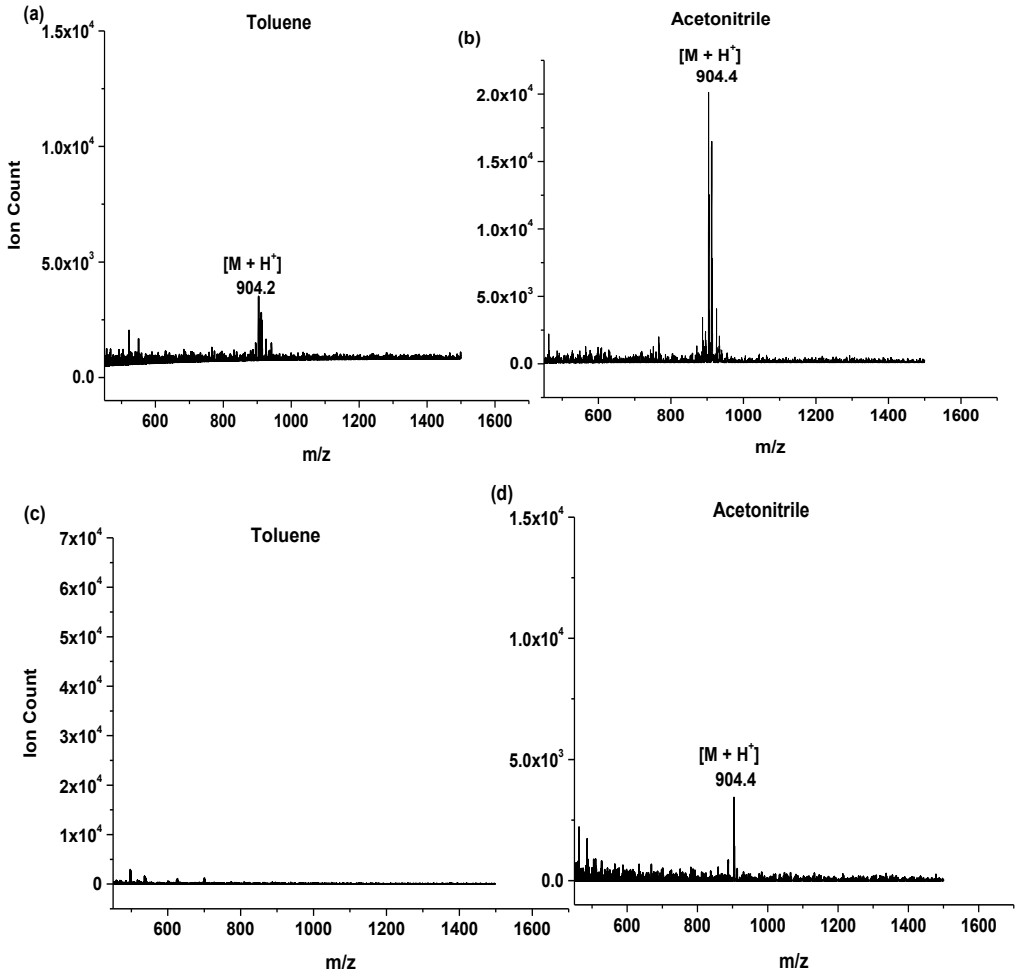

Figure 4.7. Effect of solvent on SMALDI-MS with silica GLAD films. Mass spectrum of 0.55 pmol bradykinin on 1 μm silica in (a) toluene, (b) acetonitrile and on 3 μm in (c) toluene and (d) acetonitrile taken at laser fluence 2700 a.u.

Silicon films were able to generate signals at all the thicknesses tested, Figure 4.3, even at 5 μm, while silica films only gave signals at 1 μm, Figures 4.5 and 4.6. Comparing the S/N, ion counts and the general quality of the spectra of silicon and silica at 1 μm also showed silicon to be superior to silica for LDI. However, based on the positive results for LDI on both silica and silicon GLAD films at 1 μm, we chose to further investigate UTLC performance with both materials at this thickness.

4.3.3 UTLC-SMALDI-MS Performance of Silicon films

Retention on silicon films tended to be poor and compounds migrated as lines rather than completely resolved spots, despite efforts to adjust the mobile phase using the PRISMA model.[190,191] However, the bands were distinct, with very little tailing. In order to quickly and easily identify the separated bands of carbohydrates, we used the visualization agent naphthoresorcinol, structure in Figure 4.8, which develops specifically coloured carbohydrates after UTLC.[188,192]

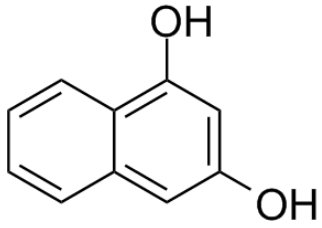

Figure 4.8. Structure of naphthoresorcinol (1,3-Dihydroxynaphthalene).

The coloured pigments are formed when the by-product of naphthoresorcinol condensation reacts with the carbonyl groups of sugars[193-195]. For a mixture of three carbohydrates, we were able to identify three distinct colour bands corresponding to each sugar; ribose-yellow, 498 MW carbohydrate - pink and β-cyclodextrin-blue.

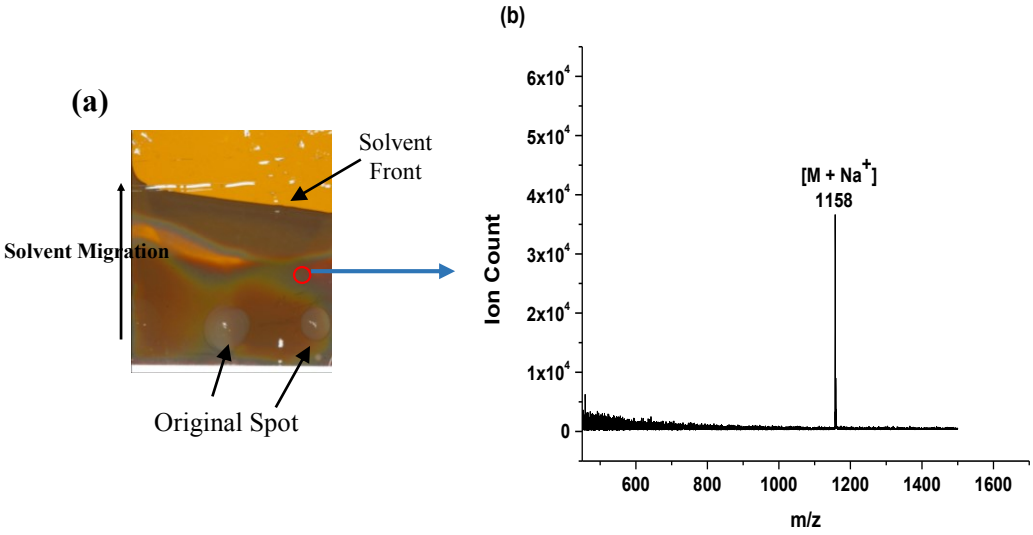

Figure 4.9. (a) UTLC separation of ribose, 498 MW carbohydrate and β cyclodextrin on 1 μm thick Si on ITO-glass substrate following development with naphthoresorcinol and (b) SMALDI spectrum of β cyclodextrin acquired from (a) taken at laser fluence 2000 a.u.

However, one of the drawbacks of redeveloping the plates with naphthoresorcinol is that the separated bands were pushed back from the front and spread in all directions horizontally along the film, ruining the separation, Figure 4.9 (a). To better contain the mobile phase and bands for a more uniform separation, we devised films with narrow strips of GLAD columns, Figure 4.10 (b), which we called the "zebra" chip.

A PDMS template (master wafer shown in Figure 4.9 (a)) was used to remove portions of the GLAD film from the substrate, leaving behind only narrow strips of GLAD columns, Figure 4.9 (b). Figure 4.9 (c) shows an expansion of one strip, highlighted in red in (b) and the separation of β cyclodextrin and 498 MW carbohydrate using the zebra technique. If we compare Figure 4.9 (a) to Figure 4.10 (c), the zebra strips did managed to contain the lateral spreading of the separated lines, for a better separation overall.

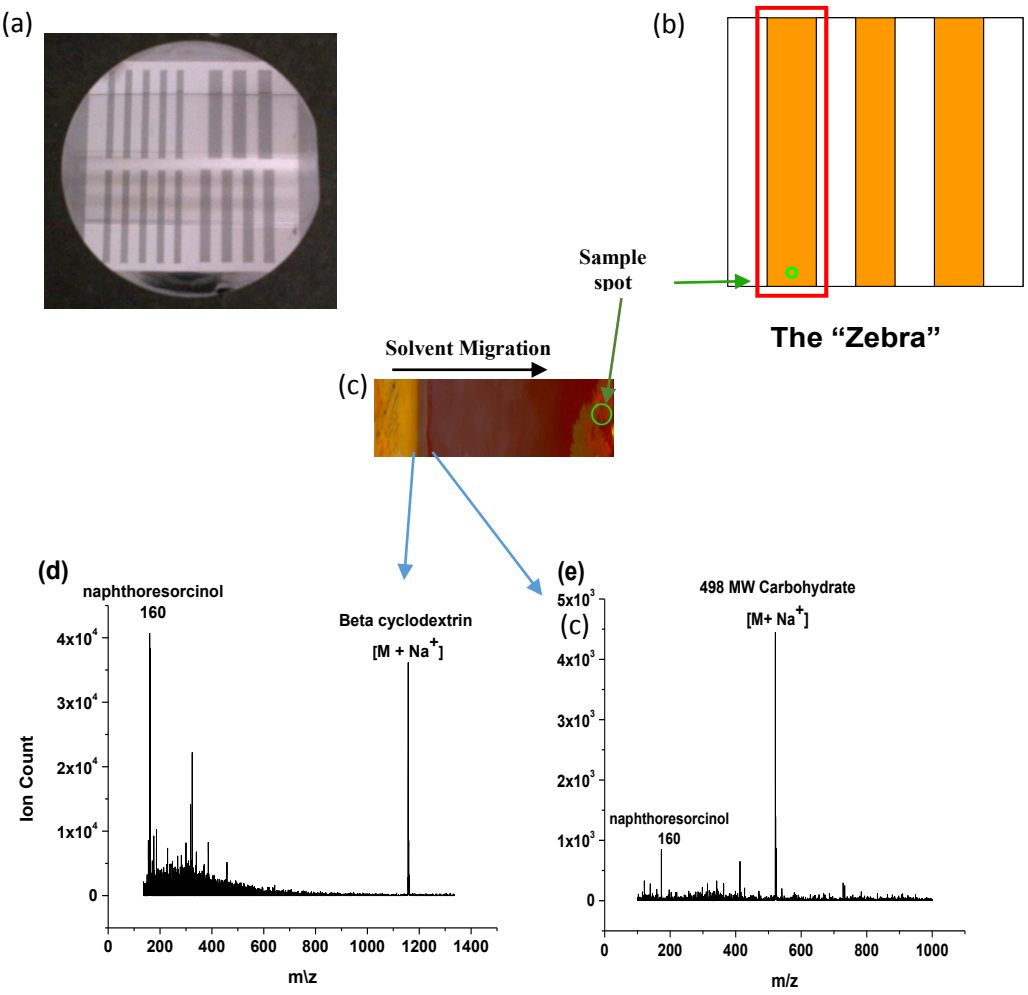

Figure 4.10. (a) Master wafer of zebra template, used to remove portions of GLAD film, (b) Zebra of 1 μm Si-ITO GLAD film created with zebra template, (c) section of film from zebra in shown in (b) after UTLC, and mass spectrum of (d) β cyclodextrin (blue) and (e) 498 MW carbohydrate (pink) taken from film shown in (c). Laser fluence of 2000 a.u. used for spectra.

4.3.4 UTLC-SMALDI-MS Performance of Silica films

Attempts to achieve resolved spots rather than lines were more successful with silica films than with the previously described silicon, Section 4.3.3. Despite the significant tailing for β cyclodextrin, Figure 4.11, the first attempt at separating a mixture of just two carbohydrates with a mobile phase of isopropanol:ethyl acetate (1:1), was promising, with one completely resolved spot for glucose.

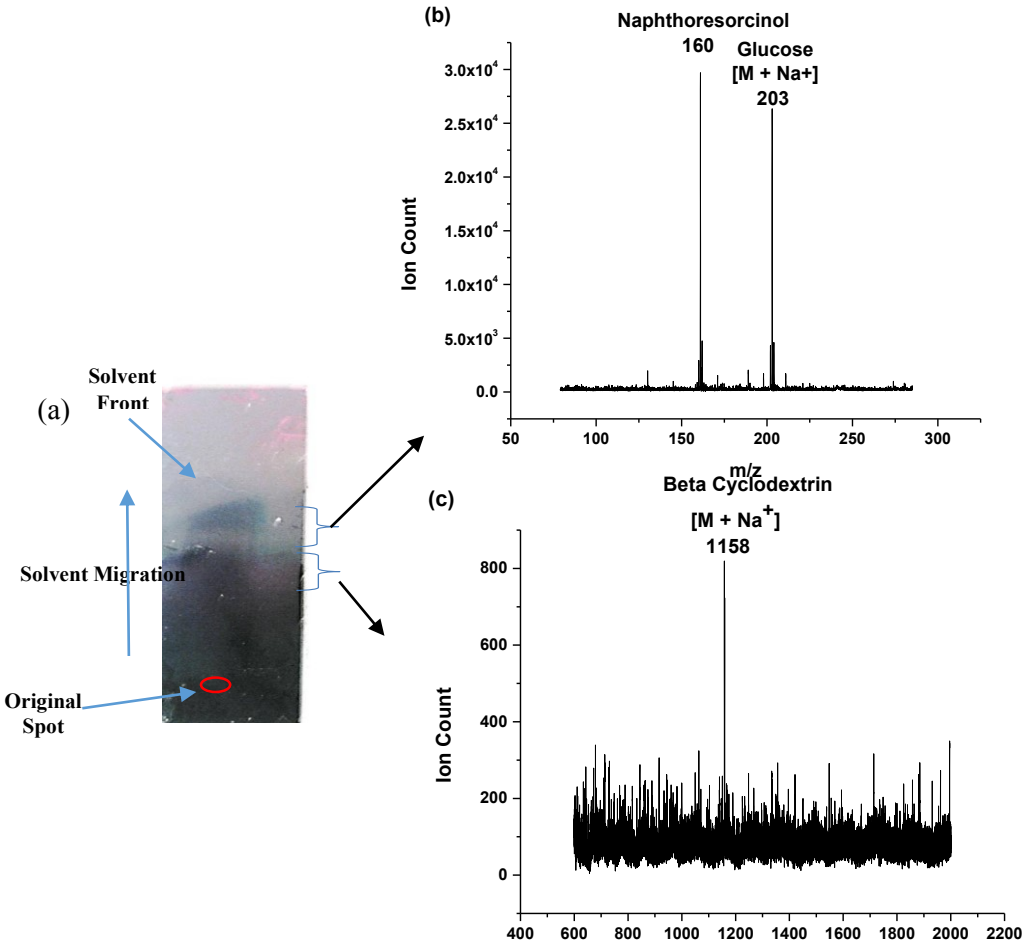

Figure 4.91. (a) UTLC separation of glucose and β cyclodextrin on 1 µm silca, SMALDI spectrum of (b) taken from bands shown in (a) taken at laser fluence 2700 a.u.

Initally, naphthoresorcinol was used with silica films, to clearly determine the extent of tailing, by observing the portions of the film that were stained. Later, as the resolution was improved, this step became unnecessary.

These silica films were also more responsive to changes in the composition of the mobile phase than silicon films. Systematic adjustments to the strength of the mobile phase produced marked improvement in the separation.

4.3.5 Elution on Silicon vs. Silica GLAD

Separation on silica GLAD did not follow the elution order one would expect for normal phase chromatography (stationary phase is polar, like silica GLAD), where the least polar analytes elute first and the more polar compounds are highly retained and elute last. Rather, the elution on GLAD films tended to follow a more size based order, with the smaller molecules eluting first, Figures 4.12 and 4.14.

We conclude that the elution order is mostly influenced by the macroporous/mesoporous nature of the GLAD films and to a lesser extent, by molecular interactions of the solutes, solvents and the functional groups on the surface of the films (stationary phase). For GLAD films deposited with an oblique angle of 87^{o}, the dominant spacing between columns is 85 nm, but ranges from approximately 50 to 250 nm.[86]

Retention was difficult to achieve with 1 μm silicon films and over all, the migration of mobile phase tended to be rapid. The fabrication procedure for GLAD films is highly controllable and reproducible, and in terms of structure, 1 μm silicon and 1 μm silica films are identical. Therefore differences in both solute and solvent retention are most likely due to the differences in the chemical nature of silicon and silcia GLAD. The silicon films have fewer silanol groups for interactions as compared to silica and are more likely to consist of a mixed SiO_x oxide on the surface, with a wide range of surface chemistries and high chemical reactivity.[196-199]

The difficulty with retention on silicon films was the main reason why we concentrated our efforts on 1 μm silica films for hyphenation of UTLC-SMALDI-

MS. We first tested the separation of a mixture of carbohydrate compounds - 35.5 pmol ribose, 45.6 pmol sucrose, 50.4 pmol β cyclodextrin and 48.8 pmol methyl galactopyranoside, Figure 4.12. The final adjusted mobile phase was isopropanol:hexane:ethyl acetate (6:2:2) and the R_F values reported in Table 4.1 were calculated after a development time of 40 seconds. This was the minimum amount of time required for the spots to completely resolve on the film, as seen in Figure 4.12 (a).

For a mixture of peptides and a metabolite - 38.5 pmol angiotensin I, 48.7 pmol angiotensin II, 55.3 pmol bradykinin and 50.3 pmol verapamil, Table 4.2, the mobile phase was acetonitrile:ethylacetate:0.1% TFA (4:4:1:1). The optimum separation time for completely resolved spots, Figure 4.14 (a), for this mixture was 75 seconds. The larger size of these compounds, Figures 4.13 and 4.15, and the apparent size-dependent nature of the separations on GLAD films probably influenced the longer separation time when compared to the carbohydrates.

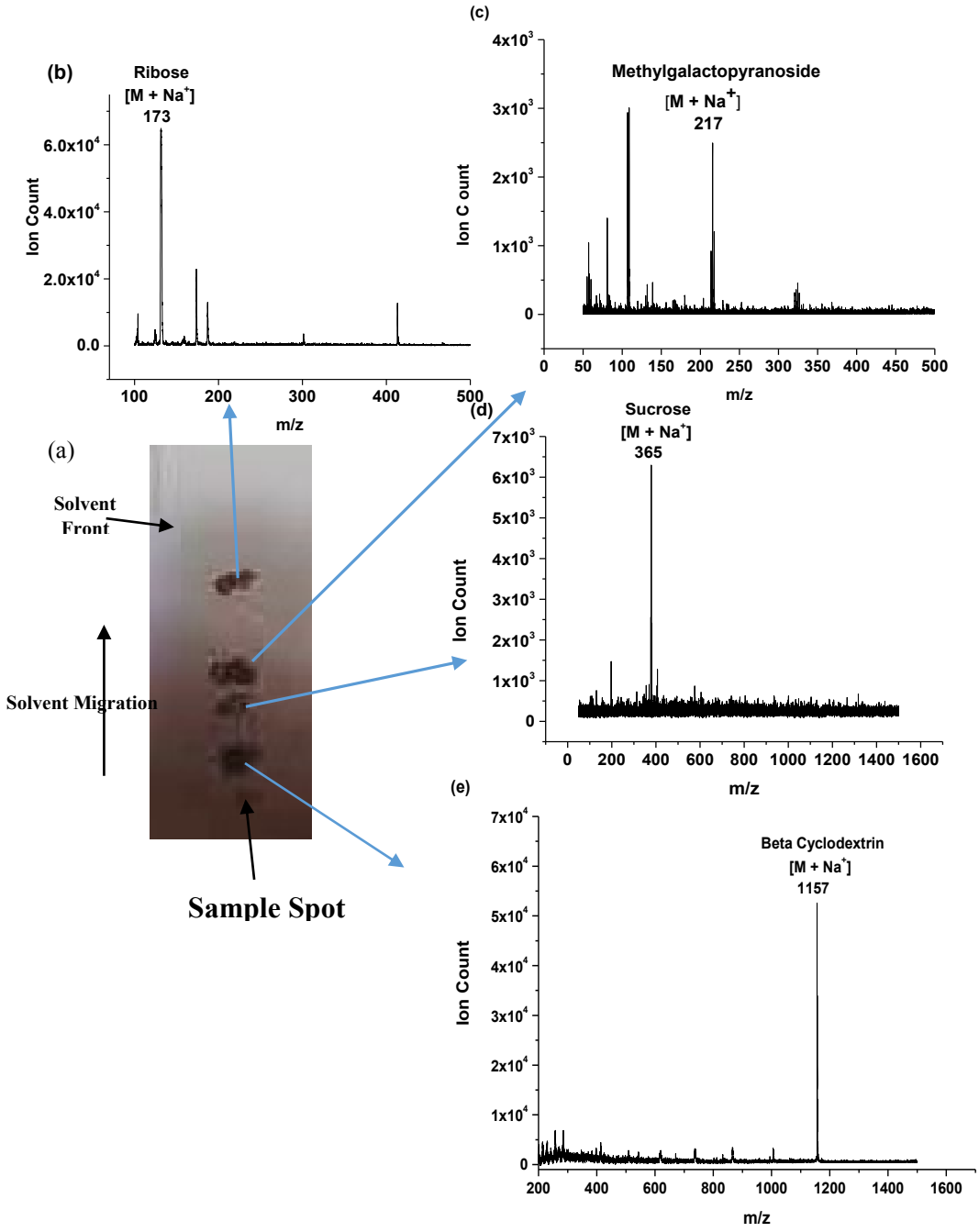

Figure 4.102. UTLC SMALDI-MS of a mixture of carbohydrates. (a) 1 µm silica GLAD film used for UTLC, mass spectra obtained from each spot following UTLC, (b) ribose, (c) methylgalactopyranoside, (d) sucrose and (e) β cyclodextrin taken at laser fluence 2700 a.u.

Table 4.1. R_F values and signal to noise ratios for carbohydrate compounds, 35.5 pmol ribose, 45.6 pmol sucrose, 50.4 pmol β cyclodextrin and 48.8 pmol methyl galactopyranoside.

Compound (Sep. Time 40)	R_F	S/N
β cyclodextrin	0.14 ± 0.007	314 ± 23.9
Methylgalactopyranoside	0.18 ± 0.008	46 ± 8.55
Ribose	0.21 ± 0.006	159 ± 21.76
Sucrose	0.43 ± 0.045	197 ± 39.43

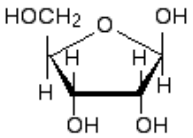

Ribose

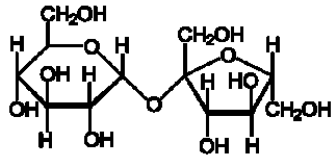

Sucrose

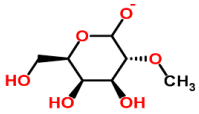

Methyl - galactopyranoside

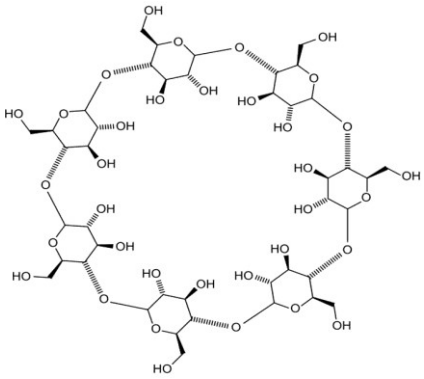

Beta Cyclodextrin

Figure 4.113. Structure of carbohydrates separated and detected with UTLC-SMALDI-MS.

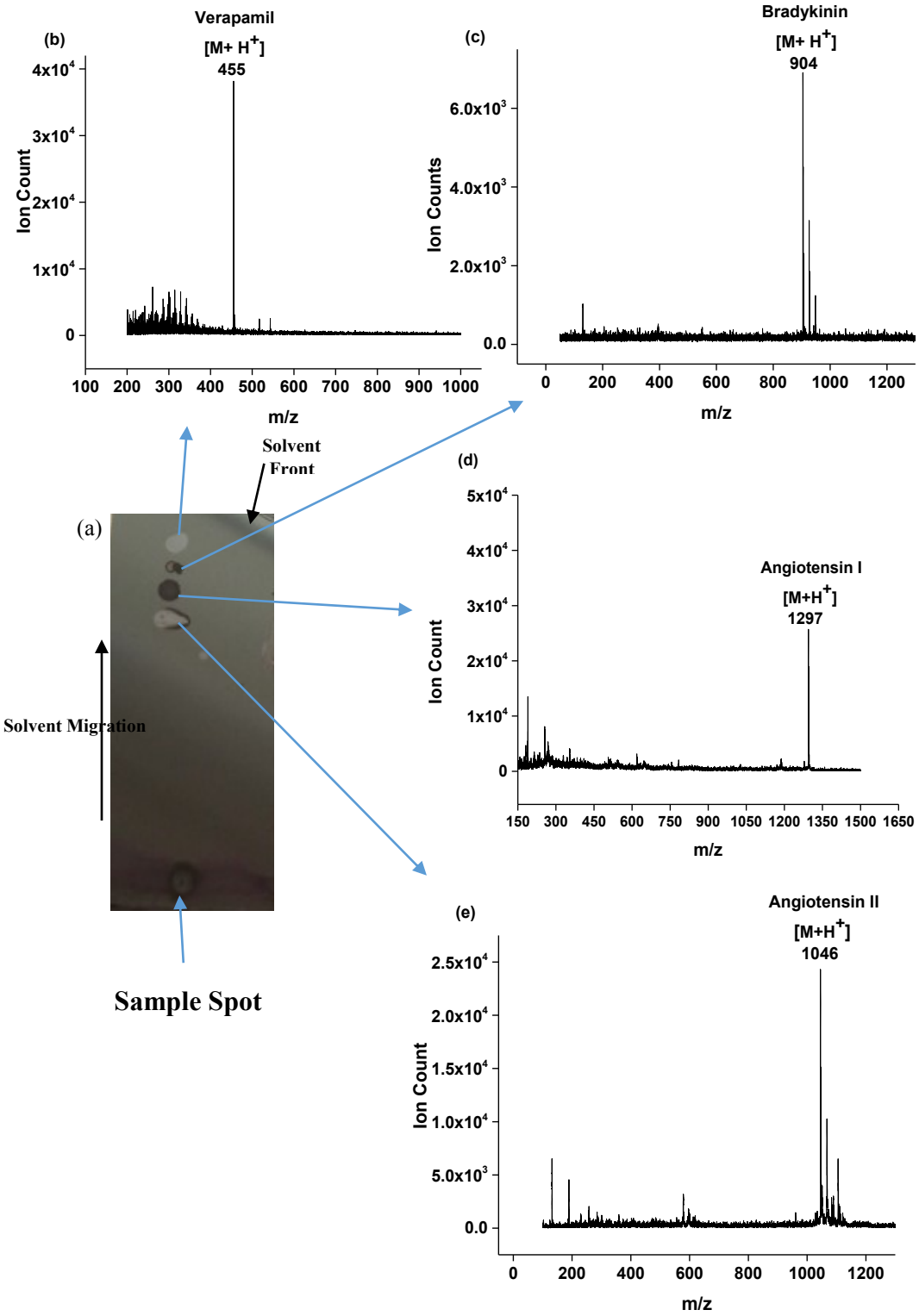

Figure 4.124. UTLC SMALDI-MS of a mixture of peptides and a metabolite. (a) 1 µm silica GLAD film used for UTLC, mass spectra obtained from each spot following UTLC, (b) verapamil, (c) bradykinin, (d) angiotensin I and (e) angiotensin II taken at laser fluence 2700 a.u.

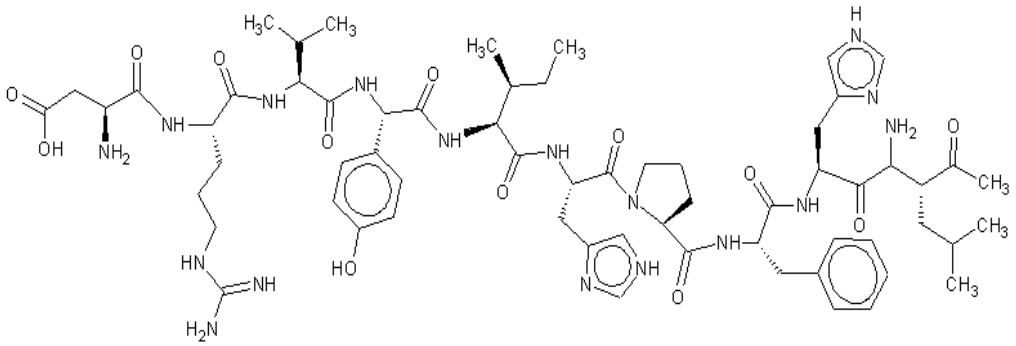

Angiotensin II

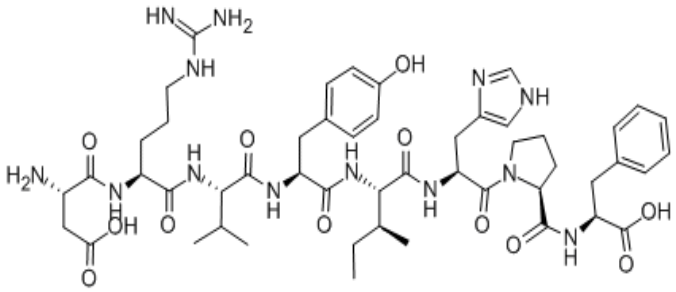

Verapamil

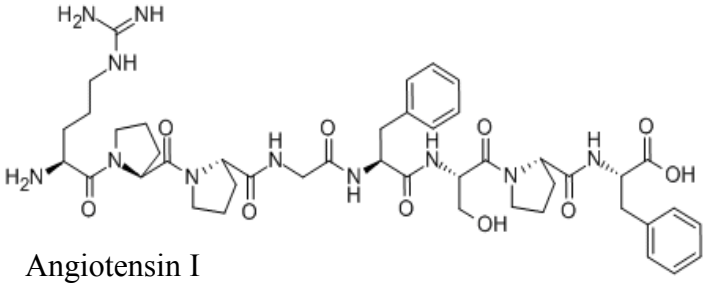

Angiotensin I

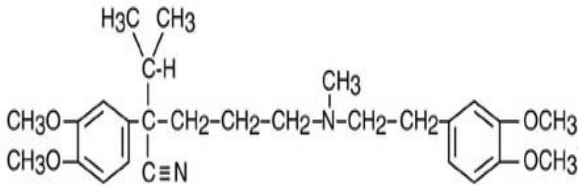

Bradykinin Fragment 1-8 acetate salt hydrate

Figure 4.135. Structures of compounds separated and detected with UTLC-SMALDI-MS.

Table 4.2. R_F values and signal to noise ratios for peptides, 38.5 pmol angiotensin I, 48.7 pmol angiotensin II, 55.3 pmol bradykinin and 50.3 pmol verapamil.

Compound (Sep. Time 75 s)	R_F	S/N
Verapamil	0.29 ± 0.007	168 ± 34.1
Angiotensin II	0.72 ± 0.017	254 ± 22.21
Angiotensin I	0.45 ± 0.018	255 ± 14.84
Bradykinin	0.66 ± 0.023	140 ± 32.12

The mass spectra generated from the resolved spot served to quickly identify each compound, and were generally free of major background peaks. This offers a significant advantage in cases where mixtures of unknown compounds are being studied and it might not be practical to have standards on hand for band comparison and identification. As mentioned before, once the mobile phases had been correctly adjusted, there was no need to use naphthoresorcinol for visualisation or to track tailing.

Both the separation times and the R_F values for our two groups of compounds are well within the range reported for other UTLC methods.[181,200,201] Separation and detection at the picomole level was also in keeping with other hypenated UTLC-MS techniques.[41,184] However, on closer comparison with these other studies, we have found that our results are superior. The estimated detection limit of the eluted compounds in our study, at a S/N of 3, ranges from 0.5-1.1 pmol; for verapamil it is 0.9 pmol. In the study of UTLC plates hyphenated to AP-MALDI,[184] the LOD for verapamil is 1.3 pmol. However, this is the lowest detection limit achieved out of the seven compounds tested, without verapamil, the LOD range jumps to 4.8-300 pmol, which is significantly higher than our results.

The subpicomole detection with HPTLC plates hypentated to ESI-MS was not matched with UTLC-SMALDI-MS.[155,187] We recommend that UTLC separations on silicon GLAD films be revisited, since silicon films have superior SMALDI-MS sensitiviy in the femtomole to attomole range[72] and this could be extended to the hyphenated UTLC-SMALDI-MS technique. It might also be possible to lower the limit of detection with SMALDI-MS with a more sensitive mass spectrometer.

UTLC-SMALDI-MS is also a lot simpler and straight forward compared to the combined UTLC ESI-MS methods attempted.[69,71,153] The technique does not require additional commerical interface equipment to bridge the UTLC and mass spectrometry functionalities. Also of note is the much shorter separation time and the smaller volume of development solvent required for peptide separation with our GLAD films compared to UTLC ESI-MS[153]; 1 mL and 1.25 minutes compared to 4 mL and 6.5 minutes respectively.

4.4 Conclusions and Future Work

One μm silica GLAD films proved to be the ideal combination of material type and film thickness for hyphenated UTLC-SMALDI-MS of peptides and small carbohydrates. The R_F values and separation times are comparable to other UTLC methods. However, it has also been demonstrated that the eluion order for the separations is size based.

Our matrix free SMALDI-MS approach, performed on the same film following the separation, also eliminates the need for additional interface equipment, standards and visualization methods for the identification of separated compounds.

We recommend that the combined UTLC-SMALDI-MS ability of silicon GLAD films be further investigated. Films of this material type has a proven record of superior LDI- MS performance when compared to films made of silica. The limit of detection for separated analyte compounds could therefore be potentially lower with silicon in future investigations.

Chapter 5

Tissue Imaging

5.1 Introduction

Mass spectrometry imaging (MSI) has been gathering momentum as a tool for providing holistic information from tissue samples.[134,202-206] It combines individual molecular distribution with the spatial orientation of the tissue sample to visualize a mapped, molecular image. The image of the molecular distribution is achieved without lengthy tissue preparation and extraction methods, which can lead to a loss of valuable compounds. This type of imaging is particularly useful for applications such as biomarker detection and for monitoring the progress of an illness in diseased tissue.[169,202,207] Simply "seeing what molecules are where" can be an important diagnostic tool. Since the technique does not require that the molecules of interest be labelled prior to detection, sample preparation is simple and the information collected is not restricted to specific species/types. In fact, it has been applied to several classes of compounds: proteins, lipids, metabolites and glycomes.[208] An extensive amount of information can be gathered based on the molecules located and detected from a single tissue sample, without prior knowledge of exactly what molecules are present and without the need for labelling specific molecules for detection. This can make the discovery of unknown biomarkers easier.[209]

There are several ionization methods being used. The first and simplest is MALDI MSI. The image is generated by stitching together the distribution of individual molecules from the surface of the tissue. The laser is spatially monitored as it is rastered over the surface, ionizing the molecules which are then detected. Pixel sizes range from 1-10 μm and corresponds to one LDI spot. MALDI MSI offers the advantage of being able to not only detect the molecules but also identify potentially unknown biomarkers by MS/MS fragment ion

formation. This technique has been successfully applied to identify lipid biomarkers of polycyctic kidney disease in rats,[169] metabolites in rat brain,[202] accumulation of gangliosides with age in mouse hippocampus[120] and for the spatial distribution of glycerophospholipids in the ocular tissue of pigs.[205]

However, the downfalls of MALDI MSI are its large pixel size relative to other methods and the fact that it uses an organic matrix. Organic matrices are problematic since they fragment and generate ions in the low molecular range. Since it is the nature of MSI to detect the most abundant molecules present, this reduces the overall sensitivity for small molecules. In many cases, biomarkers and metabolites of interest are found in this low mass range, between 100 to 1000 Da. Organic matrices can also negatively impact the spatial resolution due to the size of the matrix crystals. If the crystals are too large or unevenly formed, this can result in mute spots on the tissue sample, where very poor ion intensities are obtained.[210] Another spatial issue associated with matrix deposition onto a tissue sample is the matrix solvents can induce lateral diffusion of the analytes and disrupt the native location of the molecules, skewing the molecular mapping.[206]

The application of the matrix is critical for any traditional MALDI-MS, but is especially critical for tissue imaging. Ion localization in a particular section of tissue may be an indication of the state of a disease progression, especially in age related illnesses. Hot and mute spots due to irreproducible matrix applications can lead to missing information in disease diagnosis and monitoring. Successful MALDI imaging in most of the current literature[134,204,206] requires the use of an add-on matrix application device, such as a matrix sprayer. For example, Separation Associates, Napa, USA, offers a commercial pneumatic atomizer for matrix application onto tissue samples, called the SunChrom SunCollect™, Figure 5.1. The choice of matrix used is also dependent on the type of compounds being investigated. This can limit the amount of information that can be mined from a particular sample, since potentially noteworthy molecules which the selected matrix cannot detect will not be captured.

Some of the other ionization methods include secondary ion mass spectrometry (SIMS),[206] which uses an ion beam, C60 or argon, to bombard the surface. Since an ion beam is used with SIMS, much smaller pixel sizes are achieved as compared to using a laser; on the order of 300 nm. SIMS can also generate rough 3D images by molecular depth profiling. Craters are created in the tissue sample and a 3D molecular image is generated.[208] But while SIMS has the advantage of smaller pixel size, the instrumentation is not that common in most laboratories. Desorption electrospray ionization (DESI) is also used for imaging;[134] solvent droplets are sprayed onto the surface and extract the molecules, other drops then splash these molecules off the tissue to be ionized and detected. Like SIMS, DESI instrumentation is not that common in most labs.

Figure 5.1. SunChrom SunCollect™ by Separation Associates for MALDI tissue imaging.

Overall, imaging by MALDI remains the most popular mass spectrometry method. But most of the work currently being done, is still with special, commercial MSI MALDI instrumentation. Several of the manufacturers of mass spectrometers currently offer special instruments for mass spectrometry imaging. For example, AB Sciex, Bruker, JEOL, Philips, Shimadzu, Thermo Fisher Scientific and Waters. However, in recent years, the availability of free software from some of these same companies and from other independent researchers, has led to the potential of adapting conventional MALDI-MS equipment, already present in many labs, for MSI applications.

Since GLAD films have a proven SMALDI-MS ability, we have chosen to explore SMALDI MSI on silicon GLAD films by adapting the current MALDI TOF/TOF instrument available to us with free software for imaging. SMALDI MSI is a proof of concept investigation, for a simple, inexpensive, matrix-free, readily adaptable method for tissue imaging with GLAD films, without the need of a matrix or add-on equipment. Central nervous system (CNS) tissue samples were chosen for this study, since lipid molecules in CNS have been investigated as biomarkers in several illnesses including Alzheimer's disease,[118] Tay-Sachs disease[211] and dementia.[120]

5.2 Experimental

5.2.1 Materials and Reagents

9-Aminoacridine (9-AA), 2,5-dihydroxybenzoic acid (DHB) matrix and methanol were from Sigma-Aldrich Chemical Co. (Milwaukee, WI, USA). Spinal cord tissue samples from rats were provided by the Fouad research group of the Faculty of Rehabilitation Medicine, Centre for Neuroscience, University of Alberta.

5.2.2 GLAD Film Fabrication

Porous thin film deposition was performed in a high vacuum system (Kurt J. Lesker Co., Clairton, PA, USA)[57] Conductive indium tin oxide (ITO) glass substrates were cleaned prior to deposition by submersion in piranha (3:1, sulfuric acid: hydrogen peroxide) for 20 minutes followed by a deionized water rinse and drying with nitrogen gas. Silicon (99.9% pure, Cerac Inc., Milwaukee, WI, USA) was deposited onto the silicon substrate with a deposition angle of 88^{o} relative to the substrate normal. The substrate rotation rate was 1.2 rpm and the deposition rate was 0.6 nm/s.[74] Slanted posts were deposited at the specified angles, with no substrate rotation at a deposition rate of 0.3-0.7 nm/s. The films were deposited by electron beam evaporation under vacuum, base pressure $<10^{-6}$ Torr.

5.2.3 Tissue Samples

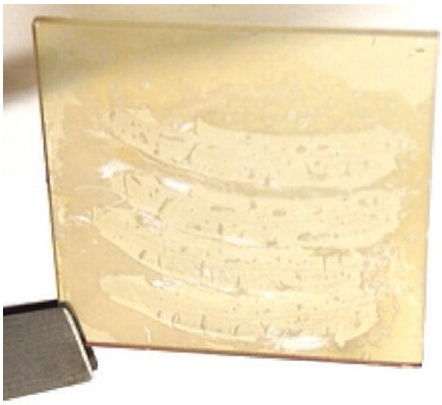

Figure 5.2. Rat tissue slices on 500 nm silicon GLAD films. GLAD films deposited onto an ITO glass substrate which was cut into 2.5 cm X 2.5 cm pieces.

Spinal cord tissue slices, 15 μm thick, extracted from rats were thaw-mounted on to 500 nm silicon GLAD films and frozen at -20^{o} C until required for analysis. Prior to MSI, films were thawed for 20 minutes at room temperature in a desiccator. The GLAD films with tissue samples were adhered to the MALDI sample plate with double sided sticky copper tape.

Figure 5.3. Picture of Si GLAD film with tissue samples attached to MALDI plate with double sided sticky copper tape.

5.2.4 Mass Spectrometry Imaging

5.2.4.1 Mass Spectrometer

Mass spectrometry imaging was performed using an Applied Biosystems (Framingham, MA, USA) Voyager STR time-of-flight mass/time-of-flight (TOF/TOF) mass spectrometer operated with a pulsed N_2 laser at 337 nm. Laser fluence was between 3800-4000 arbitrary units.

5.2.4.2 Image Acquisition Software

The 4800 Imaging Acquisition Tool software written by Markus Stoeckli of Novartis, Switzerland, was downloaded for free from http://www.maldi-msi.org. This site is dedicated to sharing information on matrix-assisted laser desorption/ionization MALDI MSI. The 4800 Imaging Acquisition Tool software was specifically written for the image acquisition on the ABI 4000 Series Proteomics Analyzers from Applied Biosystems. It integrates with the existing ABSciex Series Explorer software that comes with the TOF/TOF instrument. With the acquisition tool, a raster of mass spectra was acquired over the two dimensional sample, resulting in a MSI file containing spatial and spectral information. The output image data is stored in the Analyze 7.5 format, which can be accessed and processed by the image processing software. Spatial laser rastering in these experiments was set at 100 μm x 100 μm.

5.2.4.3 Image Processing Software

TissueView™ software was provided for free from AB SCIEX (Concord, Ontario, Canada). TissueView™ is a tool designed for displaying and processing the data from mass spectrometric imaging acquisition software, like the 4800 Imaging Acquisition Tool. It displays spectral information for every image location and shows the intensity of each ion detected.

5.3 Results and Discussion

5.3.1 SMALDI-MS with Tissue Samples

Spinal cord tissue of the CNS is composed mostly of grey and white matter. White matter is white due to the high lipid content of its myelin sheets. Gray matter is composed mostly of neurons which also have a high lipid content. In Chapter 2, the SMALDI-MS detection of CNS lipid compounds was very successful in a liquid medium. However, prior to testing GLAD films for MSI, we first needed to determine if it would be possible to generate SMALDI-MS spectra from tissue samples several micrometers thick, deposited on the surface of silicon films on ITO glass substrates.

We chose to deposit the 500 nm silicon GLAD films onto ITO glass substrates for two reasons. Firstly, tissue deposition onto a glass slide is easier as glass is more robust than silicon wafers and is easier to handle during tissue application. Secondly, silicon wafers are completely opaque, while silicon GLAD films with ITO as a substrate are semitransparent, Figure 5.2. This means that light microscope studies (light is transmitted through the bottom of the slide to illuminate the sample) is more feasible, with the semitransparent films being able to transmit light.[209] These microscope studies may be done either before or after imaging on areas of interest in the tissue sample.

DHB matrix is popular for imaging work in the positive ion mode.[167,209,211,212] So this matrix was chosen for comparison with SMALDI-MS in the positive ion mode, Figure 5.4. Not only was the GLAD film capable of producing a spectrum from the tissue sample, the background below m/z 500 with DHB matrix was eliminated.

The major lipid peaks at 782 and 810 were detected with both MALDI and SMALDI-MS and with similar ion counts. 782 is most likely the molecular ion of the phosphatidylcholine (fatty acid, 36:4), present in rat brain sections.[212] Phosphatidylcholines are the most abundant phospholipids in mammalian cells.[213] The 810 and 782 peaks differ by 28 units; these are likely the same

phosphatidylcholine compound, but with a single conjugation difference within the fatty acid chain.[120]

The peak at m/z 184, corresponds to the head group of the phosphatidylcholine detected.[214] Since phosphatidylcholines are mainly located on the outer portion of cell membranes, their head group ions are common in tissue sample spectra due to the ease of desorbing these groups. We were unable to definitively identify the major peak at 332. However, this peak is consistent with a sialic acid we detected during our studies with glycolipids, Chapter 2.

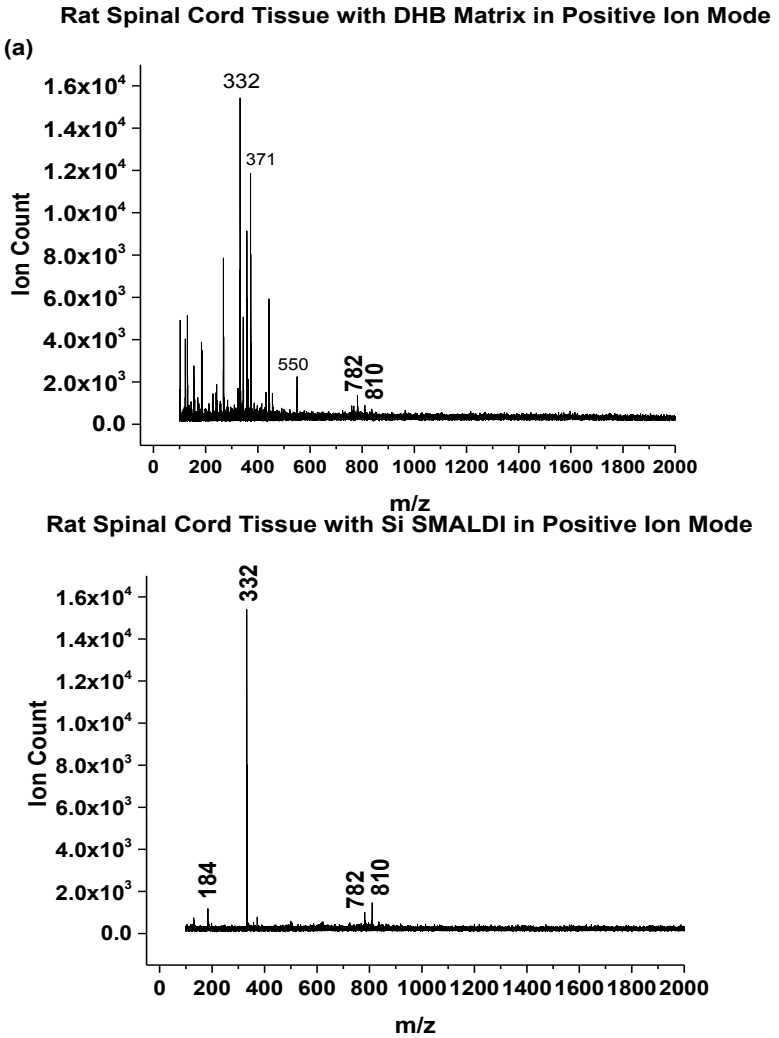

Figure 5.4. Comparison of MALDI and SMALDI-MS of tissue samples. Spectrum of rat spinal cord tissue in the positive ion mode (a) with DHB matrix, and (b) with silicon SMALDI.

In the negative ion mode, SMALDI-MS was compared with MALDI using the matrix 9-AA. This matrix is popular for negative ion mode detection of lipid compounds in imaging.[142,202,213] The most intense peak with both SMALDI and MALDI was at m/z 885, Figure 5.5. This peak is associated with the molecular ion of the phosphatidylinositol with fatty acid, 38:4, present in large amounts in the gray matter regions of rats.[169,212] The SMALDI spectra also contained peaks associated with other lipid compounds found in rats in other studies. For example, the peak at 878 corresponds to the sulfatide with fatty acid (22:0) in rat brain sections, 902 is associated with the sulfatide with 24:1 fatty acid. [142,212,215]

From our own investigations with MALDI matrices, and in comparison with studies by others, we were able to detect the same ion peaks with SMALDI-MS on rat tissue samples. This therefore meant that imaging experiments were feasible with SMALDI.

One notable potential advantage of SMALDI MSI over MALDI MSI, is the possible mapping of compounds in both the positive and negative ion modes on the same tissue sample. With MALDI, a different matrix is needed for each mode, and it is not possible to apply two matrices on the same tissue effectively.

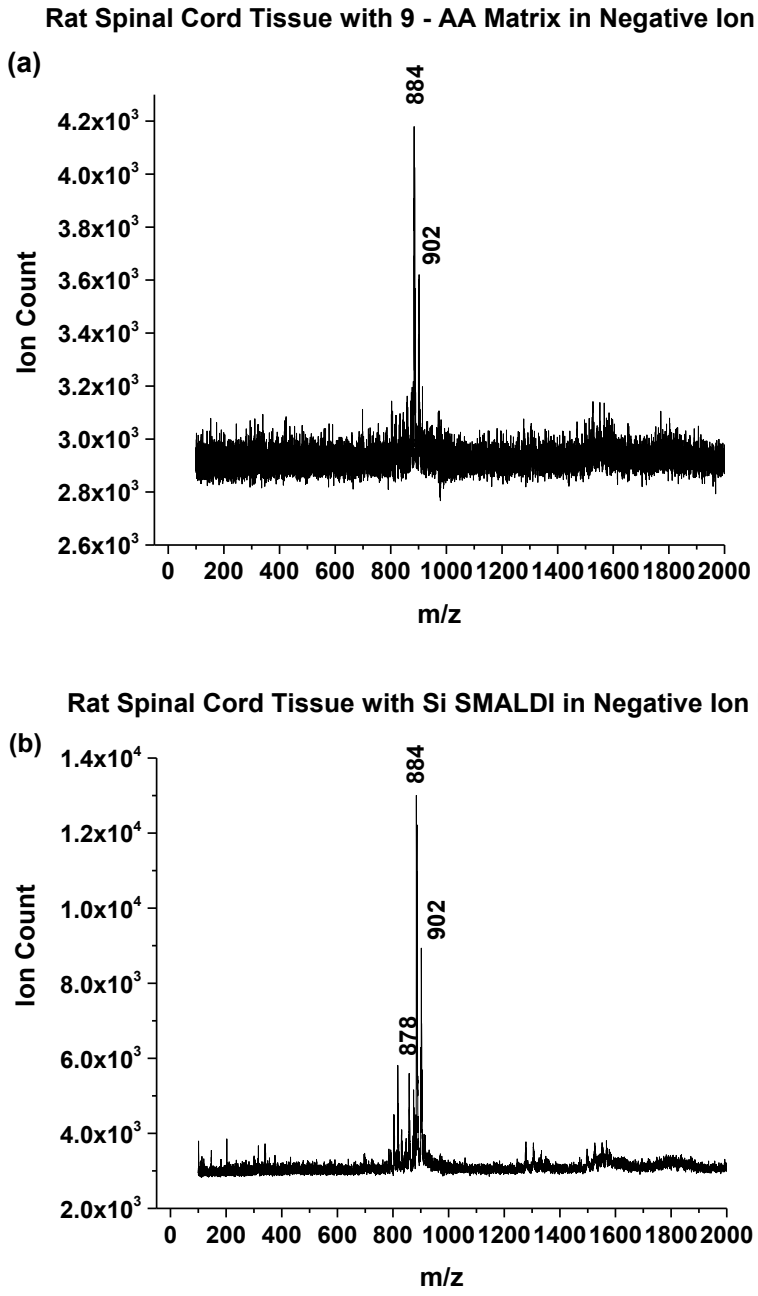

Figure 5.5. Comparison of MALDI and SMALDI-MS of tissue samples.Spectrum of rat spinal cord tissue in the negative ion mode (a) with 9-AA matrix, and (b) with silicon SMALDI.

5.3.2 SMALDI-MSI

Following the successful detection of lipid compounds from rat spinal cord tissues using 500 nm silicon GLAD films, we then proceeded to explore the potential of GLAD for MSI. The 878 peak of the sulfatide with fatty acid (22:0) was chosen for investigation. The intensity of this peak from the preliminary results indicated that while this species was present in the rat tissue samples, it was not the most abundant, and would therefore would give a better indication of the effectiveness of SMALDI-MSI.

Using the 4800 Imaging Acquisition Tool and TissueView™ software, the distribution of this ion from a section of tissue sample was determined, Figure 5.6. The image in 5.6 (b) was generated from the highlighted section of tissue in 5.6 (a) and shows where the sulfatide is located in the section. It also indicates the relative intensity of the molecule at each location. The mass spectrum shown in Figure 5.6 (c), with an ion count of only 13, was generated from a region of relatively low intensity of the molecule and serves as a good indication of the potential of SMALDI-MSI.

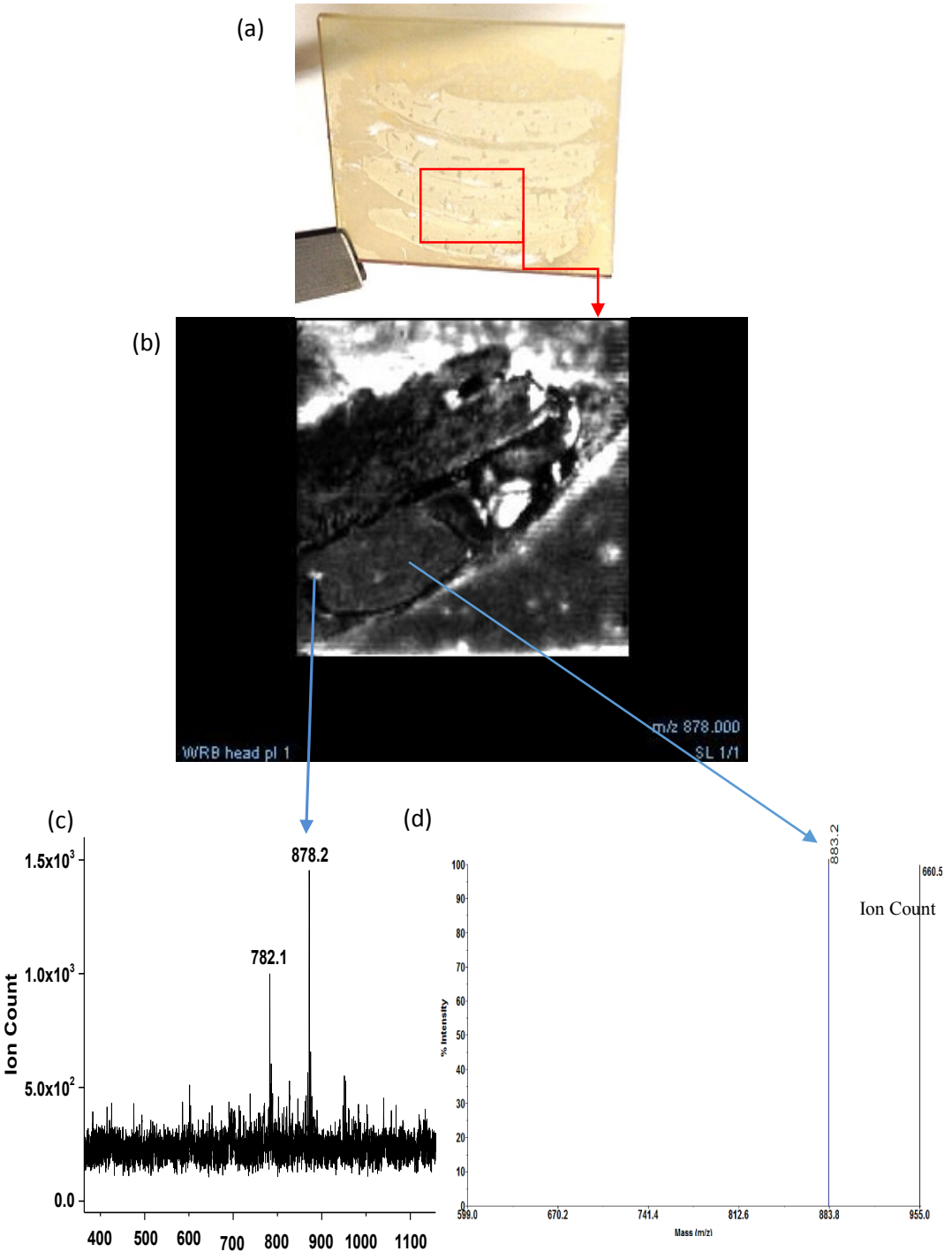

Figure 5.6. Mass spectrometry imaging, (a) Section of tissue imaged, (b) distribution of 878 sulfatide with in the section of tissue highlighted in (a), mass spectra of sulfatide (c) and (d) generated from the indicated spots of tissue in (b).

5.4 Conclusions and Future Work

These preliminary results of SMALDI-MSI have show that silicon GLAD films can be used as an imaging technique. First, the ions detected from rat spinal cord tissue samples were consistent with those reported in current literature using other techniques. We were able to combine SMALDI-MS with free imaging software and a standard MALDI TOF instrument, to generate a mass spectrometry image of a CNS lipid compound. The detection of this compound was highly sensitive, with regions of low intensity being able to generate a mass spectrum. This low detection ability, coupled with the fact that live samples maybe used, is promising for future experiments, where this technique can be possibly applied for monitoring reactions such as drug/metabolite interactions in single-cell imaging.[216] Second, using SMALDI, MSIs can be generated from the same tissue sample using both the positive and negative ion modes, since specific matrices were not required.

Chapter 6

Conclusions and Future Work

This thesis has demonstrated the application of GLAD films for matrix-free LDI-MS of small molecules below 1500 Da. The three material types examined were cobalt, silicon and silica films. In Chapter 2, cobalt films proved to be an effective substrate for the detection of small carbohydrate and metabolite molecules with low femtomole detection. Films ranging from 250 nm to 500 nm possessed the ideal combination of porosity and film material for LDI detection. Co GLAD films also produced reproducible mass spectrometry results without lengthy and complicated sample spot preparation.

In Chapter 3, silicon GLAD films were tested for the detection of glycolipids. First, after the isolation of serum contaminants on the GLAD film and, second, in the serum itself, with out clean up. The detection for glycolipids in serum, without sample clean up, was in the low femtomole range.

Isolating the contaminants on the film prior to mass spectrometry eliminated the need for a lengthy analyte extraction process, and demonstrated the potential of silicon GLAD films to be used as part of a fast and simple sample clean up in high through put analyses. The use of separation solvents as the mobile phase for the separation and isolation of glycolipids is a stepping stone for further work with relevant biomarkers in biofluids. Other separations solvents may be used as the mobile phase, as well as other biofluids such as blood, urine and saliva may be tested. This is promising for the application of SMALDI-MS as a high through put technique in biomarker studies. Diseases such as Alzheimer's disease, dementia, Type II diabetes, Tay Sach's, etc. all involve changes in glycolipid biomarkers.

Expanding on the UTLC ability of GLAD observed during the sample cleanup of serum on silicon, silica films were further examined for a hyphenated UTLC-MS application in Chapter 4. While silicon films had a superior LDI-MS performance, silica films proved to be the optimum material for the two

techniques combined. The detection on silica films was in the low picomole range for separation followed by LDI-MS detection, and the R_F values and separation times are comparable to other hypenated UTLC methods. We recommend that the combined UTLC-SMALDI-MS ability of silicon GLAD films be further investigated. Films of this material type has a proven record of superior LDI-MS performance when compared to films made of silica. The limit of detection for separated analyte compounds could therefore be potentially lower with silicon in future investigations.

The SMALDI-MS approach, performed on the same film following the separation, also eliminates the need for additional interface equipment and visualization methods for the identification of separated compounds. Two dimensional UTLC separation on GLAD films may also be investigated, with separation solvents used in series for the isolation of different classes of compounds from the same sample.

Overall, the LDI-MS results of the cobalt, silicon and silica GLAD films tested have been very promising. We have been able to detect small molecules without the use of matrices. This has led to a simple and straightforward sample preparation. The mass spectrometry detection of compounds that are less widely studied has also become easier, since the matrix selection process is eliminated. This was especially noted with some of the glycolipids. While SMALDI-MS was able to detect all of the test compounds; we were unable to find a suitable matrix from a pool of common MALDI matrices for some gangliosides.

While various classes of compounds - carbohydrates, metabolites, peptides and glycolipids- have been successfully detected throughout this work, these compounds have not all been tested on each GLAD material type. For GLAD films to be an effective and widely used substrate, the ability of each material type, i.e., cobalt, silicon and silica, must be fully explored with different classes of compounds. For future investigations, we recommend investigating the full repertoire of compounds each film type can detect.

Since a significant difference in performance was also found with different column morphology, vertical vs. slanted posts, in Chapter 2, it might also be

useful to further examine other GLAD column types for SMALDI-MS applications.

The SMALDI-MSI results in the final results Chapter of this thesis show that silicon GLAD films can be used as an imaging technique. We were able to combine SMALDI-MS with free imaging software and a standard MALDI TOF instrument, to generate a mass spectrometry image of a CNS lipid compound. The detection of this compound is promising for future experiments, where this technique can be applied for monitoring reactions such as drug/metabolite interactions in single-cell imaging. GLAD films can also be used to generate molecular distribution images for a more comprehensive molecular image of diseased tissue sections, potentially as part of a diagnostic tool.

While the mechanism of porous silicon surfaces have been studied, there is currently limited information available in literature for other types of porous materials such as GLAD films. The nature of the surface characteristics of the films could provide insight into the mechanism of matrix-free LDI-MS and provide information on how to exploit GLAD films for improved mass spectrometry results. The determination of the nature of the surface oxide formed and more in-depth studies into the porous nature of the films would be especially useful to understanding the SMALDI-MS mechanism.

Secondary Ion Mass Spectrometry (SIMS) may be employed to determine the elementary composition of the surface. However, for more comprehensive information on the oxide layers formed on the surface of the porous films, X-ray diffraction studies would provide more information on the nature of any crystalline layers formed. This would be especially useful for exploring the mechanism of cobalt GLAD films. Very little information is currently available on the nature of porous cobalt materials.

Bibliography

(1) Ramizy, A.; Aziz, W. J.; Hassan, Z.; Omar, K.; Ibrahim, K. *Microelectronics International* **2010**, *27*, 117-120.

(2) Robbie, K.; Brett, M. *Journal of Vacuum Science & Technology A* **1997**, *15*, 1460-1465.

(3) Fan, J.; Tang, X.; Zhao, Y. *Nanotechnology* **2004**, *15*, 501.

(4) Han, X.; M Holtzman, D.; McKeel, D. W., Jr.; Kelley, J.; Morris, J. C. *Journal of Neurochemistry* **2002**, *82*, 809-818.

(5) Hawkeye, M. M.; Brett, M. J. *Crystallography and Liquid Crystals* **2007**, *25*, 1317-1335.

(6) Gusev, A. I. *Fresenius J Analytical Chemistry*. **2000**, *366*, 691-700.

(7) Borman, S. *Historical Perspective, A Brief History of Mass Spectrometry Instrumentation, http://masspec.scripps.edu/mshistory/perspectives/sborman.php;* Scripps Center for Metabolomics and Mass Spectrometry, 2014.

(8) Karas, M.; Hillenkamp, F. *Analytical Chemistry* **1988**, *60*, 2299-2301.

(9) Peterson, D. S. *Mass Spectrometry Reviews* **2007**, *26*, 19-34.

(10) Lewis, J. K.; Wei, J.; Siuzdak, G. *Encyclopedia of Analytical Chemistry* **2000**.

(11) Gohl, W.; Kutscher, R.; Laue, H. J.; Wollnik, H. *International Journal of Mass Spectrometry and Ion Physics* **1983**, *48*, 411-414.

(12) Schmid, D. G.; Grosche, P.; Bandel, H.; Gunther Jung, G. *Biotechnolgy and Bioengineering* **2000**, *71*, 2001.

(13) Vestal, M. L.; Juhasz, P.; Martin, S. A. *Rapid Communications in Mass Spectrometry* **1995**, *9*, 1044-1050.

(14) Chaurand, P.; Luetzenkirchen, F.; Spengler, B. *Journal of the American Society for Mass Spectrometry* **1999**, *10*, 91-103.

(15) Jungblut, P.; Thiede, B. *Mass Spectrometry Reviews* **1997**, *16*, 145-162.

(16) Ross, P. L.; Lee, K.; Belgrader, P. *Analytical Chemistry* **1997**, *69*, 4197-4202.

(17) Griffin, T. J.; Smith, L. M. *Trends in Biotechnology* **2000**, *18*, 77-84.

(18) Mank, M.; Stahl, B.; Boehm, G. *Analytical Chemistry* **2004**, *76*, 2938-2950.

(19) Heeren, R.; Kükrer-Kaletaş, B.; Taban, I. M.; MacAleese, L.; McDonnell, L. A. *Applied Surface Science* **2008**, *255*, 1289-1297.

(20) Montaudo, G.; Samperi, F.; Montaudo, M. S. *Progress in Polymer Science* **2006**, *31*, 277-357.

(21) Wu, K. J.; Steding, A.; Becker, C. H. *Rapid Communications in Mass Spectrometry* **1993**, *7*, 142-146.

(22) Tang, K.; Taranenko, N.; Allman, S.; Chen, C.; Chág, L.; Jacobson, K. *Rapid Communications in Mass Spectrometry* **1994**, *8*, 673-677.

(23) Krause, J.; Stoeckli, M.; Schlunegger, U. P. *Rapid Communications in Mass Spectrometry* **1996**, *10*, 1927-1933.

(24) Lin, H.; Hunter, J. M.; Becker, C. H. *Rapid Communications in Mass Spectrometry* **1999**, *13*, 2335-2340.

(25) Banoub, J. H.; Newton, R. P.; Esmans, E.; Ewing, D. F.; Mackenzie, G. *Chemical Reviews* **2005**, *105*, 1869-1916.

(26) Laremore, T. N.; Zhang, F.; Linhardt, R. J. *Analytical Chemistry* **2007**, *79*, 1604-1610.

(27) Armstrong, D. W.; Zhang, L.-K.; He, L.; Gross, M. L. *Analytical Chemistry* **2001**, *73*, 3679-3686.

(28) Kawasaki, H.; Yonezawa, T.; Watanabe, T.; Arakawa, R. *The Journal of Physical Chemistry C* **2007**, *111*, 16278-16283.

(29) Dai, Y.; Whittal, R. M.; Li, L. *Analytical Chemistry* **1999**, *71*, 1087-1091.

(30) Kussmann, M.; Nordhoff, E.; Rahbek-Nielsen, H.; Haebel, S.; Rossel-Larsen, M.; Jakobsen, L.; Gobom, J.; Mirgorodskaya, E.; Kroll-Kristensen, A.; Roepstorff, P. *Journal of Mass Spectrometry* **1997**, *32*, 593-601.

(31) Tanaka, K.; Waki, H.; Ido, Y.; Akita, S.; Yoshida, Y.; Yoshida, T.; Matsuo, T. *Rapid Communications in Mass Spectrometry* **1988**, *2*, 151-153.

(32) Sunner, J.; Dratz, E.; Chen, Y.C. *Analytical Chemistry* **1995**, *67*, 4335-4342.

(33) Law, K. P.; Larkin, J. R. *Biochemical Methods* **2011**, *399*, 2597-2622.

(34) Watanabe, T.; Kawasaki, H.; Yonezawa, T.; Arakawa, R. *Journal of Mass Spectrometry* **2008**, *43*, 1063-1071.

(35) Watanabe, T.; Okumura, K.; Kawasaki, H.; Arakawa, R. *Journal of Mass Spectrometry* **2009**, *44*, 1443-1451.

(36) Chiang, C.K.; Chiang, N.-C.; Lin, Z.-H.; Lan, G.-Y.; Lin, Y.W.; Chang, H.-T. *Journal of the American Society for Mass Spectrometry* **2010**, *21*, 1204-1207.

(37) Shrivas, K.; Agrawal, K.; Wu, H.F. *Analyst* **2011**, *136*, 2852-2857.

(38) Hoang, T. T.; Chen, Y.; May, S. W.; Browner, R. F. *Analytical Chemistry* **2004**, *76*, 2062-2070.

(39) Tang, H.W.; Ng, K.M.; Lu, W.; Che, C.M. *Analytical Chemistry* **2009**, *81*, 4720-4729.

(40) Wei, J.; Buriak, J. M.; Siuzdak, G. *Biochemical Methods* **1999**, *399*, 243-246.

(41) Kauppila, T. J.; Talaty, N.; Salo, P. K.; Kotiaho, T.; Kostiainen, R.; Cooks, R. G. *Rapid Communications in Mass Spectrometry* **2006**, *20*, 2143-2150.

(42) Li, J.; Lu, C.; Hu, X.; Yang, X.; Loboda, A.; Lipson, R. *International Journal of Mass Spectrometry* **2009**, *285*, 137-142.

(43) Thomas, J. J.; Shen, Z.; Crowell, J. E.; Finn, M.; Siuzdak, G. *Proceedings of the National Academy of Sciences* **2001**, *98*, 4932-4937.

(44) Kruse, R. A.; Li, X.; Bohn, P. W.; Sweedler, J. V. *Analytical Chemistry* **2001**, *73*, 3639-3645.

(45) Alimpiev, S.; Grechnikov, A.; Sunner, J.; Karavanskii, V.; Simanovsky, Y.; Zhabin, S.; Nikiforov, S. *Surface Chemistry and Colloids* **2008**, *128*, 014711/014711-014711/014719.

(46) Okuno, S.; Arakawa, R.; Okamoto, K.; Matsui, Y.; Seki, S.; Kozawa, T.; Tagawa, S.; Wada, Y. *Analytical Chemistry* **2005**, *77*, 5364-5369.

(47) Xiao, Y.; Retterer, S. T.; Thomas, D. K.; Tao, J.-Y.; He, L. *Surface Chemistry and Colloids* **2009**, *113*, 3076-3083.

(48) Alimpiev, S.; Nikiforov, S.; Karavanskii, V.; Minton, T.; Sunner, J. *Surface Chemistry and Colloids* **2001**, *115*, 1891-1901.

(49) Northen, T. R.; Yanes, O.; Northen, M. T.; Marrinucci, D.; Uritboonthai, W.; Apon, J.; Golledge, S. L.; Nordström, A.; Siuzdak, G. *Nature* **2007**, *449*, 1033-1036.

(50) Lo, C.Y.; Lin, J.Y.; Chen, W.Y.; Chen, C.T.; Chen, Y.C. *Journal of the American Society for Mass Spectrometry* **2008**, *19*, 1014-1020.

(51) Shen, Z.; Thomas, J. J.; Averbuj, C.; Broo, K. M.; Engelhard, M.; Crowell, J. E.; Finn, M.; Siuzdak, G. *Analytical Chemistry* **2001**, *73*, 612-619.

(52) Ronkel, F.; Schultze, J. *Journal of Porous Materials* **2000**, *7*, 11-16.

(53) Wen, X.; Dagan, S.; Wysocki, V. H. *Analytical Chemistry* **2007**, *79*, 434-444.

(54) Dagan, S.; Hua, Y.; Boday, D. J.; Somogyi, A.; Wysocki, R. J.; Wysocki, V. H. *International Journal of Mass Spectrometry* **2009**, *283*, 200-205.

(55) Piret, G.; Drobecq, H.; Coffinier, Y.; Melnyk, O.; Boukherroub, R. *Langmuir* **2009**, *26*, 1354-1361.

(56) Gish, D. A.; Summers, M. A.; Jensen, M. O.; Brett, M. J. In *Emerging Technologies - Nanoelectronics, 2006 IEEE Conference on*, pp 447-451.

(57) Hawkeye, M. M.; Brett, M. J. *Journal of Vacuum Science & Technology A* **2007**, *25*, 1317-1335.

(58) Krabbe, J. D.; Brett, M. J. *Applied Physics Letters* **2010**, *97*, 041117.

(59) Krause, K. M.; Taschuk, M. T.; Brett, M. J. *Journal of Vacuum Science & Technology A* **2013**, *31*.

(60) Taschuk, M.; Harris, K.; Smetaniuk, D.; Brett, M. *Sensors and Actuators B: Chemical* **2012**, *162*, 1-6.

(61) Wakefield, N. G.; Sit, J. C. *Journal of Applied Physics* **2011**, *109*, 084332-084332-084310.

(62) Inoue, Y.; Matsui, J.; Ishikawa, H.; Tsuda, H.; Takai, O. *Thin Solid Films* **2010**, *518*, S6-S9.

(63) Chang, D.H.; YONG, J. P.; CHANG, K. H. *Journal of the Korean Physical Society* **2008**, *53*, 2700-2704.

(64) Hsu, S.Y.; Tsai, C.H.; Lu, C.Y.; Tsai, Y.T.; Huang, T.W.; Jhang, Y.H.; Chen, Y.F.; Wu, C.C.; Chen, Y.-S. *Organic Electronics* **2012**, *13*, 856-863.

(65) Bezuidenhout, L. W.; Nazemifard, N.; Jemere, A. B.; Harrison, D. J.; Brett, M. J. *Biochemical Methods* **2011**, *11*, 1671-1678.

(66) Bezuidenhout, L. W.; Brett, M. J. *Surface Chemistry and Colloids* **2008**, *1183*, 179-185.

(67) Jim, S.; Taschuk, M.; Morlock, G.; Bezuidenhout, L.; Schwack, W.; Brett, M. *Analytical Chemistry* **2010**, *82*, 5349-5356.

(68) Jim, S. R.; Oko, A. J.; Taschuk, M. T.; Brett, M. J. *Organic Analytical Chemistry* **2011**, *1218*, 7203-7210.

(69) Kirchert, S.; Wang, Z.; Taschuk, M.; Jim, S.; Brett, M.; Morlock, G. *Analytical and Bioanalytical Chemistry* **2013**, *405*, 7195-7203.

(70) Oko, A. J.; Jim, S. R.; Taschuk, M. T.; Brett, M. J. *Organic Analytical Chemistry* **2011**, *1218*, 2661-2667.

(71) Wannenmacher, J.; Jim, S. R.; Taschuk, M. T.; Brett, M. J.; Morlock, G. E. *Journal of Chromatography A* **2013**, *1318*, 234-243.

(72) Jemere, A. B.; Bezuidenhout, L. W.; Brett, M. J.; Harrison, D. J. *Rapid Communications in Mass Spectrometry* **2010**, *24*, 2305-2311.

(73) Xiao, Y.; Retterer, S. T.; Thomas, D. K.; Tao, J.-Y.; He, L. *The Journal of Physical Chemistry C* **2009**, *113*, 3076-3083.

(74) Jemere, A. B.; Bezuidenhout, L. W.; Brett, M. J.; Harrison, D. J. *Biochemical Methods* **2010**, *24*, 2305-2311.

(75) Kiema, G. K.; Jensen, M. O.; Brett, M. J.*: Crystallography and Liquid Crystals* **2005**, *17*, 4046-4048.

(76) Tsoi, S.; Fok, E.; Sit, J. C.; Veinot, J. G. C. *Surface Chemistry and Colloids* **2004**, *20*, 10771-10774.

(77) Tsoi, S.; Fok, E.; Veinot, J. G. C.; Sit, J. C. *Surface Chemistry and Colloids* **2007**, *6*, 103-107.

(78) Tanaka, K.; Waki, H.; Ido, Y.; Akita, S.; Yoshida, Y.; Yoshida, T.; Matsuo, T. *Rapid Communications in Mass Spectrometry* **1988**, *2*, 151-153.

(79) Yalcin, T.; Wallace, W. E.; Guttman, C. M.; Li, L.*: Physical Properties of Synthetic High Polymers* **2002**, *74*, 4750-4756.

(80) Yalcin, T.; Li, L. *Proceedings of the Symposium on Surface Science 2008 Festschrift in honor of Professor Şefik Süzer's 60th birthday* **2009**, *256*, 1309-1312.

(81) Bruker Daltonics. *Bruker Guide to MALDI Sample Preparation,* http://www.bruker.com/es/products/mass-spectrometry-and-separations/literature/literature-room/instruction-for-use.html?eID=dam_frontend_push&docID=49121., 2012.

(82) Sun, L.; Huang, H.H.; Liu, L.; Zhong, D.F. *Applied and Environmental Microbiology* **2004**, *70*, 2722-2727.

(83) Buzea, C.; Beydaghyan, G.; Elliott, C.; Robbie, K. *Surface Chemistry and Colloids* **2005**, *16*, 1986-1992.

(84) Gish, D.; Summers, M.; Brett, M. *Photonics and Nanostructures-Fundamentals and Applications* **2006**, *4*, 23-29.

(85) Taschuk, M. T.; Hawkeye, M. M.; Brett, M. J. *Handbook of Deposition Technologies for Films and Coatings, 3rd ed.(Elsevier, 2010)* **2010**, 621-678.

(86) Buzea, C.; Beydaghyan, G.; Elliott, C.; Robbie, K. *Nanotechnology* **2005**, *16*, 1986.

(87) Bezuidenhout, L. W. *Molecular Separations Using Nanostructured Porous Thin Films Fabricated by Glancing Angle Deposition (Thesis).* University of Alberta, 2012.

(88) Walker, B. N.; Stolee, J. A.; Pickel, D. L.; Retterer, S. T.; Vertes, A. *The Journal of Physical Chemistry C* **2010**, *114*, 4835-4840.

(89) Bezuidenhout, L. W. *Molecular Separations using Nanostructured Porous Thin Films Fabricated by Glancing Angle Deposition (Thesis)*. University of Alberta, 2012.

(90) Pradhan, N. R.; Duan, H.; Liang, J.; Iannacchione, G. S. *Thermodynamics, Thermochemistry, and Thermal Properties* **2008**, *19*, 485712/485711-485712/485718.

(91) Karabacak, T.; Singh, J. P.; Zhao, Y. P.; Wang, G. C.; Lu, T. M. *Crystallography and Liquid Crystals* **2003**, *68*, 125408/125401-125408/125405.

(92) Yuan, Y.; Lee, T. R. In *Surface Science Techniques*; *Contact Angle and Wetting Properties* Springer, 2013, pp 3-34.

(93) Bico, J.; Thiele, U.; Quéré, D. *Colloids and Surfaces A: Physicochemical and Engineering Aspects* **2002**, *206*, 41-46.

(94) Luo, G.; Chen, Y.; Siuzdak, G.; Vertes, A. *The Journal of Physical Chemistry B* **2005**, *109*, 24450-24456.

(95) Williams, T. L.; Andrzejewski, D.; Lay Jr, J. O.; Musser, S. M. *Journal of the American Society for Mass Spectrometry* **2003**, *14*, 342-351.

(96) Kuhlmann, F. E.; Apffel, A.; Fischer, S. M.; Goldberg, G.; Goodley, P. C. *Journal of the American Society for Mass Spectrometry* **1995**, *6*, 1221-1225.

(97) Trautwein, C.; Kümmerer, K.; Metzger, J. W. *Chemosphere* **2008**, *72*, 442-450.

(98) Credo, G.; Hewitson, H.; Benevides, C.; Bouvier, E. S. P. In *Mater. Res. Soc. Symp. Proc*; Cambridge Univ Press, pp 471-476.

(99) Stahl, B.; Steup, M.; Karas, M.; Hillenkamp, F. *Analytical Chemistry* **1991**, *63*, 1463-1466.

(100) Harvey, D. J. *Mass Spectrometry Reviews* **1999**, *18*, 349-450.

(101) Rohmer, M.; Meyer, B.; Mank, M.; Stahl, B.; Bahr, U.; Karas, M. *Analytical Chemistry* **2010**, *82*, 3719-3726.

(102) Ngoka, L. C.; Gal, J. F.; Lebrilla, C. B. *Analytical Chemistry* **1994**, *66*, 692-698.

(103) Harvey, D. J. *Biochemical Methods* **2012**, *31*, 183-311.

(104) Meloncelli, P. J.; Lowary, T. L. *Carbohydrates* **2009**, *62*, 558-574.

(105) Meloncelli, P. J.; Lowary, T. L. *Carbohydrates* **2010**, *345*, 2305-2322.

(106) Schmidt, D.; Schubert, E.; Schubert, M. *MRS Online Proceedings Library* **2012**, *1409*, null-null.

(107) Tompkins, H.; Augis, J. *Oxidation of Metals* **1981**, *16*, 355-369.

(108) Jia, S.; Hsia, C.-H.; Son, D. H. *The Journal of Physical Chemistry C* **2010**, *115*, 92-96.

(109) Chernavskii, P. A.; Pankina, G. V.; Chernavskii, A. P.; Peskov, N. V.; Afanasiev, P.; Perov, N. S.; Tennov, V. A. *The Journal of Physical Chemistry C* **2007**, *111*, 5576-5581.

(110) Fromhold, A. T.; Cook, E. L. *Physical Review* **1967**, *163*, 650-664.

(111) Cabrera, N.; Mott, N. *Reports on Progress in Physics* **1949**, *12*, 163.

(112) Fehlner, F. P.; Mott, N. F. *Oxidation of Metals* **1970**, *2*, 59-99.

(113) Fredman, P.; Månsson, J.E.; Rynmark, B.M.; Josefsen, K.; Ekblond, A.; Halldner, L.; Osterbye, T.; Horn, T.; Buschard, K. *Glycobiology* **2000**, *10*, 39-50.

(114) Li, G.; Hu, R.; Kamijo, Y.; Nakajima, T.; Aoyama, T.; Ehara, T.; Shigematsu, H.; Kannagi, R.; Kyogashima, M.; Hara, A. *Mammalian Pathological Biochemistry* **2009**, *14*, 658-662.

(115) NÃrskov, N. P.; Hedemann, M. S.; LÃ¦rke, H. N.; Knudsen, K. E. B. *Journal of Proteome Research* **2013**, *12*, 2818-2832.

(116) Liu, Y.; Chen, Y.; Momin, A.; Shaner, R.; Wang, E.; Bowen, N. J.; Matyunina, L. V.; Walker, L. D.; McDonald, J. F.; Sullards, M. C. *Molecular Cancer* **2010**, *9*, 186.

(117) Cutler, R. G.; Kelly, J.; Storie, K.; Pedersen, W. A.; Tammara, A.; Hatanpaa, K.; Troncoso, J. C.; Mattson, M. P. *Proceedings of the National Academy of Sciences of the United States of America* **2004**, *101*, 2070-2075.

(118) Han, X.; Holtzman, D. M. *Mammalian Pathological Biochemistry* **2004**, *9*, 78-82.

(119) Han, X. *Mammalian Pathological Biochemistry* **2004**, *18*, 73-79.

(120) Sugiura, Y.; Shimma, S.; Konishi, Y.; Yamada, M. K.; Setou, M. *PLoS ONE* **2008**, *3*, e3232.

(121) Mielke, M. M.; Lyketsos, C. G. *Mammalian Pathological Biochemistry* **2010**, *12*, 331-340.

(122) Jana, A.; Pahan, K. *The Journal of Neuroscience : the Official Journal of the Society for Neuroscience* **2010**, *30*, 12676-12689.

(123) Di Pardo, A.; Maglione, V.; Alpaugh, M.; Horkey, M.; Atwal, R. S.; Sassone, J.; Ciammola, A.; Steffan, J. S.; Fouad, K.; Truant, R.; Sipione, S. *Proceedings of the National Academy of Sciences* **2012**.

(124) Hu, R.; Li, G.; Kamijo, Y.; Aoyama, T.; Nakajima, T.; Inoue, T.; Node, K.; Kannagi, R.; Kyogashima, M.; Hara, A. *Mammalian Pathological Biochemistry* **2007**, *24*, 565-571.

(125) Zhou, P.; Li, J.; Shao, L.; Lv, G.; Zhao, L.; Huang, H.; Zhang, A.; Pan, X.; Liu, W.; Xie, Q.; Chen, D.; Guo, Y.; Hao, S.; Xu, W.; Li, L. *Metabolomics* **2012**, *8*, 869-879.

(126) Zou, Y.; Albohy, A.; Sandbhor, M.; Cairo, C. W. *Bioorganic & Medicinal Chemistry Letters* **2010**, *20*, 7529-7533.

(127) Sandbhor, M. S.; Soya, N.; Albohy, A.; Zheng, R. B.; Cartmell, J.; Bundle, D. R.; Klassen, J. S.; Cairo, C. W. *Biochemistry* **2011**, *50*, 6753-6762.

(128) Moody, D. B.; Reinhold, B. B.; Guy, M. R.; Beckman, E. M.; Frederique, D. E.; Furlong, S. T.; Ye, S.; Reinhold, V. N.; Sieling, P. A.; Modlin, R. L. *Science* **1997**, *278*, 283-286.

(129) Sugiyama, E.; Hara, A.; Uemura, K.-i. *Analytical Biochemistry* **1999**, *274*, 90-97.

(130) Moss, J. P. *Nomenclature of Glycolipids,* www.chem.qmul.ac.uk/iupac/misc/glylp.html International Union of Pure and Applied Chemistry (IUPAC) and International Union of Biochemistry and Molecular Biology (IUBMB), 1997.

(131) Bode, L.; Beermann, C.; Mank, M.; Kohn, G.; Boehm, G. *The Journal of Nutrition* **2004**, *134*, 3016-3020.

(132) Ikeda, K.; Shimizu, T.; Taguchi, R. *Journal of Lipid Research* **2008**, *49*, 2678-2689.

(133) Lee, H.; An, H. J.; Lerno Jr, L. A.; German, J. B.; Lebrilla, C. B. *Special Issue: In Recognition of Catherine Costello, Recipient of the 2010 Field & Franklin Award* **2011**, *305*, 138-150.

(134) Nimesh, S.; Mohottalage, S.; Vincent, R.; Kumarathasan, P. *International Journal of Molecular Sciences* **2013**, *14*, 11277-11301.

(135) McNaught, A. D., Wilkinson, A. *IUPAC Compendium of Chemical Terminology - the Gold Book,* http://goldbook.iupac.org/; International Union of Pure and Applied Chemistry, 2005–2014.

(136) Zhu, J.; Li, Y.-T.; Li, S.-C.; Cole, R. B. *Glycobiology* **1999**, *9*, 985-993.

(137) Han, X.; Fagan, A. M.; Cheng, H.; Morris, J. C.; Xiong, C.; Holtzman, D. M. *Mammalian Pathological Biochemistry* **2003**, *54*, 115-119.

(138) Cairo Research Group. *Membrane Glycobiology,* http://www.chem.ualberta.ca/~cairo/aboutus.html, 2014.

(139) Varki, A.; Cummings, R. D.; Esko, J. D.; Freeze, H. H.; Stanley, P.; Bertozzi, C. R.; Hart, G. W.; Etzler, M. E.; Varki, A.; Schauer, R. **2009**.

(140) Cairo, C. W.; Key, J. A.; Sadek, C. M. *Current Opinion in Chemical Biology* **2010**, *14*, 57-63.

(141) Loka, R. S.; Sadek, C. M.; Romaniuk, N. A.; Cairo, C. W. *Bioconjugate Chemistry* **2010**, *21*, 1842-1849.

(142) Cheng, H.; Sun, G.; Yang, K.; Gross, R. W.; Han, X. *Journal of Lipid Research* **2010**, *51*, 1599-1609.

(143) Endo, S.-i.; Morita, M.; Ueno, M.; Maeda, T.; Terabayashi, T. *Biochemical and Biophysical Research Communications* **2009**, *378*, 890-894.

(144) Torretta, E.; Vasso, M.; Fania, C.; Capitanio, D.; Bergante, S.; Piccoli, M.; Tettamanti, G.; Anastasia, L.; Gelfi, C. *Electrophoresis* **2014**, *35*, 1319-1328.

(145) Fuchs, B.; Schiller, J. *European Journal of Lipid Science and Technology* **2009**, *111*, 83-98.

(146) Östman, P.; Pakarinen, J. M. H.; Vainiotalo, P.; Franssila, S.; Kostiainen, R.; Kotiaho, T. *Rapid Communications in Mass Spectrometry* **2006**, *20*, 3669-3673.

(147) Knochenmuss, R.; Stortelder, A.; Breuker, K.; Zenobi, R. *Journal of Mass Spectrometry* **2000**, *35*, 1237-1245.

(148) McAlpin, C. R.; Voorhees, K. J.; Corpuz, A. R.; Richards, R. M. *Analytical Chemistry* **2012**, *84*, 7677-7683.

(149) McAlpin, C. R.; Voorhees, K. J. *Rapid Communications in Mass Spectrometry* **2013**, *27*, 1763-1768.

(150) Lobasso, S.; Lopalco, P.; Angelini, R.; Baronio, M.; Fanizzi, F. P.; Babudri, F.; Corcelli, A. *Mammalian Biochemistry* **2010**, *45*, 593-602.

(151) Beausoleil, H.-E.; Lépine, F.; Daniel Dubreuil, J. *FEMS Microbiology Letters* **2002**, *209*, 183-188.

(152) Meisen, I.; Peter-Katalinic, J.; Müthing, J. *Analytical Chemistry* **2004**, *76*, 2248-2255.

(153) Vovk, I.; Popović, G.; Simonovska, B.; Albreht, A.; Agbaba, D. *Journal of Chromatography A* **2011**, *1218*, 3089-3094.

(154) Morlock, G. E. In *Mass Spectrometry Handbook*; John Wiley & Sons, Inc., 2012, pp 1181-1206.

(155) Bokka, R.; Kothapalli, H. B.; Vanka, U. M. S.; Potturi, S. D. *J. Pharm. Res.* **2011**, *4*, 4541-4545, 4545 pp.

(156) Guittard, J.; Hronowski, X. L.; Costello, C. E. *Rapid Communications in Mass Spectrometry* **1999**, *13*, 1838-1849.

(157) Dreisewerd, K.; Müthing, J.; Rohlfing, A.; Meisen, I.; Vukelic, Z.; Peter-Katalinic, J.; Hillenkamp, F.; Berkenkamp, S. *Analytical Chemistry* **2005**, *77*, 4098-4107.

(158) DeLong, C. J.; Baker, P. R. S.; Samuel, M.; Cui, Z.; Thomas, M. J. *Journal of Lipid Research* **2001**, *42*, 1959-1968.

(159) Brügger, B.; Erben, G.; Sandhoff, R.; Wieland, F. T.; Lehmann, W. D. *Proceedings of the National Academy of Sciences* **1997**, *94*, 2339-2344.

(160) Honda, A.; Yamashita, K.; Miyazaki, H.; Shirai, M.; Ikegami, T.; Xu, G.; Numazawa, M.; Hara, T.; Matsuzaki, Y. *Journal of Lipid Research* **2008**, *49*, 2063-2073.

(161) Milne, S.; Ivanova, P.; Forrester, J.; Alex Brown, H. *Methods* **2006**, *39*, 92-103.

(162) Xiao, Y.; Chen, Y.; Kennedy, A. W.; Belinson, J.; Xu, Y. *Annals of the New York Academy of Sciences* **2000**, *905*, 242-259.

(163) Hall, J. Z.; Taschuk, M. T.; Brett, M. J. *Biochemical Methods* **2012**, *1266*, 168-174.

(164) de Souza, L. M.; Iacomini, M.; Gorin, P. A.; Sari, R. S.; Haddad, M. A.; Sassaki, G. L. *Chemistry and Physics of Lipids* **2007**, *145*, 85-96.

(165) Jiang, X.; Cheng, H.; Yang, K.; Gross, R. W.; Han, X. *Analytical Biochemistry* **2007**, *371*, 135-145.

(166) Kyogashima, M.; Tamiya-Koizumi, K.; Ehara, T.; Li, G.; Hu, R.; Hara, A.; Aoyama, T.; Kannagi, R. *Glycobiology* **2006**, *16*, 719-728.

(167) Zaima, N.; Goto-Inoue, N.; Adachi, K.; Setou, M. *Journal of Oleo Science* **2011**, *60*, 93-98.

(168) Yuki, D.; Sugiura, Y.; Zaima, N.; Akatsu, H.; Hashizume, Y.; Yamamoto, T.; Fujiwara, M.; Sugiyama, K.; Setou, M. *Neuroscience* **2011**, *193*, 44-53.

(169) Ruh, H.; Salonikios, T.; Fuchser, J.; Schwartz, M.; Sticht, C.; Hochheim, C.; Wirnitzer, B.; Gretz, N.; Hopf, C. *Journal of Lipid Research* **2013**, *54*, 2785-2794.

(170) Zhang, Y.; Lu, H. *Chinese Journal of Chemistry* **2012**, *30*, 2091-2096.

(171) Ikeda, K.; Taguchi, R. *Rapid Communications in Mass Spectrometry : RCM* **2010**, *24*, 2957-2965.

(172) O'Connor, P. B.; Budnik, B. A.; Ivleva, V. B.; Kaur, P.; Moyer, S. C.; Pittman, J. L.; Costello, C. E. *Journal of the American Society for Mass Spectrometry* **2004**, *15*, 128-132.

(173) Xu, C.; Pinto, E. C.; Armstrong, D. W. *Analyst* **2014,** 139, 4169-4175.

(174) Floegel, A.; Stefan, N.; Yu, Z.; Muhlenbruch, K.; Drogan, D.; Joost, H. G.; Fritsche, A.; Haring, H. U.; Hrabe de Angelis, M.; Peters, A.; Roden, M.; Prehn, C.; Wang-Sattler, R.; Illig, T.; Schulze, M. B.; Adamski, J.; Boeing, H.; Pischon, T. *Diabetes* **2013**, *62*, 639-648.

(175) Fenselau, C.; Heller, D. N.; Olthoff, J. K.; Cotter, R. J.; Kishimoto, Y.; Uy, O. M. *Biochemical Methods* **1989**, *18*, 1037-1045.

(176) Manicke, N. E.; Wiseman, J. M.; Ifa, D. R.; Cooks, R. G. *Journal of the American Society for Mass Spectrometry* **2008**, *19*, 531-543.

(177) Ekroos, K.; Ejsing, C. S.; Bahr, U.; Karas, M.; Simons, K.; Shevchenko, A. *Journal of Lipid Research* **2003**, *44*, 2181-2192.

(178) Tanaka, Y.; Higashi, T.; Rakwal, R.; Shibato, J.; Wakida, S.; Iwahashi, H. In *Biological Responses to Chemical Pollutants*; Health Engineering Research Center,
National Institute of Advanced Industrial Science and Technology (AIST),
Midorigaoka-1-8-31, Ikeda, Osaka 563-8577, Japan; and
Tsukuba west, Tsukuba, Ibaraki 305-8569, Japan, 2008, pp 123–132.

(179) Floegel, A.; Stefan, N.; Yu, Z.; Mühlenbruch, K.; Drogan, D.; Joost, H.-G.; Fritsche, A.; Häring, H.U.; de Angelis, M. H.; Peters, A. *Diabetes* **2013**, *62*, 639-648.

(180) Hauck, H.; Schulz, M. *Chromatographia* **2003**, *57*, S313-S315.

(181) Hauck, H. E.; Schulz, M. *Journal of Chromatographic Science* **2002**, *40*, 550-552.

(182) Ivleva, V. B.; Sapp, L. M.; O'Connor, P. B.; Costello, C. E. *Journal of the American Society for Mass Spectrometry* **2005**, *16*, 1552-1560.

(183) Li, F.; Dong, M.; Miller, L. J.; Naylor, S. *Rapid Communications in Mass Spectrometry* **1999**, *13*, 464-466.

(184) Salo, P. K.; Salomies, H.; Harju, K.; Ketola, R. A.; Kotiaho, T.; Yli-Kauhaluoma, J.; Kostiainen, R. *Journal of the American Society for Mass Spectrometry* **2005**, *16*, 906-915.

(185) Zlatkis, A.; Kaiser, R. E. *HPTLC-High Performance Thin-layer Chromatography*; Elsevier, 2011; Vol. 9.

(186) Park, H.; Zhou, Y.; Costello, C. E. *Journal of Lipid Research* **2014**, *55*, 773-781.

(187) Biasone, A.; Cianci, G.; Di Tommaso, D.; Piaggesi, A.; D'Alessandro, N. *Journal of Chromatography A* **2013**, *1312*, 58-68.

(188) Lato, M.; Brunelli, B.; Ciuffini, G.; Mezzetti, T. *Journal of Chromatography A* **1968**, *34*, 26-34.

(189) Jim, S. R.; Taschuk, M. T.; Morlock, G. E.; Bezuidenhout, L. W.; Schwack, W.; Brett, M. J. *Organic Analytical Chemistry* **2010**, *82*, 5349-5356.

(190) Nyiredy, S.; Erdelmeier, C.; Meier, B.; Sticher, O. *Planta Medica* **1985**, *51*, 241-246.

(191) Heftmann, E. *Chromatography: Fundamentals and Applications of Chromatography and Related Differential Migration Methods-Part B: Applications*; Elsevier, 2004.

(192) Lato, M.; Brunelli, B.; Ciuffini, G.; Mezzetti, T. *Journal of Chromatography A* **1969**, *39*, 407-417.

(193) Grauer, A.; Neuberg, C. *Analytica Chimica Acta* **1953**, *8*, 422-425.

(194) Hanson, S.; Mills, G.; Williams, R. *Biochemical Journal* **1944**, *38*, 274.

(195) Guerrero, A.; Williams, R. T. *Nature* **1948**, *161*, 930-930.

(196) Terman, L. M. *Solid-State Electronics* **1962**, *5*, 285-299.

(197) Berglund, C. *Electron Devices, IEEE Transactions on* **1966**, *13*, 701-705.

(198) Deal, B. E.; Sklar, M.; Grove, A.; Snow, E. *Journal of The Electrochemical Society* **1967**, *114*, 266-274.

(199) Morita, M.; Ohmi, T.; Hasegawa, E.; Kawakami, M.; Ohwada, M. *Journal of Applied Physics* **1990**, *68*, 1272-1281.

(200) Pasilis, S. P.; Kertesz, V.; Van Berkel, G. J.; Schulz, M.; Schorcht, S. *Analytical and Bioanalytical Chemistry* **2008**, *391*, 317-324.

(201) Malinowska, I.; Studziński, M.; Niezabitowska, K.; Gadzikowska, M. *Chromatographia* **2013**, *76*, 1327-1332.

(202) Benabdellah, F.; Touboul, D.; Brunelle, A.; Laprevote, O. *Analytical Chemistry* **2009**, *81*, 5557-5560.

(203) Hölscher, D.; Shroff, R.; Knop, K.; Gottschaldt, M.; Crecelius, A.; Schneider, B.; Heckel, D. G.; Schubert, U. S.; Svatoš, A. *The Plant Journal* **2009**, *60*, 907-918.

(204) Liu, Q.; Xiao, Y.; Pagan-Miranda, C.; Chiu, Y. M.; He, L. *Journal of the American Society for Mass Spectrometry* **2009**, *20*, 80-88.

(205) Pól, J.; Vidová, V.; Hyötyläinen, T.; Volný, M.; Novák, P.; Strohalm, M.; Kostiainen, R.; Havlícek, V.; Wiedmer, S. K.; Holopainen, J. M. *PLoS ONE* **2011**, *6*, 1-9.

(206) Rubakhin, S. S.; Jurchen, J. C.; Monroe, E. B.; Sweedler, J. V. *Drug discovery today* **2005**, *10*, 823-837.

(207) Dufresne, M.; Thomas, A.; Breault-Turcot, J.; Masson, J.F.; Chaurand, P. *Analytical Chemistry* **2013**, *85*, 3318-3324.

(208) Perkel, J. M. *Science* **2013**, *340*, 1119-1121.

(209) Zaima, N.; Hayasaka, T.; Goto-Inoue, N.; Setou, M. *International Journal of Molecular Sciences* **2010**, *11*, 5040-5055.

(210) Arakawa, R.; Kawasaki, H. *Analytical Sciences* **2010**, *26*, 1229-1240.

(211) Chen, Y.; Allegood, J.; Liu, Y.; Wang, E.; Cachón-González, B.; Cox, T. M.; Merrill, A. H.; Sullards, M. C. *Analytical Chemistry* **2008**, *80*, 2780-2788..

(212) Wang, H.Y. J.; Post, S. N.; Woods, A. S. *International Journal of Mass Spectrometry* **2008**, *278*, 143-149.

(213) Touboul, D.; Brunelle, A.; Laprévote, O. *Bioactive Lipids, Nutrition and Health* **2011**, *93*, 113-119.

(214) Yang, H. J.; Ishizaki, I.; Sanada, N.; Zaima, N.; Sugiura, Y.; Yao, I.; Ikegami, K.; Setou, M. *Medical Molecular Morphology* **2010**, *43*, 158-164.

(215) Chen, Y.; Allegood, J.; Liu, Y.; Wang, E.; Cachón-González, B.; Cox, T. M.; Merrill, A. H.; Sullards, M. C. *Analytical Chemistry* **2008**, *80*, 2780-2788.

(216) Sun, X.; Liu, Z.; Welsher, K.; Robinson, J. T.; Goodwin, A.; Zaric, S.; Dai, H. *Nano Research* **2008**, *1*, 203-212.

Appendix 1

Data for Figure 2.3. Effect of deposition angle on SMALDI-MS performance. S/N was measured for 1 pmol verapamil on Co GLAD films deposited at 70, 85 and 88°.

Deposition Angle	**70°**	**85°**	**88°**
Spectrum 1 S/N	14.5	174.9	218.7
Spectrum 2 S/N	13.1	94.5	265.7
Spectrum 3 S/N	17.7	155.1	260.8
Spectrum 4 S/N	14.3	135.5	283.2
Spectrum 5 S/N	12.2	117.8	213.7
Mean	14.4	135.6	248.4
Standard Deviation	2.09	31.35	30.62
Error	0.93	14.02	13.69

Five spectra were collected per deposition angle and the mean S/N calculated.

Error was calculated as a measure of the spread in data points.

Error = $\frac{\text{Standard Deviation}}{\sqrt{n-1}}$, where n is the total number of replicates.

Appendix 2

Data for Figure 2.5. Effect of film thickness on SMALDI-MS performance. (a) S/N of 1 pmol verapamil obtained from Co GLAD films of different thicknesses. The same laser intensity was used for each film. (b) The UV absorption at 337 nm wavelength for Co GLAD films at different thicknesses. Optical absorption of cobalt films was measured using a Variable Angle Spectroscopic Ellipsometer in the reflectance mode. Column height, is monitored during deposition by measuring the deposition rate using a quartz-crystal microbalance.

Film Thickness (nm)	S/N					Mean	Standard Deviation	Error
250	295.7	368.6	499.4	356.5	462.8	396.6	82.95	37.10
500	410.1	459.1	506.3	291.5	278.9	389.18	90.27	40.37
750	82.5	116.2	156.5	160.7	222	147.58	52.46	23.46
1000	7.8	33.4	9.5	20.9	14.6	17.24	10.37	4.64

S/N ratios were measured for five spectra at each thickness.

Film Thickness (nm)	Absorbance		Mean	Standard Deviation	Error
250	0.307	0.297	0.302	0.007	0.005
500	0.530	0.529	0.530	0.001	0.001
750	0.766	0.750	0.758	0.011	0.008
1000	1.004	1.001	1.002	0.003	0.002

Error = $\frac{\text{Standard Deviation}}{\sqrt{n-1}}$, where n is the total number of replicates.

Appendix 3

Data for Figure 2.7. Contact angle measurements for a) 168 nm, b) 250 nm, c) 500 nm, d) 750 nm and e) 1000 nm Co films, f) contact angle vs film thickness

Film Thickness (nm)	Contact Angle (°)				Average	Standard Deviation	Error
168	84.18	84.3	62.47	56.88	71.96	14.36	7.18
250	30.24	27.51	37.17	32.12	31.64	4.98	2.87
500	17.87	20.44	22.17	18.84	19.83	1.89	0.94
750	25.62	23.82	24.3	23.84	24.72	1.27	0.90
1000	27.82	21.59	25.49	28.00	25.725	2.98	1.49

Error = $\frac{\text{Standard Deviation}}{\sqrt{n-1}}$, where n is the total number of replicates.

Appendix 4

Data for Figure 2.8. Determination of the optimum arbitrary unit (a.u.) laser fluence for SMALDI-MS on 250 nm Co films. S/N for 1 pmol verapamil was measured for five spectra at each a.u. laser fluence.

Laser Fluence (a.u.)	S/N			Average	Standard Deviation	Error
1500	13.5	48.6	19.3	27.1	18.8	10.9
1550	34.5	31.2	21.6	29.1	6.7	3.9
1600	507.7	481	485.3	491.3	14.3	8.3
1610	394.6	434	564.5	499.1	100.5	50.3
1620	615.3	443.2	442.9	502.0	81.3	40.6
1630	549.6	409.5	542.4	464.3	97.0	48.5
1640	335.8	497.3	490.8	483.8	113.1	56.5
1650	503.3	468.2	469.4	480.3	19.9	11.5
1660	494.4	420.6	401.6	431.9	42.4	21.2
1670	382.3	334	342.4	350.3	21.7	10.9
1680	386.1	263.7	268	334.7	80.7	40.4
1690	321.1	235.9	223	283.18	63.6	31.8
1700	299.4	297.7	223.3	273.47	43.5	25.1
1750	152.5	201.5	168	174	25.0	14.5
1800	54.2	237.8	189.7	160.6	95.2	55.0
1850	61.4	154.6	112.2	109.4	46.7	26.9
1900	29.5	93.6	62.6	61.9	32.1	18.5
1950	41.6	78.7	54.7	58.3	18.8	10.9
2000	38.5	80.8	39.2	52.8	24.2	14.0
2050	18.6	57.1	38.6	38.1	19.3	11.1
2100	24.1	58.5	29.1	37.2	18.6	10.7

Error = $\frac{\text{Standard Deviation}}{\sqrt{n-1}}$, where n is the total number of replicates.

Appendix 5

Data for Figure 2.9. Determination of the optimum arbitrary unit (a.u.) laser fluence for SMALDI-MS on 250 nm Co films. S/N for 10 pmol verapamil was measured for five spectra at each a.u. laser fluence.

Spot Number	S/N	Relative Intensity
spot 1	25.1	77
spot 2	33.9	96
spot 3	57	100
spot 4	47	100
spot 5	35.9	100
spot 6	30.9	100
spot 7	64	100
spot 8	17.2	67
spot 9	44.3	100
spot 10	18.5	50
spot 11	77.5	100
spot 12	48.6	100
spot 13	52.2	100
spot 14	56.2	100
spot 15	11	100

Single shot analysis data (red curve)

Spot Number	Relative Intensity
1	100
2	100
3	100
4	100
5	100
6	88.9
7	94.2
8	78.4
9	68.0
10	100
11	96.6
12	82.6
13	86.1
14	75.1
15	63.7

100 shots per spot analysis data (black curve)

Appendix 6

Data for Figure 2.10. Comparison of SMALDI-MS performance of Co films fabricated on different dates. S/N of 50 pmol verapamil was measured for five spectra from films produced on each date.

Fabrication Date	S/N					Average	Standard Deviation	Error
27/10/2010	488.1	510.4	509.6	482.9	535.7	505.34	21.01	9.39
24/11/2010	487.9	498.1	491.3	431.5	380.3	457.82	50.87	22.74
26/01/2011	295.7	368.6	499.4	356.5	462.8	396.6	82.95	37.10

Error = $\frac{\text{Standard Deviation}}{\sqrt{n-1}}$, where n is the total number of replicates.

Appendix 7

Data for Figure 2.11. Plot of S/N and ion count vs. amount of verapamil on 250 nm Co GLAD films for limit of detection.

Quantity (fmol)	Ion Count					Mean	Standard Deviation	Error
100	10285	9683	10362	9311	10591	1.0E+04	531	237
50	5674	4748	4250	8196	2997	5.2E+03	723	323
25	2449	2829	2240	3676	2819	2.8E+03	549	245
12.5	1062	1178	1923	1954	2031	1.6E+03	469	210
6.25	1256	1052	1275	1135	1108	1.2E+03	97	43

S/N and ion counts were calculated for the verapamil peak for five spectra and the mean calculated. Concentration of verapamil was 1 pmol.

Quantity (fmol)	S/N					Mean	Standard Deviation	Error
100	120.6	151.8	138.3	159.0	174.0	148.74	20.3	9.1
50	70.1	25.0	101.8	91.9	90.1	75.78	30.6	13.7
25	26.1	23.1	34.4	34.3	33.6	30.3	5.3	2.4
12.5	18.6	20.7	19.3	18.2	18.9	19.14	1.0	0.4
6.25	10.1	6.6	8.3	11.9	7.9	8.96	2.1	0.9

Error = $\frac{\text{Standard Deviation}}{\sqrt{n-1}}$, where n is the total number of replicates.

Appendix 8

Data for Figure 3.18. (a) limit of quantification of standard sulfatide spiked in pig serum, S/N vs amount of standard sulfatide spiked in serum.

Standard Sulfatide (fmol)	S/N	Error
64	1090.7	38.4
32	620.4	20.2
16	378.4	65.7
8	241.6	19.3
4	84.8	12.5
0.04	17.5	2.2

Error = $\frac{\text{Standard Deviation}}{\sqrt{n-1}}$, where n is the total number of replicates.

Appendix 9

Data for Table 4.1. R_F values and signal to noise ratios for carbohydrate compounds. See Section 4.2.4 for more information obtaining measurements for RF values.

Distance travelled by solvent front and separated spots in 40 seconds for a mixture of carbohydrate compounds.

Distance to solvent front, *y* (mm)	**14.0**	**16.0**	**15.0**
Beta cyclodextrin, *x* (mm)	2.0	2.5	2.0
Methylgalactopyranoside, *x* (mm)	2.5	3.0	2.4
Ribose, *x* (mm)	3.0	3.5	3.0
Sucrose, *x* (mm)	7.0	5.5	6.5

Calculation of R_F values for carbohydrates.

	x/y					
Compound	**Run 1**	**Run 2**	**Run 3**	**Average**	**Standard Deviation**	**Error**
Beta cyclodextrin	0.14	0.16	0.13	0.14	0.012	0.007
Methylgalactopyranoside	0.18	0.19	0.16	0.18	0.014	0.008
Ribose	0.21	0.22	0.20	0.21	0.010	0.006
Sucrose	0.50	0.34	0.43	0.43	0.078	0.045

S/N values for carbohydrate separated spots.

Compound	**S/N**					**Average**	**Standard Deviation**	**Error**
Sucrose	137.8	152.0	118.7	253.1	324.6	197.2	88.2	39.4
Ribose	223.7	154.7	125.9	188.9	101.8	159.0	48.7	21.8
Methylgalactopyranoside	34.0	52.0	45.0	25.0	75.0	46.2	19.1	8.6
Beta cyclodextrin	378.7	346.2	269.8	326.3	250.1	314.2	53.4	23.9

Error = $\frac{\text{Standard Deviation}}{\sqrt{n-1}}$, where n is the total number of replicates.

Distance travelled by solvent front and separated spots in 75 seconds for a mixture of peptides and metabolite compounds.

Distance to solvent front, *y* (mm)	**18.0**	**20.0**	**18.5**
Verapamil, *x* (mm)	5	6	5.5
Angiotensin I, *x* (mm)	8	8.5	9
Bradykinin, *x* (mm)	12	14	11.5
Angiotensin II, *x* (mm)	12.5	15	13

Calculation of R_F values for separated compounds.

	x/y					
Compound	**Run 1**	**Run 2**	**Run 3**	**Average**	**Standard Deviation**	**Error**
Verapamil	0.28	0.30	0.30	0.29	0.012	0.007
Angiotensin I	0.44	0.43	0.49	0.45	0.031	0.018
Bradykinin	0.67	0.70	0.62	0.66	0.039	0.023
Angiotensin II	0.69	0.75	0.70	0.72	0.030	0.017

S/N values for carbohydrate separated spots.

Compound	**S/N**					**Average**	**Standard Deviation**	**Error**
Verapamil	153.5	146.9	106.4	130.9	299.9	167.5	76.2	34.1
Angiotensin 1	293.8	279.3	247.9	249.4	207.8	255.6	33.2	14.8
Bradykinin	219.4	142.2	189.7	119.3	33.1	140.7	71.8	32.1
Angiotensin 11	206.3	218.7	249.7	264.8	332.8	254.5	49.7	22.2